National Library
of Canada

Acquisitions and
Bibliographic Services Branch

395 Wellington Street
Ottawa, Ontario
K1A 0N4

Bibliothèque nationale
du Canada

Direction des acquisitions et
des services bibliographiques

395, rue Wellington
Ottawa (Ontario)
K1A 0N4

Your file Votre référence

Our file Notre référence

NOTICE

The quality of this microform is heavily dependent upon the quality of the original thesis submitted for microfilming. Every effort has been made to ensure the highest quality of reproduction possible.

If pages are missing, contact the university which granted the degree.

Some pages may have indistinct print especially if the original pages were typed with a poor typewriter ribbon or if the university sent us an inferior photocopy.

Reproduction in full or in part of this microform is governed by the Canadian Copyright Act, R.S.C. 1970, c. C-30, and subsequent amendments.

AVIS

La qualité de cette microforme dépend grandement de la qualité de la thèse soumise au microfilmage. Nous avons tout fait pour assurer une qualité supérieure de reproduction.

S'il manque des pages, veuillez communiquer avec l'université qui a conféré le grade.

La qualité d'impression de certaines pages peut laisser à désirer, surtout si les pages originales ont été dactylographiées à l'aide d'un ruban usé ou si l'université nous a fait parvenir une photocopie de qualité inférieure.

La reproduction, même partielle, de cette microforme est soumise à la Loi canadienne sur le droit d'auteur, SRC 1970, c. C-30, et ses amendements subséquents.

Canada

UNIVERSITY OF ALBERTA

A PALEO-GEOMAGNETIC INVESTIGATION OF THE PERMO-CARBONIFEROUS SUPERCHRON

BY

J.M.MAILLOL

©

A thesis submitted to the Faculty of Graduate Studies and Research in partial fulfillment of the requirements for the degree of DOCTOR OF PHILOSOPHY

IN

GEOPHYSICS

DEPARTMENT OF PHYSICS

EDMONTON, ALBERTA

FALL 1992

National Library of Canada
Bibliothèque nationale du Canada

Canadian Theses Service
Service des thèses canadiennes

Ottawa, Canada
K1A 0N4

The author has granted an irrevocable non-exclusive licence allowing the National Library of Canada to reproduce, loan, distribute or sell copies of his/her thesis by any means and in any form or format, making this thesis available to interested persons.

L'auteur a accordé une licence irrévocable et non exclusive permettant à la Bibliothèque nationale du Canada de reproduire, prêter, distribuer ou vendre des copies de sa thèse de quelque manière et sous quelque forme que ce soit pour mettre des exemplaires de cette thèse à la disposition des personnes intéressées.

The author retains ownership of the copyright in his/her thesis. Neither the thesis nor substantial extracts from it may be printed or otherwise reproduced without his/her permission.

L'auteur conserve la propriété du droit d'auteur qui protège sa thèse. Ni la thèse ni des extraits substantiels de celle-ci ne doivent être imprimés ou autrement reproduits sans son autorisation.

ISBN 0-315-77221-2

Canada

UNIVERSITY OF ALBERTA

RELEASE FORM

NAME OF AUTHOR: JEAN-MICHEL MAILLOL

TITLE OF THESIS: A Paleo-geomagnetic Study of the Permo-Carboniferous Superchron

DEGREE: Doctor of Philosophy

YEAR THIS DEGREE GRANTED: 1992

Permission is hereby granted to the University of Alberta Library to reproduce single copies of this thesis and to lend or sell such copies for private, scholarly or scientific research purposes only.

The author reserves all other publication and other rights in association with the copyright in the thesis, and except as hereinbefore provided neither the thesis nor any substantial portion thereof may be printed or otherwise reproduced in any material form whatever without the author's prior written permission.

2001 GH Michener Pk
Edmonton, Alberta, T6H 5B5

DATE: May 20, 1992

UNIVERSITY OF ALBERTA

FACULTY OF GRADUATE STUDIES AND RESEARCH

The undersigned certify that they have read, and recommend to the Faculty of Graduate Studies and Research for acceptance, a thesis entitled A PALEO-GEOMAGNETIC STUDY OF THE PERMO-CARBONIFEROUS SUPERCHRON submitted by JEAN-MICHEL MAILLOL in partial fulfillment of the requirements for the degree of Doctor of Philosophy in Geophysics.

M. E. EVANS

G. ROSTOKER

E. H. PINNINGTON

D. R. SCHMITT

R. MORTON

D. W. COLLINSON

DATE: May 6, 1992

To my mother, and to the
fond memory of my father.

ABSTRACT

A paleomagnetic study of a Permian redbed formation located in the Lodève Basin (Southern France) has been carried out. Two hundred and one stratigraphically ordered samples have been collected at an average of 10m intervals from a 1220 m thick sequence representing approximately 10 Ma. An additional 605 samples were obtained by small interval sampling (7 mm) of short (30 cm to 2 m) sequences.

The origin of redbed magnetization has long been controversial. The closely sampled sections reveal magnetic intensity variations with a characteristic "saw tooth" shape and a strong stratigraphic control. These variations can be best explained by a variation in efficiency of alignment of the magnetic grains, which points to an early post-depositional origin for the magnetization of the Lodève redbeds.

The Permo-Carboniferous reversed superchron (PCR) is the longest known interval of constant polarity of the Earth's magnetic field. Entirely located within this interval, both large and small interval data series show the presence of coherent, serially correlated magnetic direction variations that are interpreted as recordings of paleosecular variation. A statistical analysis of the VGP scatter indicates that the geomagnetic activity was reduced during the PCR as predicted by models linking secular variation amplitude and frequency of reversals. Spectral analysis reveals the presence of periods in the range 100 to 1000 yrs in the closely sampled sections and in the range 0.2 to 0.5 Ma in the traverse of the entire Basin.

The paleomagnetic pole (154.1°E, 44.6°N, A_{95}=1.6°) is in general agreement with the Late Paleozoic apparent polar wander path for stable Europe. However, a slight discrepancy towards more southerly latitude is observed and is possibly due to local tectonic motions.

ACKNOWLEDGEMENTS

I wish to express my thanks to my supervisor Dr. M.E. Evans for his help and for giving me the opportunity to spend a very enriching part of my life in Canada.

I am indebted to all the members of my family who have always, in all circumstances, given me the support and encouragements I needed. I am most particularly thinking of my parents Suzanne and Etienne Maillol to whom I owe everything. Above all, I would have liked them to be able to share with me the joy of this accomplishment. Life has decided otherwise.

I am thankful to the friends who made more enjoyable my stay in Edmonton and at the University of Alberta. Among them, I wish to specially thank Antonio Correia. During all these years we have spent facing various difficulties, his generous help in scientific matters and every-day life was of paramount importance to me.

Finally, I wish to express all my gratitude to the most wonderful person in the world, my wife Dominique. Her loving presence makes everything seem easy. Her direct contribution must also be recognized since she has been a very efficient help in field work and in measuring hundreds of samples. If one person has made this thesis possible, it is undoubtedly her. For all we have shared, thank you Dominique.

TABLE OF CONTENTS

Page

1. INTRODUCTION 1

1.1 General 1

1.2 The magnetization of continental redbeds 4

1.3 Geomagnetic field reversals and paleosecular variation 7

1.3.1 The Kiaman interval (PCR) 7

1.3.2 Reversals and secular variation 9

1.4 The reconstruction of Pangea 11

2. GEOLOGICAL SETTING OF THE LODEVE BASIN AND SAMPLING PROCEDURES 15

2.1 Geography 15

2.2 Tectonic setting 17

2.3 Lithostratigraphy 17

2.3.1 Overview of the Permian system 17

2.3.2 Lodève lithostratigraphy 21

2.4 Sampling details 24

2.4.1 Basin traverse 24

2.4.2 Small scale, detailed sampling 29

2.5 Sample preparation 34

2.5.1 Basin Traverse samples 34

2.5.2 Closely spaced samples 35

3. ORIGIN OF THE MAGNETIZATION IN LODEVE REDBEDS 38

3.1 Introduction 38

3.2 Samples used for the intensity investigation .. 39

3.3 Results and analysis 42
3.3.1 Remanent Magnetization Intensity Variations 42
3.3.2 Thermal and Alternating Field (AF) demagnetization 49
3.3.3 Susceptibility and Isothermal Remanent Magnetization (IRM) 50
3.4 Petrographic Analysis 59
3.5 Quantitative characterization of the intensity patterns 66
3.5.1 Statistical considerations 66
3.5.2 Trends in intensity variations 72
3.6 Discussion 80
3.7 Conclusions 85
4. DIRECTION OF MAGNETIZATION 88
4.1 Introduction 88
4.2 Pilot demagnetizations 90
4.2.1 Alternating field (AF) demagnetization 90
4.2.2 Thermal demagnetization 94
4.3 Presentation of directional data 118
4.3.1 Basin Traverse 118
4.3.2 Closely spaced samples 127
5. GEOPHYSICAL INTERPRETATION OF DIRECTIONAL DATA 135
5.1 Introduction 135
5.2 Interpretation of directional variations 136
5.3 Angular dispersion 142
5.3.1 Existing paleosecular variation (PSV) models 142
5.3.2 Lodève results 148
5.4 Time series 155
5.4.1 Basin Traverse 155
5.4.2 Closely sampled sections 162

5.5 Paleogeographic considerations 165

6. SUMMARY AND CONCLUSIONS 174

6.1 Scalar magnetic properties of the Lodève strata 174

6.2 Directional magnetic properties 176

BIBLIOGRAPHY 180

APPENDIX 1 - DATA SETS 187

a) Samples used for rock magnetic experiments 187

b) Data from the Basin Traverse and closely sampled sections 188

APPENDIX 2 - LABORATORY INSTRUMENTATION 197

a) Molspin Spinner Magnetometer 197

b) AF demagnetizer 198

c) Thermal demagnetization furnace 198

d) Magnetically shielded room 196

e) Other instruments 201

APPENDIX 3 - GEOMAGNETIC FORMULAS 203

a) Magnetic potential-Gauss coefficients 203

b) Virtual geomagnetic poles (VGP) 204

APPENDIX 4 - GLOSSARY 205

LIST OF TABLES

Table		Page
3.1	Summary of lithological, sampling, and paleodirectional data.	41
3.2	Statistical parameters R_N and R_Δ	67
4.1	List of specimens used for pilot thermal demagnetization experiments represented in Fig4.2.	99
4.2	Statistics of directional data from the Basin Traverse.	121
5.1	Results of Watson & Beran's test.	138
5.2	Average angular dispersion in degrees for 4 successive specimens, in VGP reference frame.	153
5.3	Virtual geomagnetic poles from the Basin Traverse	167
5.4	Combined mean paleopoles for Europe and North America in European coordinates	168

LIST OF FIGURES

Figure ..... Page

1.1 Schematic representation of the evolution of polarity reversal rate for the last 350Ma 8

1.2 Schematic representation of the relationship between PSV and polarity reversals 12

2.1 Map of France showing the location of the Lodève Basin 16

2.2 Simplified geological map of the Lodève Basin 18

2.3 Geological cross section of the Lodève Basin 18

2.4 Stratigraphic classification of the Permian system 20

2.5 Main lithostratigraphic divisions of the Lodève Basin 23

2.6 Location of sampling sites 26

2.7 Stratigraphic logs of the basin traverse 30

2.8 Schematic of the method used to sample continuously a 2m section using 25 cm cores 33

2.9 Illustration of the wax base method for preparing and measuring "plastic top" samples 37

3.1 Intensity data from a 190 cm siltstone/sandstone section (site BLF) before and after thermal demagnetization at 510°C 44

3.2 Same NRM data as in Fig.3.1 with enlargements of three particular intensity peaks 45

3.3 Intensity data from 3 siltstone cores taken at the same stratigraphic horizon (site BLP) 46

3.4 Other examples of intensity variations from different sandstone (BLJ1,3,4 and BLS) and mudstone (BLM1,3) horizons 47

3.5 Two stratigraphically equivalent intensity magnetograms from site BLF, separated by 30 meters 48

3.6 Normalized intensity decay curves after progressive thermal demagnetization 51

3.7 Normalized intensity decay curves after progressive AF demagnetization 52

3.8 NRM intensity versus susceptibility for the specimens of Fig.3.1 53

3.9 IRM intensity (1.75 T) compared to NRM intensity (left) and to susceptibility (right) for 6 stratigraphically consecutive siltstone samples .. 56

3.10 Normalized IRM acquisition/destruction curves 57

3.11 Normalized IRM acquisition curves of two siltstone specimens with NRM intensity ratio of 7.7 57

3.12 Thermal demagnetization of IRM for three distinct coercivity fractions 58

3.13 Photograph of a siltstone thin section in reflected light 62

3.14 Photograph of a siltstone thin section in transmitted light 63

3.15 Photograph of a sandstone thin section in reflected light 64

3.16 Photograph of a sandstone thin section in transmitted light 65

3.17 Explanation of the notation used for statistical analysis of the intensity variations 68

3.18 Histograms of R_N and R_Δ distributions for section BLF1 70

3.19 Same as Fig 3.18 for BLF2 71

3.20 Fourteen examples of magnetic intensity decay patterns in different lithologies 73

3.21 Stacked plot of data from Fig.3.20 after normalization 76

3.22 Stacked plot of data points from 11 monotonic intensity decay patterns 77

3.23 Stacked plot of data points from 5 intensity decay patterns in siltstones 78

3.24 Stacked plot of data points from 6 intensity decay patterns in sandstones 79

4.1 Stepwise AF demagnetization of two pilot specimens 92

4.2 Stepwise thermal demagnetization of 17 pilot samples. 101

4.3 Polar equal area projection of NRM directions of individual samples from the Basin Traverse (no bedding correction). 119

4.4 Polar and equatorial equal area projection of remanence directions of individual samples from the Basin Traverse after thermal treatment (no bedding correction) 120

4.5 Histogram of the angle α between NRM and cleaned directions calculated for each specimen 123

4.6 Histogram of the angle β between the normal to the plane defined by the present-day/Permian field directions and the normal to the plane defined by NRM/cleaned directions of each specimens 123

4.7 Declination and Inclination magnetograms for the 201 samples of the Basin Traverse 125

4.8 Declination and Inclination magnetograms for the 108 site means of the Basin Traverse 126

4.9. Declination and Inclination magnetograms for section 1 of site BLF 129

4.10. Declination and Inclination magnetograms for section 2 of site BLF 130

4.11. Compared declination records of the two sections sampled at site BLF 131

4.12 Compared declination and inclination records for 3 cores collected at site BLP (intercore distances 40 and 50cm) 132

4.13 Same as Fig.4.14 for site BLJ; intercore distances 30 cm 133

4.14 Declination and inclination records for 2 mining core segments 134

5.1 Plots of Declination and Inclination vs. susceptibility for section BLF2 140

5.2 Plots of Declination and Inclination vs. intensity for section BLF2 141

5.3 Angular dispersion of VGP for IGRF65 separated into the contributions from the quadrupole (secondary) dynamo family (S_q) and the dipole (primary) dynamo family (S_d) 145

5.4 Fit of model G to combined polarity data for the past 5Ma 147

5.5 Variation of VGP dispersion due to the quadrupole family for the last 190Ma (S_q) 147

5.6 Illustration of various remanence direction variation patterns and corresponding complex MEM spectra 157

5.7 Complex MEM spectra for the Basin Traverse 158

5.8 Smoothed Bauer plots of two parts of the Basin Traverse showing clockwise and counter-clockwise motion 161

5.9 Complex MEM spectrum for section BLF2 164

5.10 Smoothed Bauer plot for a part of section BLF2 .. 164

5.11 Maps of Pangea A and B reconstructions 166

5.12 Paleomagnetic poles from the entire Basin Traverse and from its lower and upper halves, compared to combined paleopoles for Europe and North America 169

5.13 Paleomagnetic poles from the entire Basin Traverse and from its lower and upper halves, compared to earlier results from the Lodève Basin 171

A.1 Contour plot of the field intensity in the magnetically shielded room 202

CHAPTER 1

INTRODUCTION

1.1 General

The study of the Earth's magnetic field has greatly benefitted from paleomagnetism, which is the only method that allows one to obtain information about the ancient geomagnetic field. Polarity reversals, the most dramatic type of field change, were discovered thanks to studies of the remanent magnetization of rocks. Furthermore, geomagnetists can now reach well beyond the short time of availability of observatory data and can provide field variation records spanning intervals of several thousand years and dating back hundreds of millions of years. These variations, known as paleosecular variation (PSV) can be studied using lava flows or sedimentary sequences. However, as always in earth science, resolution and accuracy decrease with increasing age of the rock formation studied.

The consequence of the difficulties inherent with older rocks is that very limited information about the PSV is available during the Paleozoic (570-250 Ma). However the end of this era is particularly interesting from a

geomagnetic point of view because it corresponds to the Permo-Carboniferous Reversed Superchron (PCR, 320-250 Ma), previously known as Kiaman interval. This superchron is one of two anomalous periods of the Earth's history (the other one is in the Cretaceous (KN, 124-83 Ma)) during which the geomagnetic field maintained a constant polarity for several tens of million of years. Clearly these periods are most important in the context of efforts to understand the mechanism of polarity reversals. Indeed, any anomaly of the field behavior detected during these periods could shed some light on the reversal causes. This made it very tempting to try to obtain some information on the secular variation during the PCR, which is the longest interval of constant polarity. This is what motivated the present study of a Permian sedimentary sequence, the Lodève Basin, with the initial prospect of recovering data from almost 2km of redbed strata, covering several million years.

Another interesting Permian topic is the long lasting controversy concerning continental reconstructions. It is now well established that at the end of the Permian all continental masses were joined together in a supercontinent called Pangea, just before their breaking up during the Mesozoic. However, marked discrepancies between paleomagnetic data from northern blocks (N. America and Eurasia) and southern blocks (mainly S.America

and Africa) have led to several conflicting reconstruction models. The Lodève Basin is located at the southern margin of the European block and therefore close to the controversial zone making the contact between Eurasia and Africa during the Permian. One could hope that a detailed paleomagnetic study in such an area would bring some useful information concerning the paleogeographic problem.

When trying to extract detailed paleomagnetic data from sedimentary rocks, one has to be very careful in assessing the meaning and reliability of the results. A prerequisite to all paleomagnetic studies is, therefore, a detailed analysis of the rock magnetic properties aimed at understanding the remanence acquisition mechanisms. This step is of paramount importance when redbeds are involved since their magnetization has been the subject of controversy ever since they started to be used in paleomagnetism.

Paleomagnetism and rock magnetism are now well established fields, and all their aspects are extensively described in many textbooks. Therefore common methods and techniques will not be fully described in this thesis. In the remainder of this introductory chapter, the three major topics constituting the body of the thesis and mentioned above will be introduced in greater detail. In Chapter 2, the particular area chosen for field work, the Lodève Basin will be described, as well as details of the

sampling. Chapter 3 will tackle the difficult problem of the origin of magnetization in the Lodève rocks. In Chapter 4 results of measurements of the direction of magnetization will be presented. These last results will be discussed and interpreted in Chapter 5 in light of the hypothesis on the magnetization origin. Finally, a general conclusion in Chapter 6 will try to evaluate the outcome of this study.

1.2 The magnetization of continental redbeds

Continental redbeds consist of a large variety of sedimentary facies spanning the whole spectrum of non-marine depositional environments including alluvial fans, flood plains, deserts, lakes and deltas. Long thought to be characteristic of arid climates, it is now recognized that they can form in all types of climatic environments. The most authoritative textbook on redbed geology is that of Turner (1980) who also gives a comprehensive account of their use in paleomagnetism. Only a brief summary of aspects relevant to this thesis will be given here.

Initially confined to strongly magnetic igneous rocks, paleomagnetic science has gradually broadened its scope to sedimentary rocks. This move was aided by progress in instrumentation that made possible the measurement of ever weaker magnetizations. In this context, continental

redbeds have a particular significance for they were the first sedimentary rocks to be studied in any detail for paleomagnetic purposes (e.g. Clegg et al., 1954; Runcorn, 1955; Irving & Runcorn, 1957). Many paleogeographic reconstructions and polar wander paths are based mainly on paleomagnetic determinations from redbeds.

The reason for this important role is, of course, that red sediments are generally strongly magnetized compared to other sedimentary rocks. However, the origin of the magnetization of these rocks has always been highly controversial and is still a major point of debate between paleomagnetists, 40 years after the first sedimentary paleomagnetic studies (see Butler, 1992).

The central point of the controversy is the origin, (chemical or detrital) of the magnetization, with the corollary of the age of this magnetization compared to the rock age. To be useful for detailed paleomagnetic studies, a magnetic remanence must have been acquired soon after the deposition of the sediments and at rate directly related to the rate of accumulation. If redbeds carry a depositional remanent magnetization (DRM) they have acquired it shortly after deposition and can thus be useful tools to study geomagnetic phenomena. On the other hand, if the remanence is due to a chemical remanent magnetization (CRM), it could have been acquired over the

millions of years of the diagenetic history of the rock, and all useful geomagnetic information could be lost.

In most cases the magnetization of redbeds is carried by hematite but whether this mineral is detrital or formed during diagenesis is rarely evident. Moreover, even if hematite is of chemical origin it may have formed within the first 100 years of the rock history (Herrero-Bervera & Hesley, 1983; Shive et al., 1984), and it can be as useful as a true depositional remanence. The problem is further complicated by the common presence of several hematite phases in the same rock, which may play different roles in the magnetization process. There lies the controversy, and its longevity is undoubtedly due to the fact that *redbed* is actually a generic name grouping many different rock types. Therefore paleomagnetic observations from redbeds should be evaluated on a case-by-case basis, and each study should be associated with careful analysis of all available information on the magnetization.

The magnetic properties of redbeds have been described by many authors, prominent amongst which are Creer (1962), Collinson (1965a, b; 1966a, b; 1967; 1968a, b), and Dunlop (1972). The study of these properties is often instrumental in deciphering the complex problem of magnetization origin, by helping to identify the magnetic carriers. This is what was attempted in this study and the outcome will be reported in Chapter 3.

1.3 Geomagnetic field reversals and paleosecular variation

1.3.1 The Kiaman interval

The first evidence that the geomagnetic field could reverse its polarity was discovered by David (1904) and Brunhes (1906) who observed magnetizations in lava flows roughly opposed to the present Earth's field. It is now widely acknowledged that in nearly all cases these reversed directions are indeed due to field reversals and not to a petrological self-reversal mechanism (Hospers, 1953-54). Hundreds of reversals have been recognized and serve to establish the geomagnetic polarity time scale (see e.g Hailwood, 1989). Relatively well defined back to the middle Jurassic thanks to the presence of marine magnetic anomalies, this scale loses more and more definition when one goes back in time. The reversal frequency has changed over geological time but no definite pattern has as yet been discovered (Fig.1.1).

In the polarity scale, two anomalously long constant polarity intervals have been recognized. The most recent, in the Cretaceous, has lasted for some 35 Ma and is uniformly normal. It is called the *Cretaceous normal polarity superchron* (Cox, 1982). The older one occurs in the Permian. It has long been known that almost all Permian rocks worldwide have a reverse polarity characteristic magnetization (see e.g. Irving and Parry, 1963, Khramov, 1967; McElhinny, 1969). This very long

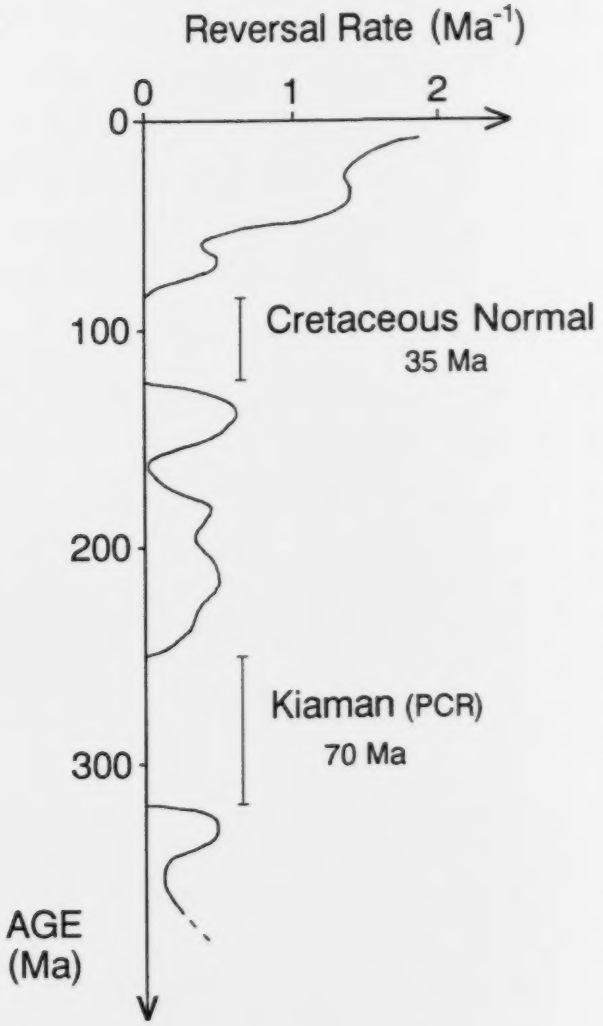

Figure 1.1. Schematic representation of the evolution of polarity reversal rate for the last 350Ma.

reverse polarity interval was first called the *Kiaman* interval from a locality in SE Australia (McElhinny, 1969) and is now preferably referred as the *Permo-Carboniferous reversed polarity superchron*. Its duration was approximately 70 Ma, making it the longest known interval of constant geomagnetic polarity. Its upper limit is ill defined but it is generally located near the Paleozoic-Mesozoic boundary (~250 Ma), thus close to the top of the Permian. The position of its base is even more disputed but most likely occurs somewhere in the Westphalian (Upper Carboniferous, ~320 Ma).

1.3.2 Reversals and secular variation

Complete reversals of polarity are the most dramatic aspect of the Earth's magnetic field. They clearly constitute the major, and least easily satisfied, constraint in attempts to model field behaviour. With durations ranging from 10^5 to 10^8 years, polarity intervals are also the longest period features of the geomagnetic field.

However, another very important aspect is the presence of smaller amplitude, shorter period (1 to 10^5 year) variations, known as secular variations. First detected in direct records of magnetic field fluctuations, the longer period (10^2 to 10^5 year) variations are also found in paleomagnetic records and become known as paleosecular

variation (PSV). When directions of the field are measured, this variation expresses itself through an angular dispersion of the data.

It is convenient, although rather artificial, to separate the total angular dispersion of the geomagnetic field into three contributions:

(i) variation in the intensity and direction of the non-dipole field

(ii) variation of the dipole moment with time

(iii) changes in the orientation of the geomagnetic dipole such that on average the dipole axis coincides with the rotation axis of the Earth (the so-called dipole wobble).

A most important characteristic of the angular dispersion is that it varies in latitude, and several models using the separation of contributions mentioned above have been proposed to account for this. These have been referred to as model A (Irving and Ward, 1964), model B (Creer et al., 1959), model C (Cox, 1962), model D (Cox, 1970), model E (Baag and Helsley, 1974), model M (McElhinny and Merrill, 1975), model F (McFadden and McElhinny, 1984) and finally, the most recent, model G (McFadden et al., 1988). A description of these models up to model F can be found in Merrill and McElhinny (1983), and model G will be discussed in greater detail in Chapter 5.

In addition to these modeling efforts concerning the paleosecular variation, attempts, initiated by Cox(1968), have been made to link the reversal mechanism to the amplitude of PSV. The basic idea is that PSV can be thought of as the expression of a perturbation phenomenon, which under favorable circumstances can trigger a complete inversion of the field polarity (Fig 1.2). The direct consequence is that PSV amplitude should be related to reversal frequency. In this context, detailed study of the PSV during very long intervals of constant polarity like the Kiaman are of considerable interest. If the coupling between reversal rate and PSV exists, one would expect to find a reduced activity of the field during the Kiaman. In addition, because of the peculiar length of this interval, one might hope to uncover new information on the field behaviour that would be masked during periods of higher reversal rate. These two aspects constitute the major goal of this study and will be addressed mainly in Chapter 5.

1.4 The reconstruction of Pangea

It is now widely recognized that by the end of Paleozoic times, all continental plates had clustered together into a single landmass called Pangea (see e.g. Piper, 1987). This reconstruction was first proposed by Wegener (1924), and has since then been supported by a

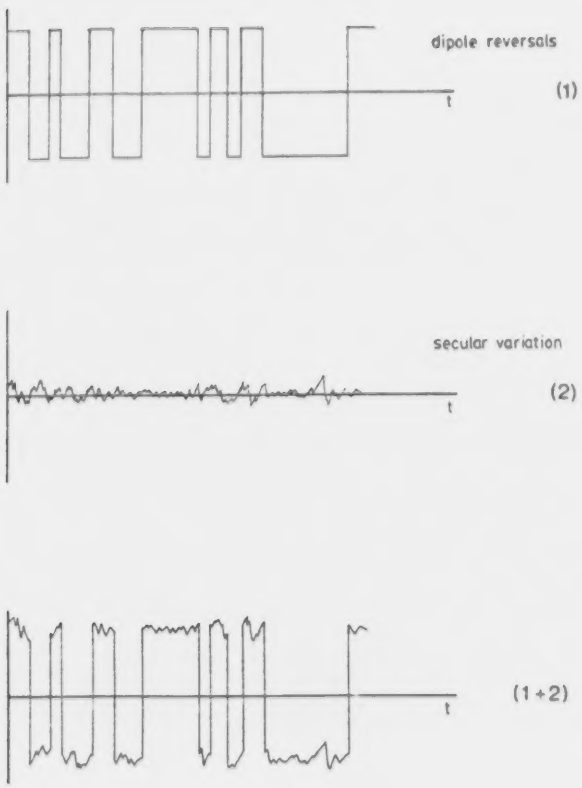

Figure 1.2. Schematic representation of the relationship between PSV and polarity reversals. PSV can be thought of as a perturbation of the main dipole behaviour.

wide range of geological evidence. Wegener's reconstruction, later quantified by Bullard et al. (1965) is referred to as *Pangea A*. Although it accommodates nicely all paleomagnetic data from the Upper Triassic and Lower Jurassic, it does not bring the Upper Carboniferous-Early Triassic poles from the northern continents (Laurasia) into precise conformity with data from the southern continents (comprising Gondwanaland).

Three causes have been proposed for this discrepancy:

(i) relative motion took place between the Laurasian and Gondwanaland parts of Pangea so that a different reconstruction from Pangea A existed prior to mid-Triassic times;

(ii) the apparent polar wander paths (APWP) are still insufficiently well constrained because of a lack of data mainly in the Upper Permian;

(iii) significant non-dipole components existed in the late Paleozoic geomagnetic field thus invalidating the dipole assumption used to calculate the paleopoles (Briden et al.,1971).

The first hypothesis has been most widely investigated and three alternative reconstructions have been proposed: Pangea A2 (Van der Voo and French, 1979), Pangea B (Irving 1977) and Pangea C (Smith et al., 1980). However, all these reconstructions require that important and rapid motion took place between Laurasia and Gondwanaland during

late Permian-early Triassic to achieve the classical Pangea A configuration in Upper Triassic times. This is not supported by geological evidence that poses serious problems to the acceptance of any of these reconstructions. Therefore, the two other hypotheses merit more attention.

Within this context, paleomagnetic data from the Lodève Basin are of interest since, as pointed out earlier, the basin sits close to the boundary between Laurasia and Gondwanaland, and the data collected would cover several million years at the very end of the Permian. We will examine in Chapter 5 what information the present study can bring to this paleogeographical problem.

CHAPTER 2

GEOLOGICAL SETTING OF THE LODEVE BASIN AND SAMPLING PROCEDURES

2.1 Geography

Located in Southern France (Fig 2.1), the Lodève Basin marks a transition between the French Massif Central and the Mediterranean region. Its shape is that of an elongated basin covering an area of about 310 km^2, and it represents a very-well defined entity among the surrounding geographical and geological units (Fig 2.2). The brittle red rocks, locally known as "ruffes", that make up the main part of the basin support very little vegetation and create a typical badland landscape where summer temperatures can be extreme. On the lower ground, along the main river (La Lergue) and its tributaries, thin Quaternary deposits support vineyards. The center of the basin is occupied by an artificial lake (Lac du Salagou).

The Lodève basin has high economic interest due to the presence of rich uranium deposits. First discovered in 1957, the deposits are now mined in several locations, and a processing plant has been installed by the French company COGEMA.

Figure 2.1. Map of France showing the location of the Lodève Basin.

2.2 Tectonic setting

Several studies of the structure have been carried out by Ruhland et al. (1977), Horrenberger and Ruhland (1981), Arthaud et al. (1977) and Santouil (1980). The general structure of the basin is that of a half-graben controlled by major faults to the South (Aires fault), and to the East (Cevennes fault) (Fig 2.2 and 2.3). The modern geometry of the basin is not representative of its original dimensions since all faults have been active long after the end of Permian sedimentation. Tectonic analysis shows that sediments have been progressively deformed during lithification, in a general context of extension and subsidence. The deformation has remained small and the result is a monoclinal dip southwards at an average angle of 12°. All the tilting had been acquired before the end of the Permian, as indicated by the horizontal Triassic strata unconformably overlying the Permian deposits.

2.3 Lithostratigraphy

2.3.1 Overview of the Permian system

Murchison in 1841 (in Harland et al., 1990) was the first to name the Permian system to take in the thick deposits overlying the Carboniferous throughout a great arc stretching from the Volga to the Urals and from the sea of Archangelsk to the southern steppes of Orenburg.

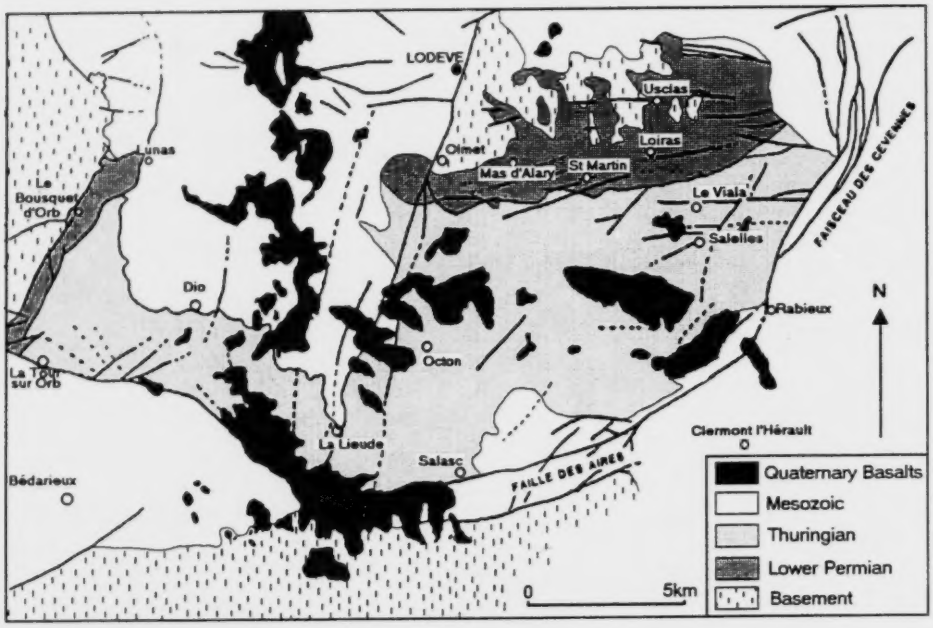

Figure 2.2. Simplified geological map of the Lodève Basin (adapted from Carte Géologique au 1/50000, Lodève, 1982)

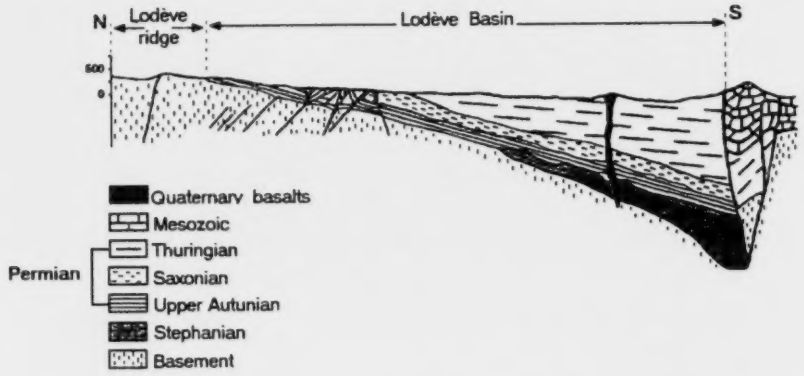

Figure 2.3. Geological cross section of the Basin (from Carte Géologique au 1/50000, Lodève, 1982)

The name came from the city of Perm and the ancient kingdom of Permia in the center of that area.

The subdivisions of the Permian have been mainly established using Russian stratotypes, but the later stages are best represented in East Asia and especially South China. There is still confusion as to whether a two- or three-fold division is more appropriate and no international consensus yet exists concerning this issue. To make matters worse several different classifications can be used depending on the geographical area of the globe and on the nature - continental or marine - of the deposits. In western Europe the continental Permian is traditionally divided into 3 stages: Autunian, Saxonian, Thuringian. In Germany, the divisions are named Rotliegendes (continental), often subdivided in Ober- and Unter-Rotliegendes, and Zechstein (marine facies). A summary of this somewhat complicated stratigraphic nomenclature is given in Fig 2.4. In this thesis, the division based on the terms Autunian, Saxonian and Thuringian will be used throughout. This choice has been made for the sake of simplicity and also because this scale has traditionally been used in all studies of the Lodève Basin.

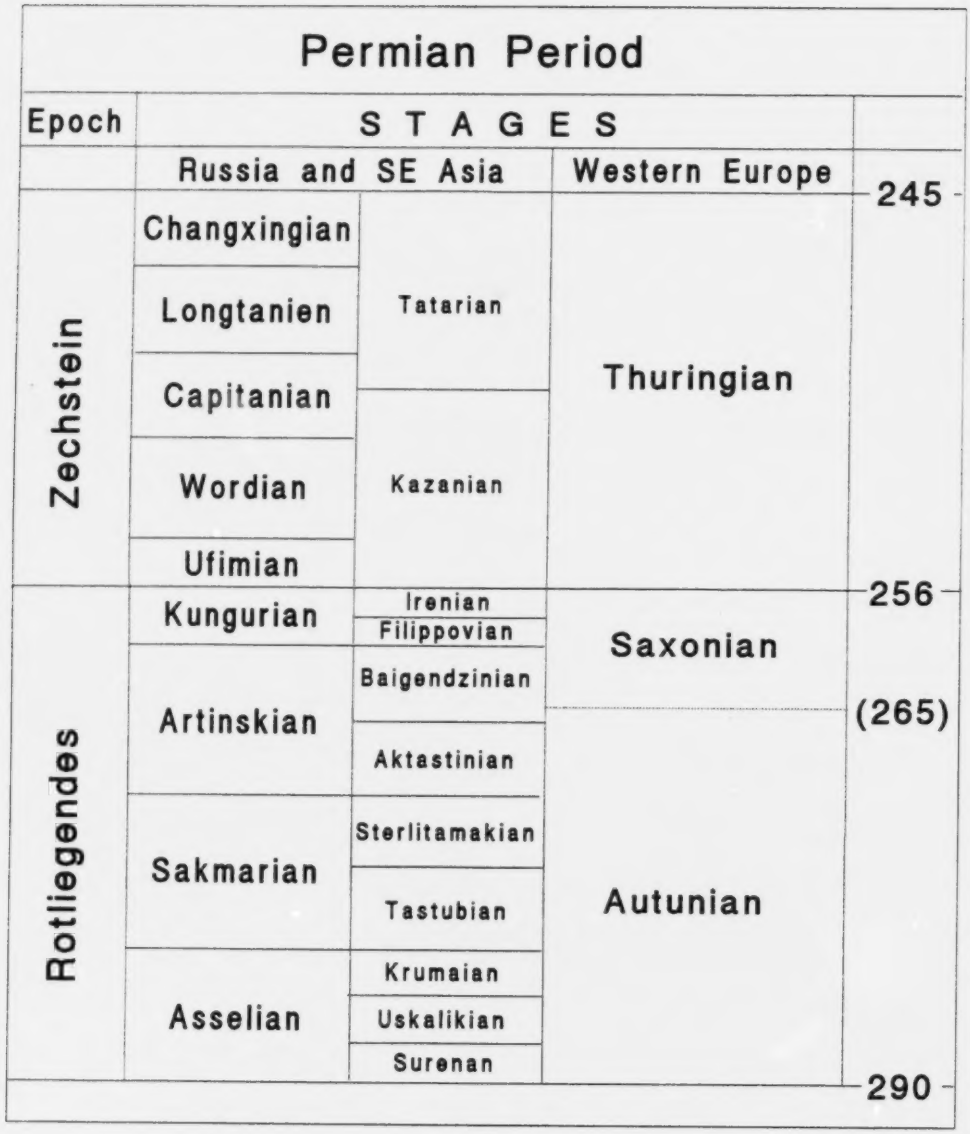

Figure 2.4. Stratigraphic classification of the Permian system (adapted from Harland et al., 1989). Ages of major boundaries are given in millions of years.

2.3.2 Lodève lithostratigraphy

The Permian sequence of the Lodève Basin has been extensively studied by Laversanne (1976) and Odin (1986), who also integrated data provided by COGEMA's geologists. It consists of 3000m of continental, clastic or bioclastic deposits, in which subdivisions can be made following structural and sedimentological criteria (Fig. 2.5). Briefly, three major divisions can be made (Odin, 1986; Odin et al., 1987). From older to younger these are:

(i) A uniformly gray 160 to 240 m thick sequence (Usclas-St Privat Formation) dated to the upper Autunian (lower Rotliegendes), and interpreted as representing a fluvio-deltaic and lacustrine environment.

(ii) An alternating sequence of gray and red rocks, approximately 200 m thick (Tuilières-Loiras Formation), belonging to the Saxonian (upper Rotliegendes) and deposited in lacustrine environment.

(iii) A very thick (up to 2000m) sequence of red sandstones, siltstones and mudstones dated by palynological analysis to the Thuringian (Zechstein). Its depositional environment is thought to have evolved from deltaic to playa-style sedimentation, under a tropical, semi-arid climate. It corresponds to the Viala, Rabejac and Salagou Formations.

The two last formations (Rabejac and Salagou) are the exclusive subject of this study. It must be noted that

their Thuringian age is based on the renewed palyno-stratigraphy of Odin (1986, see also Odin et al., 1986). This age is different from the one used in all previous studies of the basin, which traditionally give a Saxonian, therefore older, age for the thick red sequence.

The beginning of the Rabejac Formation is marked by a conglomerate lying on an eroded paleosurface developed after an intra-Thuringian tectonic phase. This layer varies in thickness from 1 to several metres and is followed by approximately 200m of alternating sandstones, siltstones and mudstones, with an increasing dominance of the finer members toward the top. In the coarser members a complete range of sedimentary structures is observed. A playa-style sedimentation characterizes the overlying Salagou Formation, with nearly 2000m of redbeds deposited during a strong subsidence of the basin. The rocks consist of uniformly red very fine sediments organized in siltstone/mudstone detrital sequences. The siltstones are limited to thin (a few cm) beds while the mudstone beds are usually several metres thick. Sedimentary structures are scarce but numerous desiccation marks occur. The overall trend in the environmental evolution clearly demonstrates the increasingly arid character of the climate as the Lodève strata were deposited (Fig 2.5).

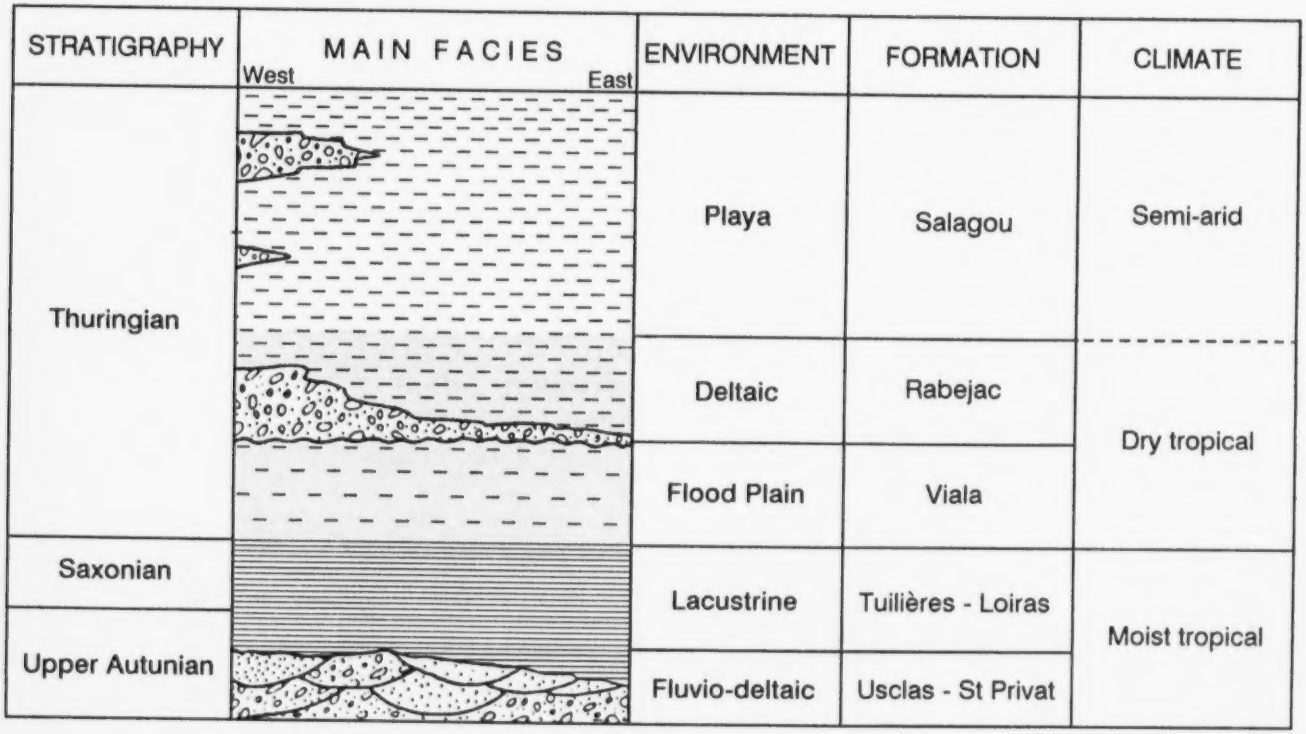

Figure 2.5. Main lithostratigraphic divisions of the Lodève Basin (adapted from Odin, 1986).

2.4 Sampling details

2.4.1 Basin traverse

The structure of the basin, a half graben with gently southerly dipping strata, makes it easy to access the whole sequence along road cuts and river beds. The first aim of the sampling campaign was to recover stratigraphically ordered paleomagnetic information from the entire sedimentary column. We deliberately chose to ignore the gray rocks likely to give less reliable information than the red ones, because of their much lower magnetization intensities. We therefore chose as a lower limit the conglomerate layer marking the limit between the Viala and Rabejac Formations, and sampled from North to South, up to the youngest Permian rocks available. This sequence represented a substantial 1220m of sedimentary column corresponding to Odin's Thuringian. It also offered at least the possibility to reach the end of the Kiaman superchron, should it be present in the Basin. The actual Basin area was selected so as to offer the best sampling line, i.e. easy to follow along an unbroken path and with the best possible outcropping conditions along road cuts and river beds (Fig 2.6). Care was also taken to avoid the proximity of basalt flows and intrusions in order to eliminate the risk of thermal remagnetization.

Figure 2.6. Location of sampling sites. BL and BLA correspond to the basin traverse, which is indicated by a thick line. Numbers refer to sampling sites along the traverse. BLF, BLJ, BLP and BLS correspond to fine scale sampling sites. The location of the mining core studied by Evans & Maillol (1986) is also indicated.

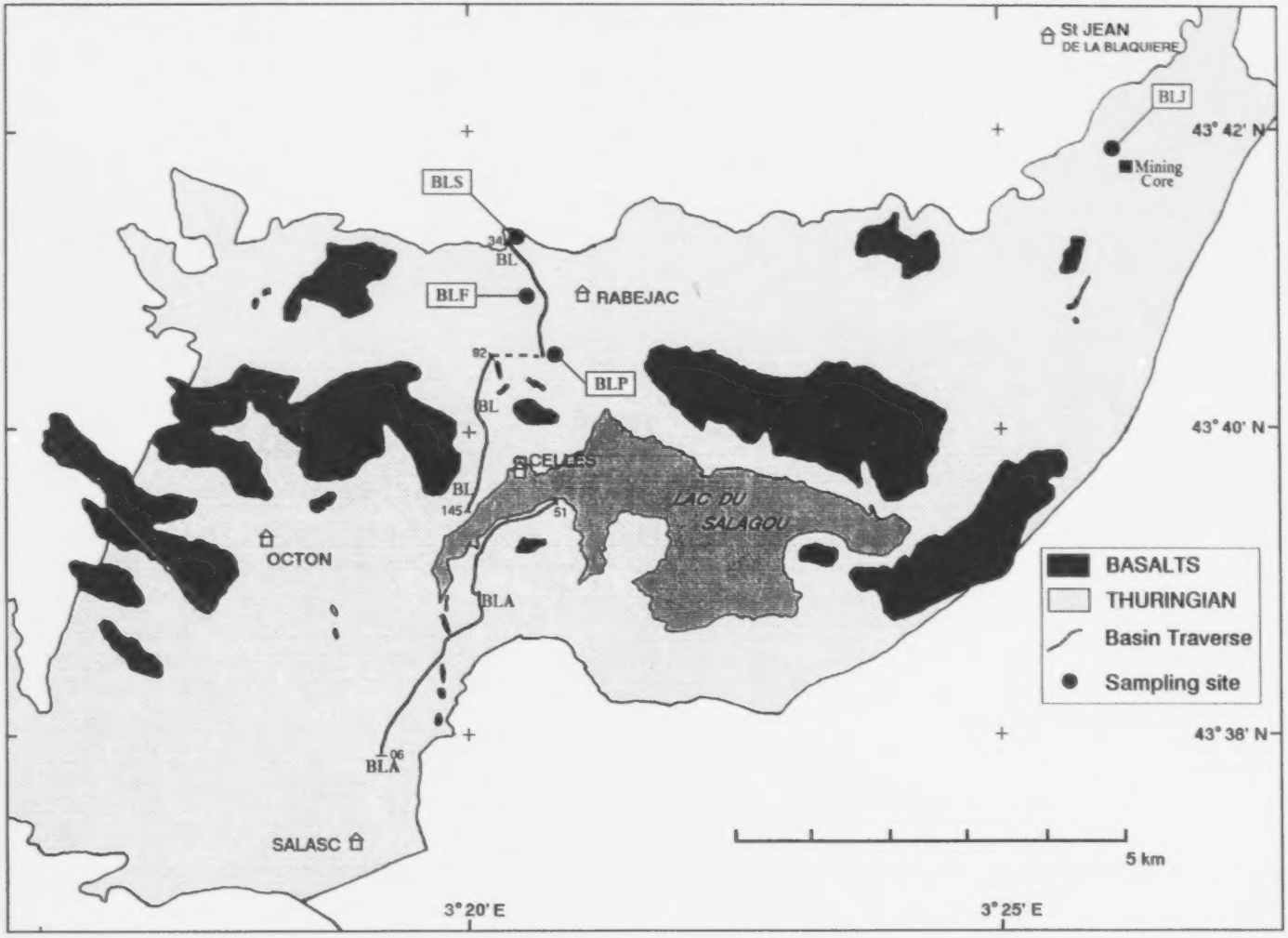
St JEAN
DE LA BLAQUIERE
BLJ
43° 42' N
Mining
Core
BLS
34
BL
BLF
RABEJAC
92
BLP
BL
43° 40' N
CELLES
BL
145
51
LAC DU
SALAGOU
OCTON
BLA
BLA
06
SALASC
43° 38' N
BASALTS
THURINGIAN
Basin Traverse
Sampling site
5 km
3° 20' E
3° 25' E

Ideally the sampling interval should have been kept as small as possible to obtain the finest possible resolution in the resulting paleomagnetic record. However, the collection of suitable samples was complicated by the lithological nature of the rocks and it soon became evident that the task at hand would be more difficult than initially thought. The sandstones and siltstones could be easily drilled using a portable gasoline drill, but these hard beds are abundant only in the lower 300 m of the profile; in the rest of the sequence they are either scarce and too thin, or most often totally absent. In addition, the need to collect samples along a well defined traverse, at relatively regular intervals, allowed little freedom in the selection of the best outcrop for sampling. Large lateral displacements of the sampling line had also to be avoided because good stratigraphic markers are very rare. All this made it necessary to sample the mudstone, which proved terribly difficult to drill. When it is fresh, this material is very hard, but tiny cracks make it very brittle when it outcrops. In order to drill the mudstone it was thus necessary to clear a crack-free surface which required digging a cavity typically 80 x 80 x 50 cm, occasionally deeper. Sometimes it was necessary to repeat this operation two or three times, and even so, the surface appropriate for drilling was seldom larger than the bare minimum to cut a 1 inch core. In addition,

more than one sample had to be obtained at each location to achieve a better reliability of the measurements. Another difficulty was that several very careful drilling attempts had to be done, which consumed a lot of water, a very scarce resource in the Lodève Basin during summer months. Replenishing the reserves often required several kilometres of driving to the Lac du Salagou. The consequence of these difficulties was that the whole process was simply too time consuming and that persisting with this technique would make it impossible to accomplish more than half of what was originally intended.

As a result it was decided to abandon drilling and to use a completely different technique. White plastic squares, 2x2 cm in size, were bonded in situ on rock fragments that could be later removed. Orientation was achieved by means of solar bearings and clinometer readings. The advantage of this technique is that it permits one to collect small, irregularly-shaped, samples typically a few cubic centimetres in size. It was only necessary to remove the first few centimetres of most altered rock and several suitable samples could be extracted at each site. For the rest of this thesis and for simplicity, these samples will be referred to as "plastic top". Despite the use of this faster method, three months of intensive field work were needed to obtain the collection corresponding to the basin traverse.

The sampling interval could be kept as small as 1 metre in the lower, coarser 200m of the sequence, but in the rest the basic interval chosen was 10 metres. In reality, the difficulties described previously caused this interval to vary between 5 and 20 metres. Where possible, i.e. along road cuts or other steep outcrops, stratigraphic distances were measured directly using a tape. Elsewhere, especially in the rather flat central part of the basin it was calculated by simple surveying. Although relatively inaccurate this method leads to an estimated error of about 50cm.

The result of the first field season was a total collection of 241 samples, consisting of 107 cores and 134 "plastic tops". They had been taken along a 7 km traverse corresponding to 1250m of stratigraphic column, with a sampling interval ranging from 1 to 20 metres (Fig. 2.7).

2.4.2 Small scale, detailed sampling

Following the first results obtained from the basin traverse, it became evident that more information concerning the small scale (a few cm) behaviour of the magnetization was needed. Lateral variations of the magnetization and their possible correlations were also of interest. A second shorter field season was therefore planned so as to obtain suitable data.

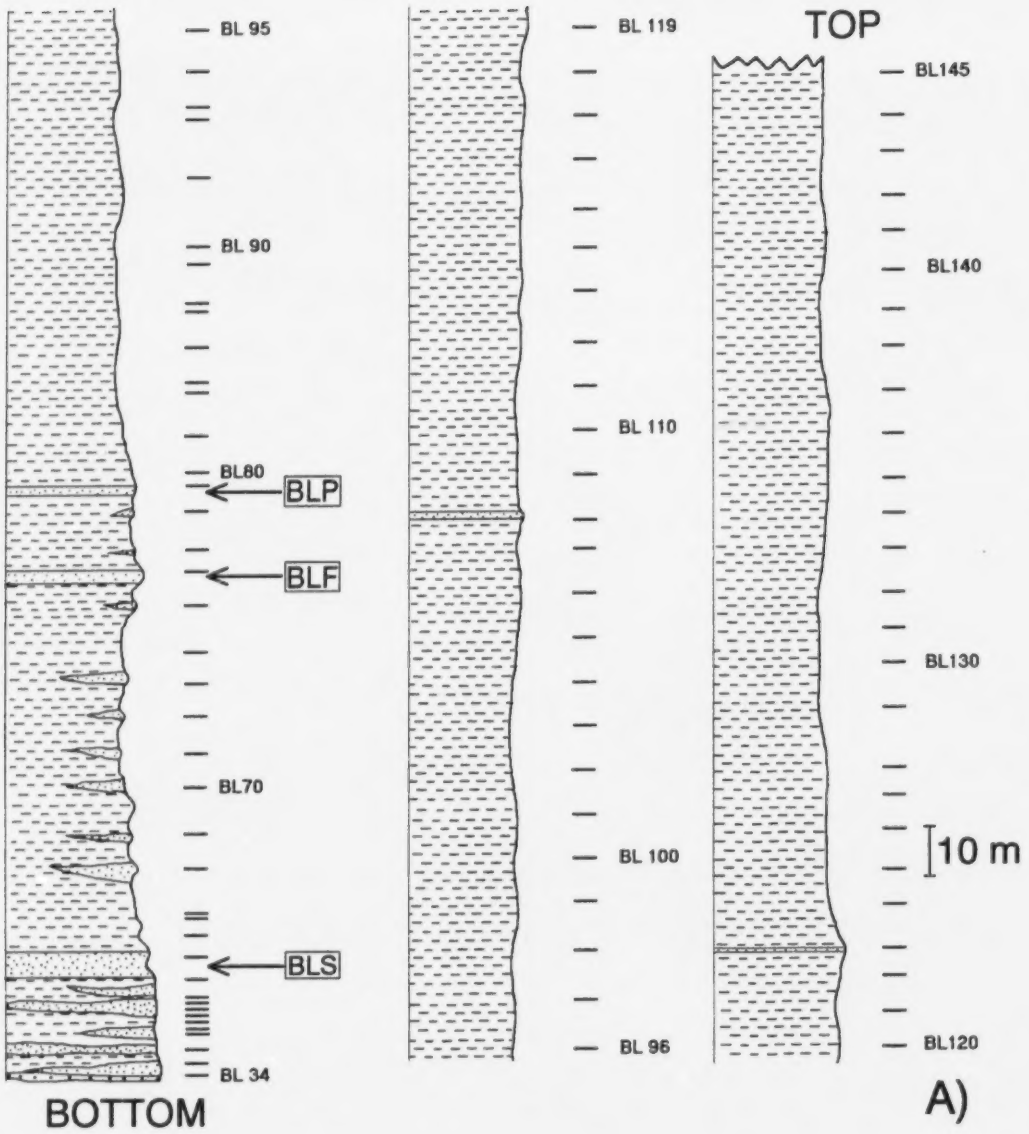

Figure 2.7. Stratigraphic logs of the basin traverse (continued next page). A) line BL; B) line BLA (see Fig. 2.6 for location). Each horizontal mark corresponds to a site where 2 to 5 samples were collected. Stratigraphic position of the small scale sampling sites are also indicated.

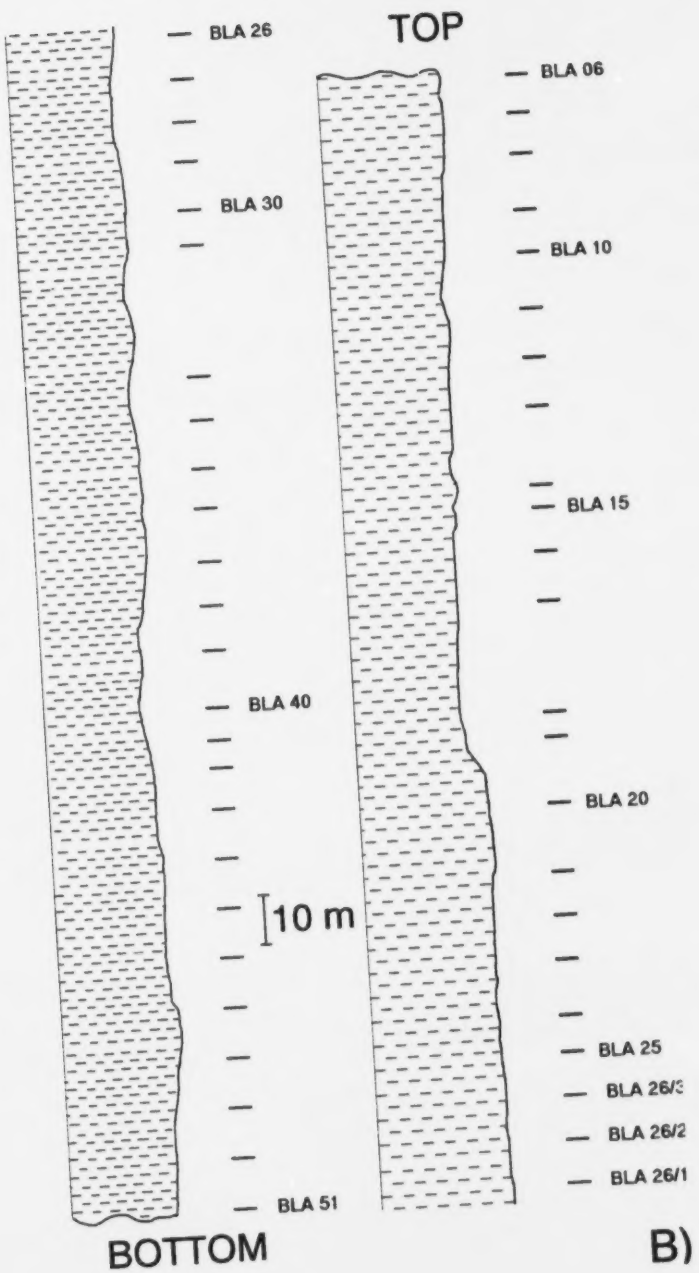
TOP
BLA 26
BLA 30
BLA 40
BLA 51
10 m
BLA 06
BLA 10
BLA 15
BLA 20
BLA 25
BLA 26/3
BLA 26/2
BLA 26/1
BOTTOM
B)

The experience of the previous year had shown that any detailed sampling of the mudstone was out of the question, so four sandstone and siltstone horizons were selected. Locations are shown in Fig 2.6. In order to obtain series of samples as continuous as possible it was decided to drill cores perpendicular to the bedding using the maximum length of the drill bits (approximately 25 cm). This method allowed the recovery of continuous cores that could be subsampled later with any degree of definition that one could require. In one case, site BLF , a 2 m horizon could be sampled continuously by drilling several cores and removing the corresponding slabs (see Fig 2.8). At all locations except BLS several laterally equivalent sections were obtained so as to allow lateral variations of magnetization to be investigated. Each core was individually marked and oriented using solar bearings.

After beginning to obtain interesting results from these closely spaced samples, we found it necessary to obtain at least minimum data from the mudstone. As explained before, this material could not be drilled in such a way as to provide long continuous records. However, we had the opportunity to use two segments (50 cm long) from the long mining core provided by the COGEMA, which was used in our previous study (Evans and Maillol, 1986).

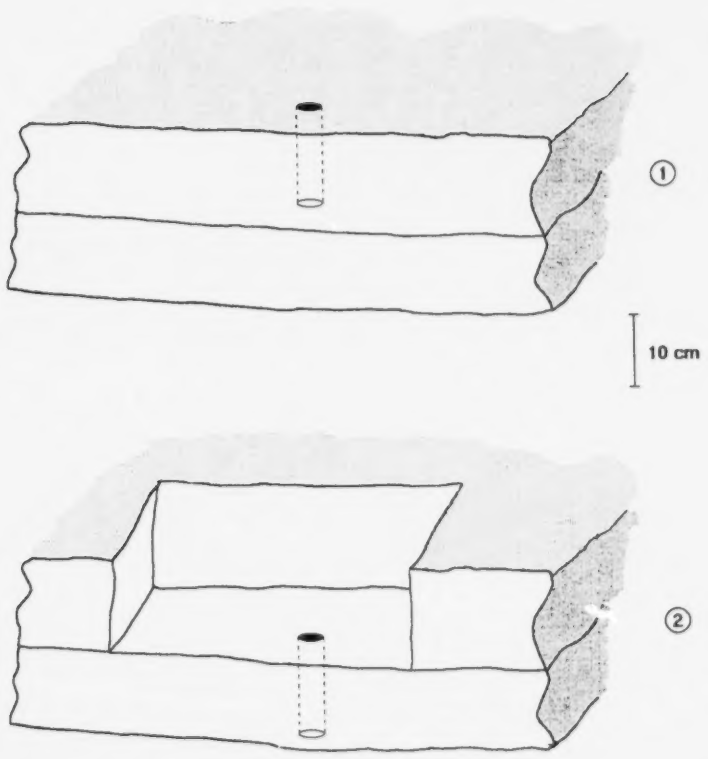

Figure 2.8. Schematic of the method used to sample continuously a 2m section using 25 cm cores. A first core is drilled (1); the corresponding slab is then removed, and a second core can be drilled below the first one (2). Each core is oriented independently.

2.5 Sample preparation

2.5.1 Basin Traverse samples

As described in the previous section, samples collected along the Basin Traverse came in two forms; 25 mm cores drilled in the field, and irregularly shaped specimens bearing a glued plastic square carrying the orientation. The former had only to be cut into 25 mm long cylinders to allow direct measurement in a Molspin spinner magnetometer, but the latter ("plastic tops") again gave rise to several problems. The initial idea was to set the samples in plaster of Paris and to drill the resulting block, but even in the much better conditions in the laboratory where very smooth drilling can be performed, most of the mudstone fragments broke in small pieces and were unusable. After several trials the only possible alternative was to measure the samples whole. This could be done by using a wide mouth magnetometer sensor, designed for archeomagnetic purposes and allowing samples up to 6 cm in diameter to be measured; this was large enough for most of the "plastic tops". However, because they were irregularly shaped, these samples had still to be included in a material which could be formed into a suitable geometrical shape and which could also reproduce the original orientation. Plaster could not be used because of the anticipated need to heat the specimens up

to 500° C and beyond. One had therefore to resort to a novel procedure.

The lower half of each specimen was dipped in melted wax and allowed to set in a cylindrical mold. After solidification of the wax the specimen could be removed from its base and the faithful print of its shape would allow it to be put back in place on its base as many times as needed (Fig. 2.9). The orientation could be reproduced on the wax base and the plastic top removed to avoid melting during heating. A cubical sample holder was made to fit the magnetometer head and to accept the cylindrical base and its sample.

2.5.2 Closely spaced samples

This collection consisted of cores 25 mm in diameter and about 25 cm long on average. We wanted to subsample these cores with intervals as small as possible and this was achieved by cutting them into disks. To avoid loss of too much material, an ultra-thin diamond saw (thickness=0.012") was used. In order to remain measurable, and also to retain their orientation, samples could not be cut too thin, but a good compromise was found with disks 5 to 7 mm thick. During this subsampling care was always taken to avoid cutting disks straddling any conspicuous sedimentary boundary, and natural breaks of

the cores were respected. These precautions were adopted in order to maximize the homogeneity of each specimen.

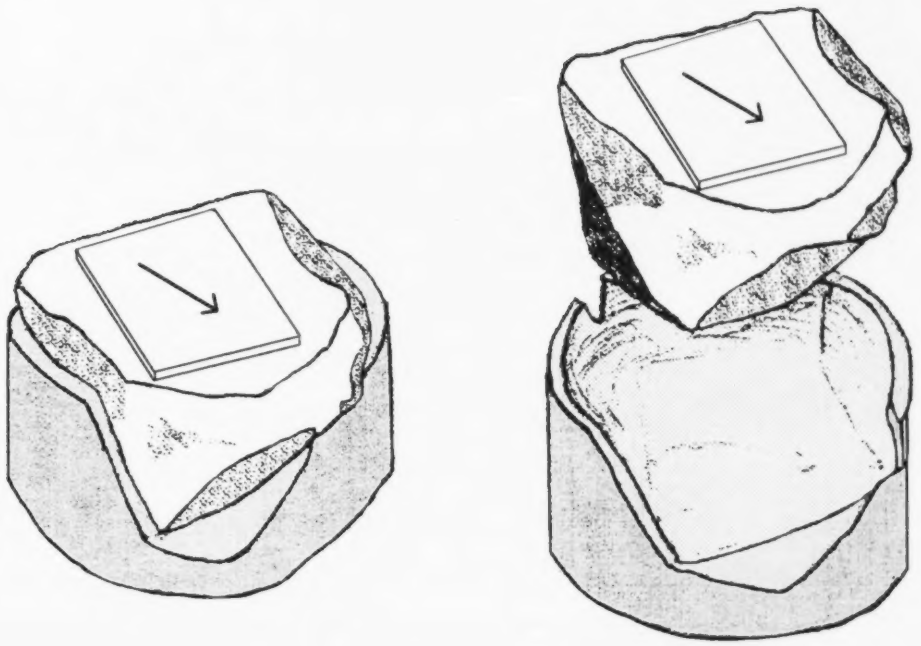

Figure 2.9. Illustration of the wax base method for preparing and measuring "plastic top" samples.

CHAPTER 3

ORIGIN OF THE MAGNETIZATION IN LODEVE REDBEDS

3.1 Introduction

Despite several decades of effort, the origin of redbed magnetization is still open to question and is much debated. In most cases the remanence can be shown to be carried by hematite but whether it is acquired at an early stage of the rock history or much later, through diagenetic processes, is always a central problem in every study dealing with redbeds.

Examples of depositional remanent magnetization (DRM) in redbeds have been documented in which hematite is believed to carry a reliable recording of the geomagnetic field (Elston and Purucker, 1979; Steiner, 1983; Van den Ende, 1977). In other cases the magnetization appears to be of chemical origin (CRM) and to have been acquired over several million years (Larson et al., 1982). It is also possible to find both types of magnetization co-existing in the same rocks, carried by different mineral phases (Tauxe et al., 1980; Tauxe et al., 1990). There is thus no easy answer to the origin of magnetization in redbeds, simply because many different types of rocks can be called

redbeds by reason of their common color (Turner, 1980). As a result one should always carry out a careful analysis of the magnetization characteristics in each study dealing with such rocks.

The initial goal of this entire project was to investigate the possibility of extracting paleosecular variation data from the Lodève strata, and the results obtained will be presented in Chapter 4. The eventual need to assess the reliability of such results, and to investigate the "resolution" of the material, motivated a study of the fine scale variations of magnetization. This led to the discovery of large magnetization intensity variations exhibiting strong lithostratigraphic control. Although the results presented in this chapter were acquired in the later stage of the study, it seems more appropriate to discuss them first since they are essential in assessing the significance of the directional data. This chapter will therefore deal exclusively with the interpretation of intensity variations and their bearing on the origin of the magnetization.

3.2 Samples used for the intensity investigation

As explained in the previous section, the initial goal of the close interval sampling was to study the fine scale variations of remanence directions. It was only after the

discovery of the intensity variations that it appeared that these samples could effectively be used to investigate the rock magnetic properties. Consequently, all the results presented in this chapter were obtained as described in section 2.4.2. Table 3.1 gives more details about the sample collection as well as relevant paleomagnetic information. The geographic and stratigraphic locations of the sites are indicated in Figs. 2.6 and 2.7. A complete listing of the specimens actually used for the experiments described in this chapter can be found in Appendix 1.a.

Most of the samples used in this part of the study are representative of the sandstone and siltstone members of the sequence. Only the samples obtained from the mining core (Evans and Maillol, 1986) are mudstone (see section 2.4.2). However, because of the high level of similarity found in the magnetic properties of the different lithologies, it seems reasonable to extend the conclusions about the magnetization origin to the whole stratigraphic profile. It was deemed preferable not to use any of the samples from the Basin Traverse because by the time the small scale investigation was started, they had already all been heated with possible risk of alteration of the magnetic properties. In addition, most experiments required cutting the samples into definite shapes to fit

Code Name	Description	Thickness of sampled section (cm) (number of sampled sections)	N	Dec/Inc/α_{95}
BLF	2 fine sandstone (50 and 70 cm) units bracketing 1 siltstone (80 cm) unit	190 (1) and 70 (1)	353	198.1/ -8.6 /1.0
BLJ	60cm thick red sandstone bed with abundant cross-laminations	22 (3)	90	198.6/-13.3 /0.9
BLP	50 cm thick red siltstone unit consisting of several beds separated by dessication surfaces	22 (3)	81	195.6/-6.9 /1.1
BLS	1 m thick massive red sandstone bed	46 (1)	11	199.5/-12.3/2.4
BLM1	red mudstone segment from mining core (unoriented)	45 (1)	30	
BLM3	same as BLM1	38 (1)	40	

Table 3.1. Summary of lithological, sampling, and paleodirectional data.

N: number of disks investigated. Dec, Inc, α_{95}: mean declination, mean inclination and half angle of 95% confidence cone. These should be compared with corresponding published results of 198.5, -6.5 (Kruseman, 1962), 203.5, -11.3 (Evans & Maillol, 1986), and 199.4, -11.8 (Merabet & Guillaume, 1988)

the instruments such as the electro-magnet used for Isothermal Remanent Magnetization (IRM) experiments; this could not have been done with the brittle outcrop mudstones.

3.3 Results and analysis

3.3.1 Remanent Magnetization Intensity Variations

Previous studies (Kruseman, 1962; Evans and Maillol, 1986; Merabet and Guillaume, 1988), and additional stepwise thermal demagnetizations carried out in the present work, show that the red rocks of the Lodève Basin carry two components of magnetization. A modern overprint is removed between 400°C and 500°C, leaving a characteristic magnetization in the direction of the Permian field. These directional properties will be fully discussed in Chapter 4.

The most immediate observation is that substantial variations in the intensity of magnetization can take place over stratigraphic distances of only a few centimetres. Figure 3.1 is an intensity magnetogram obtained from the 265 discs cut from the 190 cm of the sequence labelled BLF2, which consists of fine sandstone and siltstone. Large, rapid, fluctuations occur, which are remarkably similar before and after thermal treatment. Sharp peaks are observed in which the intensity may vary

by an order of magnitude over a few centimetres (e.g. factors of 36.5 between 498 and 528 mm, 24.4 between 1089 and 1121 mm, and 7.0 between 1326 and 1346 mm). These intensity highs often exhibit asymmetric shapes with a gradual build-up terminated by an abrupt decrease at the top (Fig 3.2). Moreover, these abrupt decreases systematically coincide with bed boundaries or sedimentation discontinuities. Figure 3.3 shows data from three siltstone cores taken from a single stratigraphic horizon with inter-core distances of 40 and 50cm. Intensity variations are again noticeable and correlate well between cores. Similar intensity patterns (Fig. 3.4) are found at all the locations that were investigated, in sandstones as well as in siltstones, and also for the mudstone segments from the deep mining core. Figure 3.5 shows two magnetograms from the same section, separated by a horizontal distance of 30 m. One (labelled BLF2) is a portion of the data presented in Fig.3.2, between 1100 and 1800 mm. The new section (labelled BLF1) also displays marked intensity variations, but despite certain similarities, correlations between both magnetograms are not obvious.

All intensity values are mass normalized; the magnetic moments range from 10 to 200×10^{-9} Am^2. The noise level of the instrument is always less than $0.4 \times 10^{-9} Am^2$.

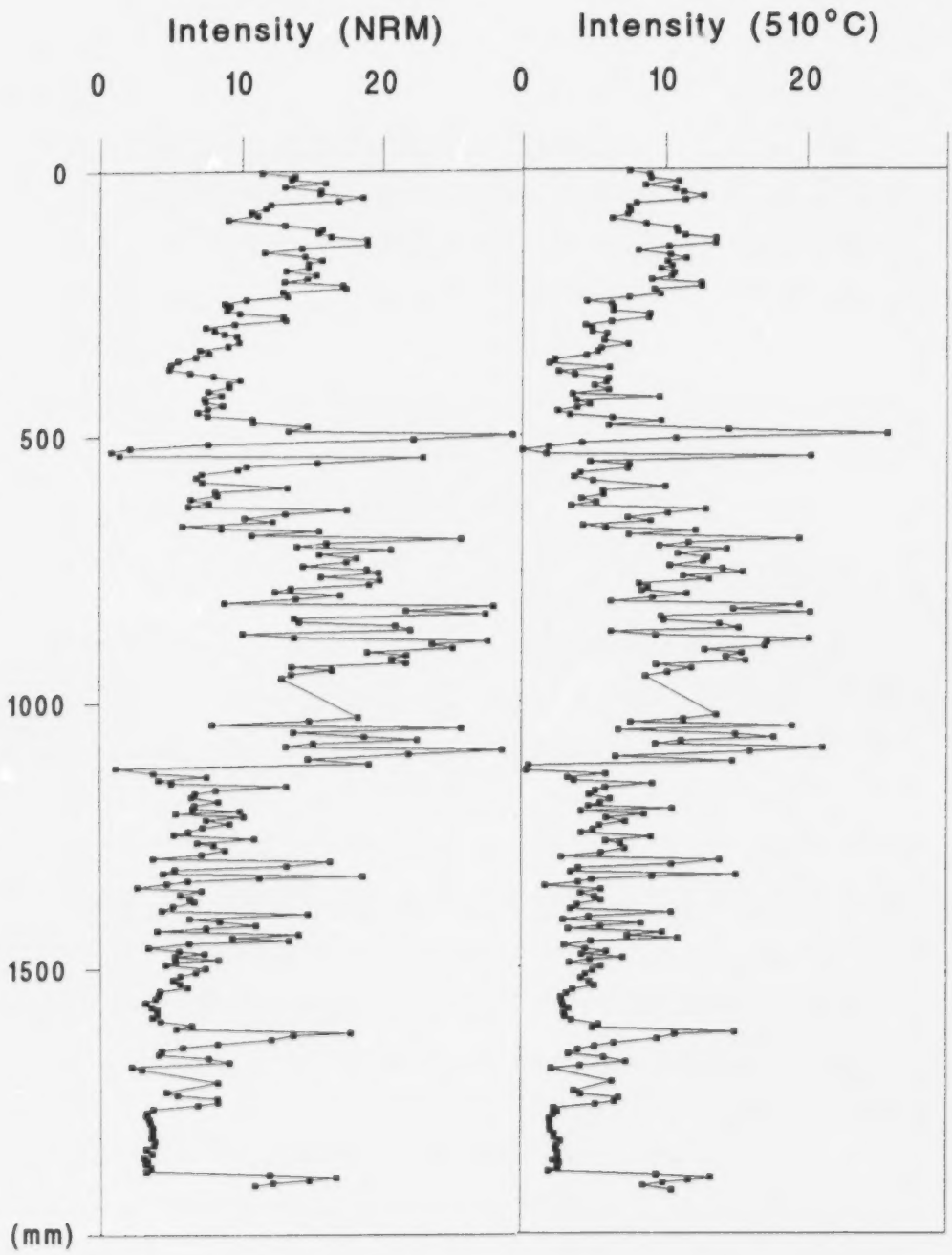

Figure 3.1. Intensity data from a 190 cm siltstone/sandstone section (site BLF) before and after thermal demagnetization at 510°C. Depths are given in mm, intensity of magnetization in 10^{-6} Am^2/kg.

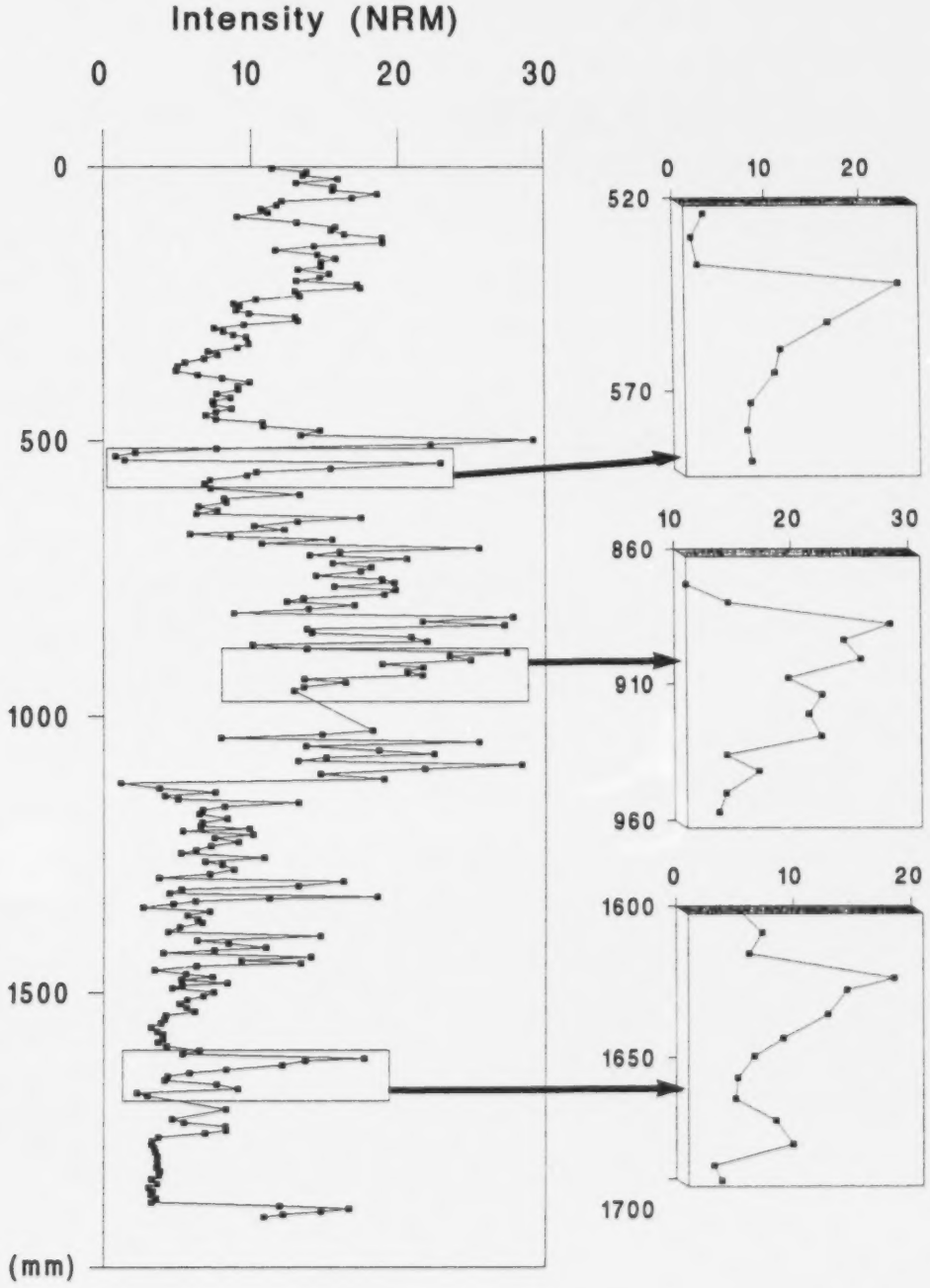

Figure 3.2. Same NRM data as in Fig.3.1 with enlargements of three particular intensity peaks.

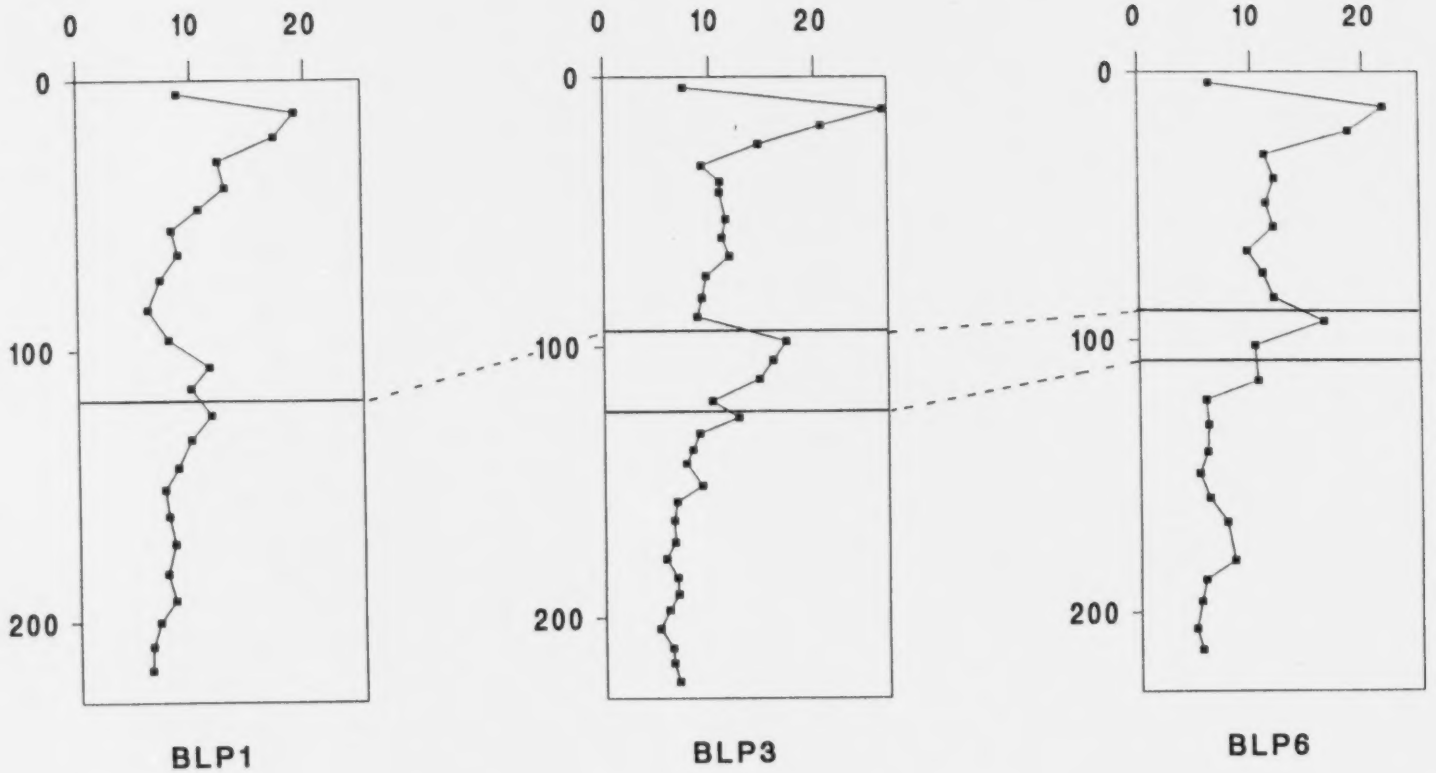

Figure 3.3. Intensity data from 3 siltstone cores taken at the same stratigraphic horizon (site BLP). Horizontal lines indicate observable sedimentary boundaries marked by desiccation surfaces. Inter-core distances are 40 cm and 50 cm. Units as in Fig. 3.1.

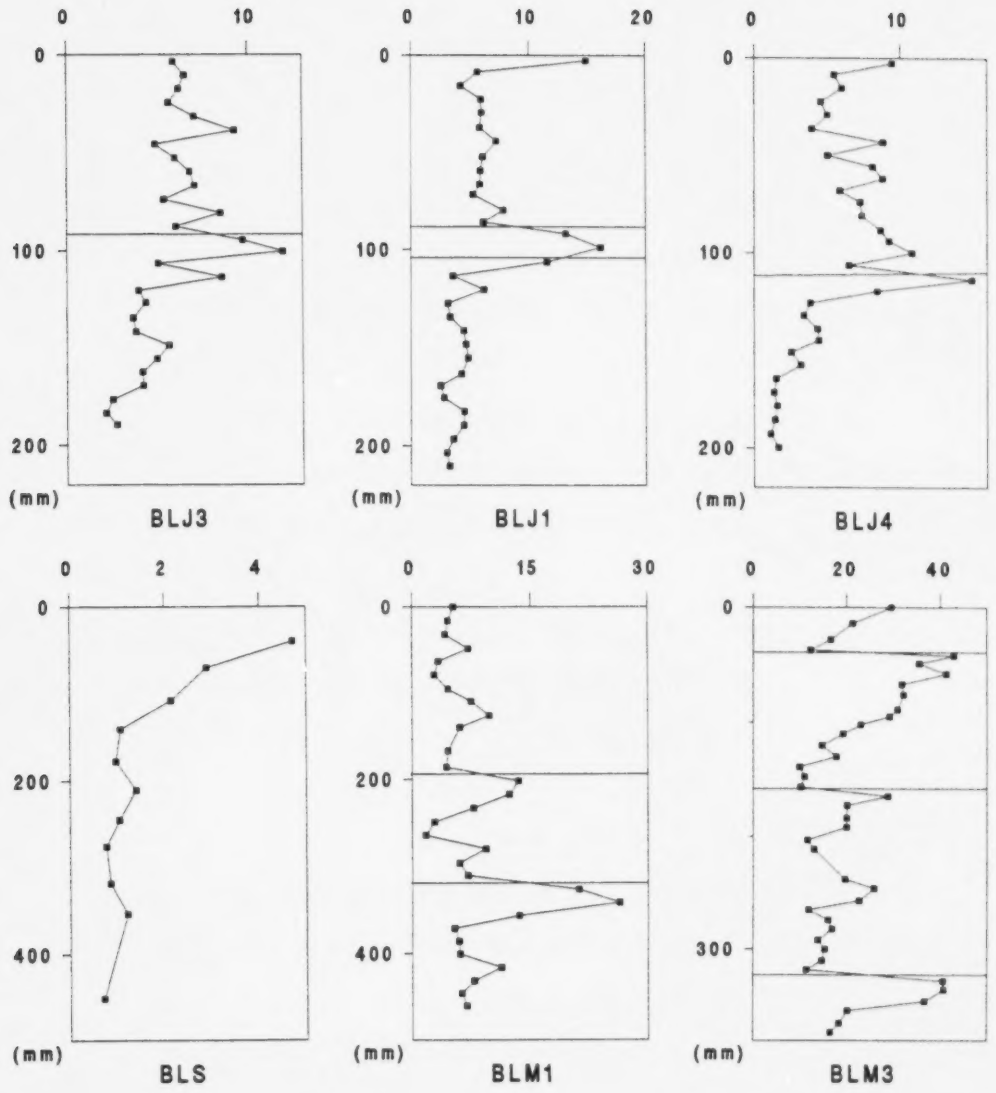

Figure 3.4. Other examples of intensity variations from different sandstone (BLJ1,3,4 and BLS) and mudstone (BLM1,3) horizons. BLJ1, 3 and 4 have inter-core distances of 30 cm. Horizontal lines indicate observable sedimentary boundaries (desiccation surfaces, changes in cross-lamination patterns). Units as in Fig. 3.1.

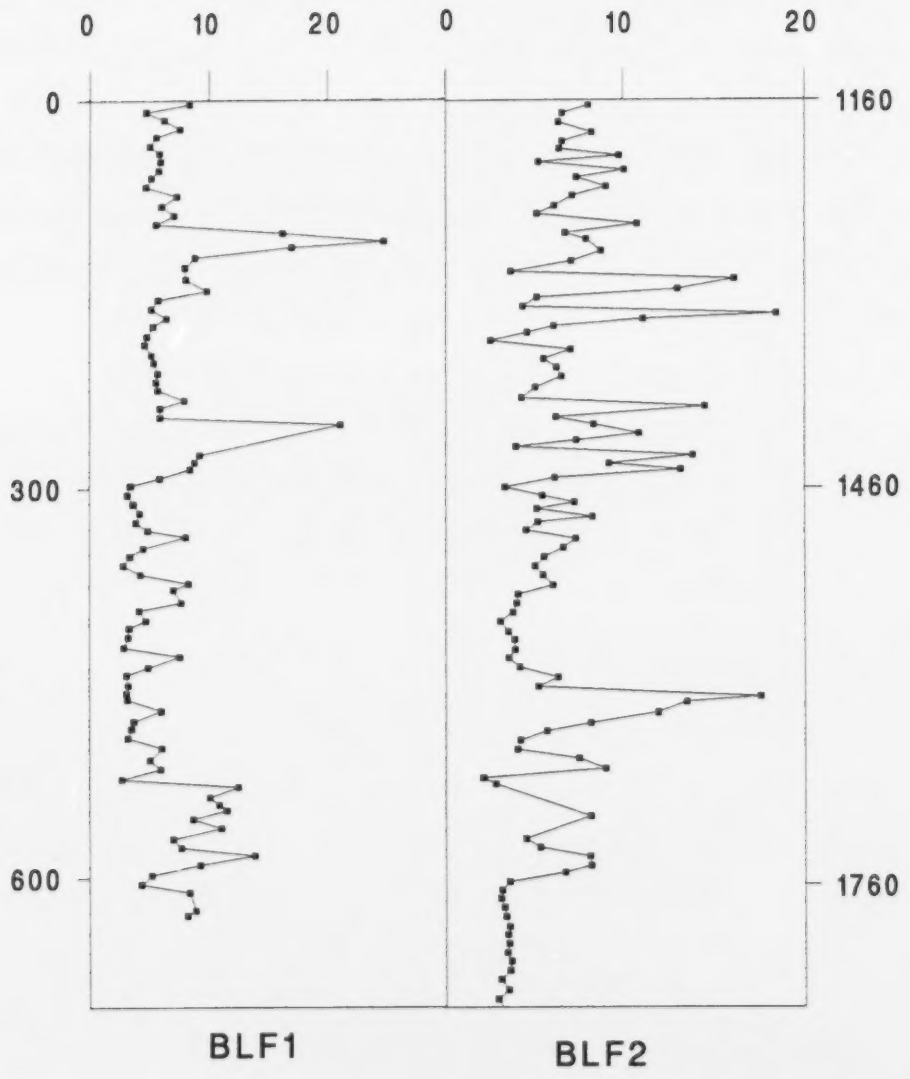

Figure 3.5. Two stratigraphically equivalent intensity magnetograms from site BLF, separated by 30 meters. Units as in Fig. 3.1.

The intensity variations described above are a ubiquitous feature of the red rocks of the Lodève Basin and it is felt that they might well shed some light on the process of acquisition of the magnetization. Several processes can cause magnetization intensity variations; among them are fluctuations of the geomagnetic field, interplay of antipodal components, and changes in the amount, type, and properties of the magnetic mineral present. In an attempt to identify which mechanism is responsible, a rock magnetic study was undertaken using a variety of techniques, to see if any systematic differences between "high" and "low" intensity samples could be found. "High" refers to those specimens responsible for the intensity peaks (intensities >13 $x10^{-6}$ Am^2/kg) and corresponding to the top 2 cm of a sedimentary unit. "Low" refers to those samples cut in the bottom 2-3 cm of the same units (intensities <7 $x10^{-6}$ Am^2/kg).

3.3.2 Thermal and Alternating Field (AF) demagnetization

Thermal decay curves show the removal of a small component with blocking temperature below 500° C followed by a decrease of the remanence to a final sharp drop at 670°C (Fig.3.6). This behaviour points to hematite as the main remanence carrier. The change in slope between 500°C and 600°C might possibly be due to the presence of

magnetite but none of the other experiments confirm the presence of a significant amount of this mineral.

The maximum field available for AF demagnetization is 0.18T, which is too low to achieve a complete demagnetization of hematite bearing rocks. Still, even incomplete results are interesting for they show that between 37 and 55% of the NRM is destroyed at 0.18T (Fig.3.7). This suggests that a good deal of the NRM is carried by relatively low coercivity grains. Unlike thermal treatment, AF demagnetization proves ineffective in removing the recent overprint, which thus appears to have a coercivity comparable to or higher than the characteristic remanence. In both thermal and AF demagnetizations no systematic differences can be observed between specimens with high and low NRM intensity.

3.3.3 Susceptibility and Isothermal Remanent Magnetization (IRM)

If remanence intensity variations were due to changes in the total amount of magnetic grains, one would expect to find a correlation between intensity and susceptibility. This is not so in our case as is shown in figure 3.8 that presents data corresponding to figure 3.1. Susceptibility variations exist but show no correlation with NRM intensity values. However, it must be born in mind that susceptibility by itself is not necessarily a

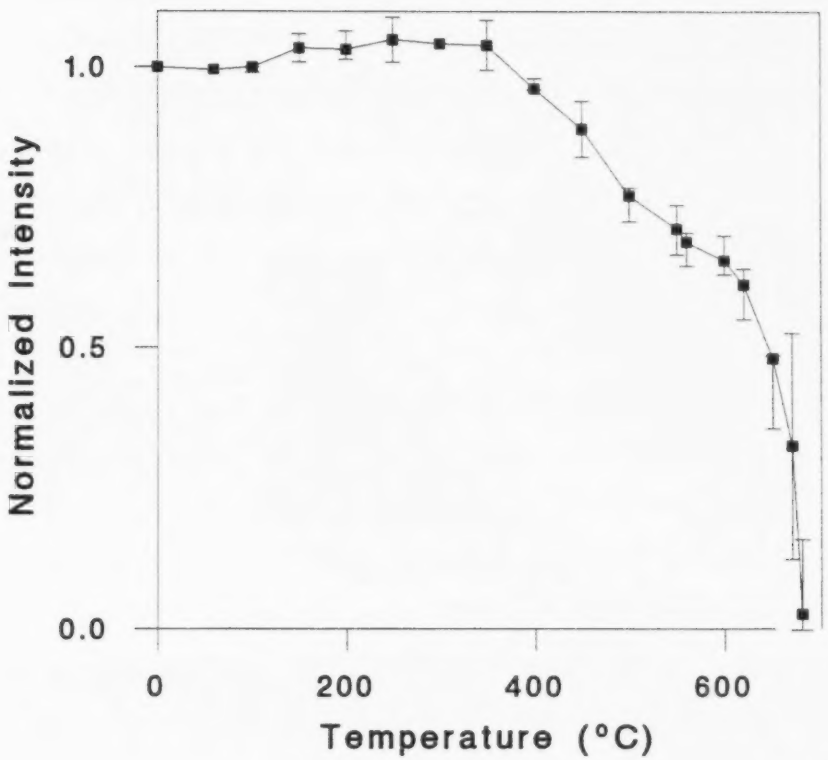

Figure 3.6. Normalized intensity decay curves after progressive thermal demagnetization. Squares represent means at each temperature step, and bars give the ranges. NRM intensities in 10^{-6} Am^2/kg are, for siltstones: 5.1, 5.3, 7.1, 13.0, 18.9, 26.5; for sandstones: 1.1, 2.8, 14.9, 16.1.

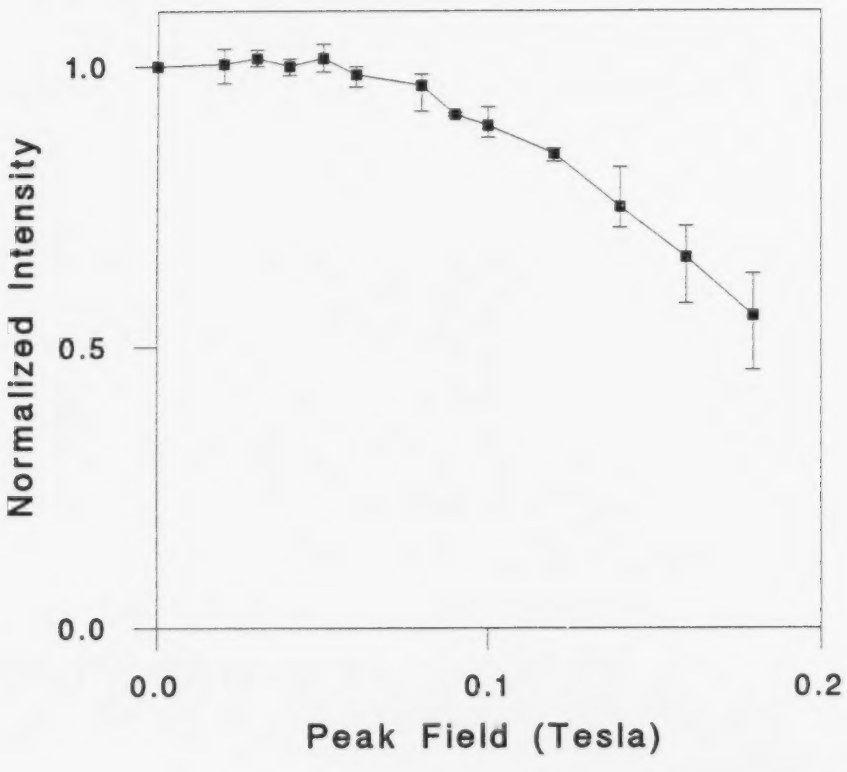

Figure 3.7. Normalized intensity decay curves after progressive AF demagnetization. NRM intensities in 10^{-6} Am^2/kg are, for siltstones: 5.6, 13.5, 14.5, 18.5; for sandstones: 6.4, 16.5.

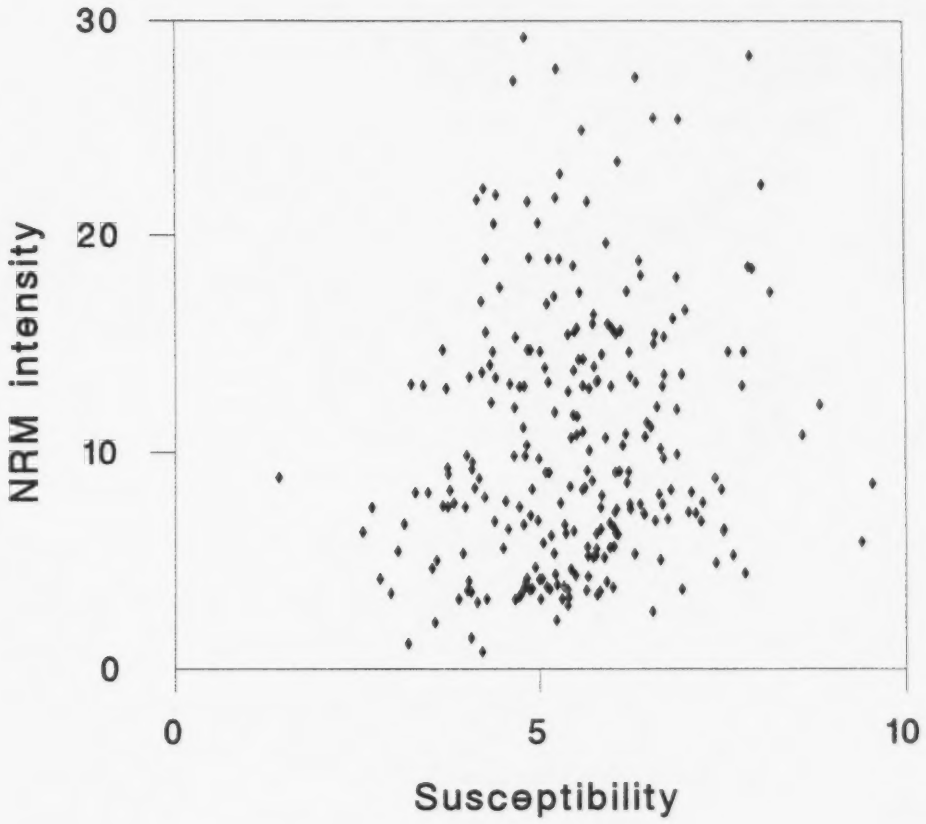

Figure 3.8. NRM intensity versus susceptibility for the specimens of Fig.3.1. NRM units as in Fig.3.1. Susceptibility is given in 10^{-8} m^3kg^{-1}.

good test for this purpose since it may be partly controlled by minerals (ferromagnetic, diamagnetic or paramagnetic) playing little or no role at all in the remanence.

A parameter directly related to remanence is more appropriate, and specimens with low and high NRM were therefore subjected to IRM acquisition experiments. The maximum field available, 1.75 T, is not quite sufficient to achieve a complete saturation in our rocks, but the shape of the acquisition curves indicates that this was approached. One example consisting of six stratigraphically consecutive samples provides no evidence for a relationship between the intensity of maximum IRM and NRM, although a good correlation is found between maximum IRM and susceptibility (Fig.3.9). The consequence is that there is little doubt that NRM intensity variations are not due to fluctuations of the total amount of magnetic material.

Five examples of IRM acquisition/destruction curves are given in Fig.3.10. The observed behaviour is typical for redbeds (see e.g. Dunlop, 1972), with a generally lower coercivity for the coarser-grained samples. There is no evidence of two distinct magnetic phases in the siltstone, but the sandstone backfield curves exhibit a more rapid initial decrease indicative of a softer component. On the other hand, however, AF demagnetization

of NRM shows very little decrease below 0.1 T, so this component does not appear to be a significant factor in the NRM.

High and low NRM specimens do not exhibit any systematic difference in behaviour and it is felt that variations of an order of magnitude in NRM intensity, if they were due to corresponding variations of grain size, should show up in IRM curves. A particularly good example is given in Fig. 3.11 where two siltstone specimens with NRM ratio of 7.7 display almost perfectly identical behaviour.

Thermal demagnetization of the IRM's was also carried out using the method described by Lowrie (1990), in which a specimen is given an IRM at three different field values along three orthogonal axes and is then subjected to incremental heating. The evolution of the three components of magnetization gives information on fractions corresponding to three different parts of the coercivity spectrum. In the three siltstone specimens investigated here, the low coercivity fraction (< 0.12T) seems to decay more quickly than the others during the first 100°C but thereafter the three components follow a similar path with a sharp drop when 670° C is approached (Fig. 3.12). This simple behaviour confirms that the only mineral playing a significant role in the magnetization is hematite and that no large heterogeneity can be expected in the

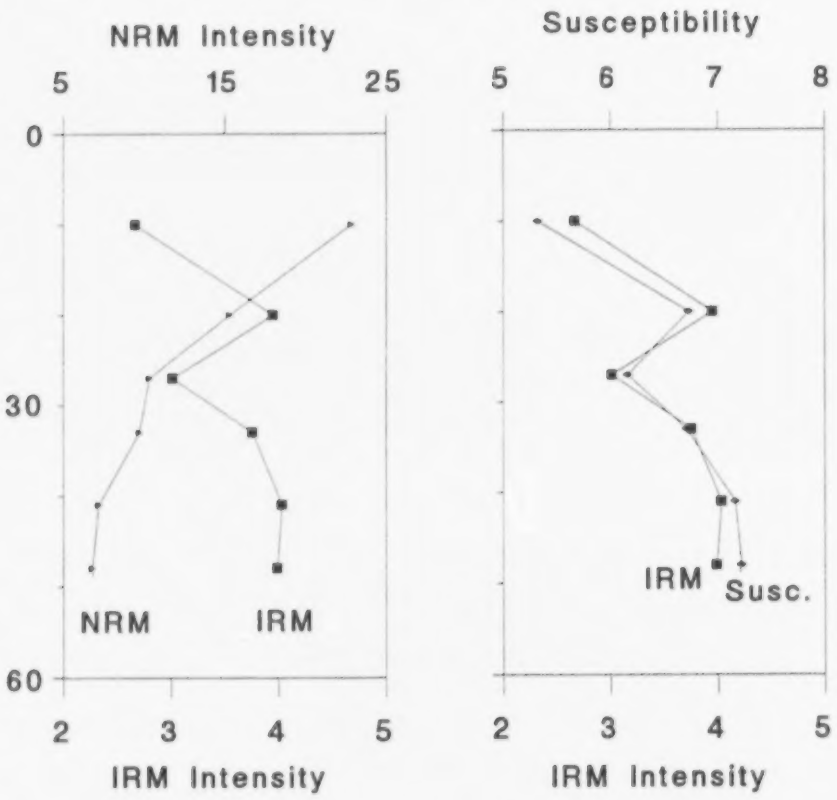

Figure 3.9. IRM intensity (1.75 T) compared to NRM intensity (left) and to susceptibility (right) for 6 stratigraphically consecutive siltstone samples. NRM units as in Fig.3.1; IRM intensities are in 10^{-3} Am^2/kg; susceptibility is given in 10^{-8} m^3kg^{-1}. Depths in mm.

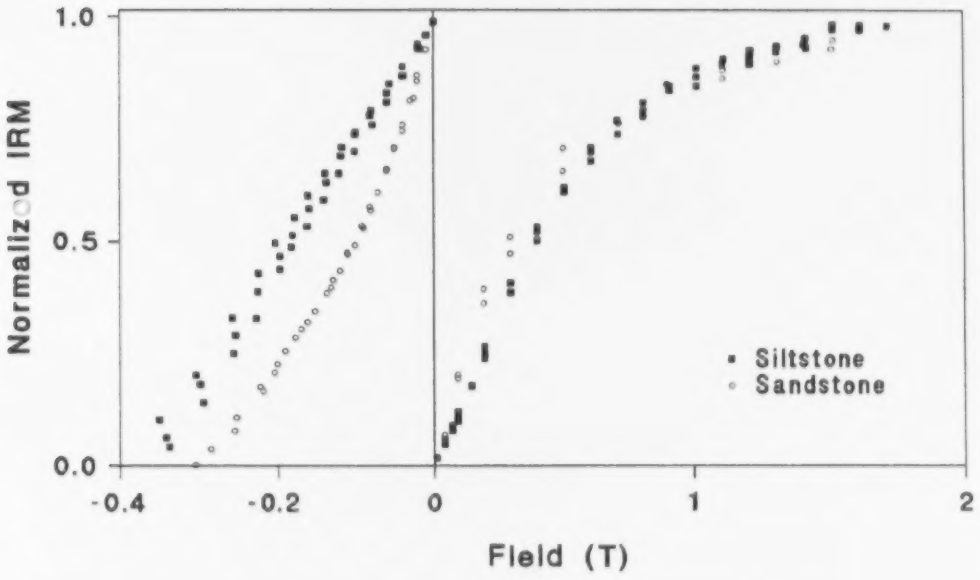

Figure 3.10. Normalized IRM acquisition/destruction curves. Corresponding NRM intensities in 10^{-6} Am^2/kg are, for siltstones: 4.3, 15.1, 18.6; for sandstones: 4.8, 17.4.

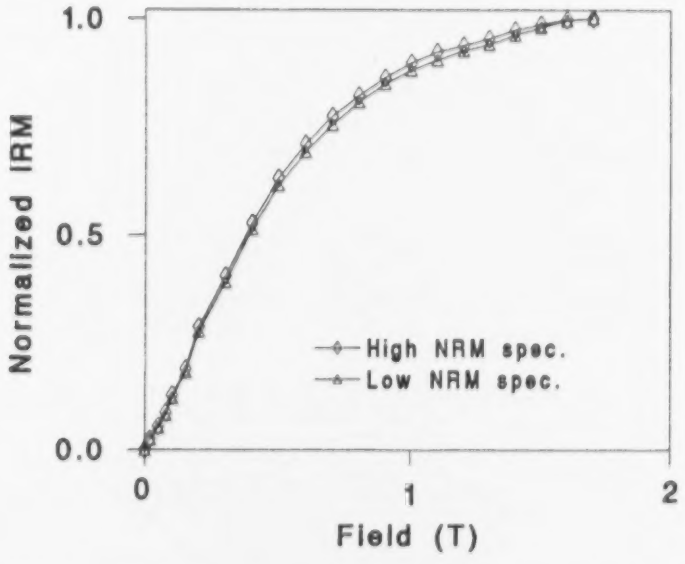

Figure 3.11. Normalized IRM acquisition curves of two siltstone specimens with NRM intensity ratio of 7.7 (i.e. 2.4 and 18.3x10^{-6} Am^2/kg).

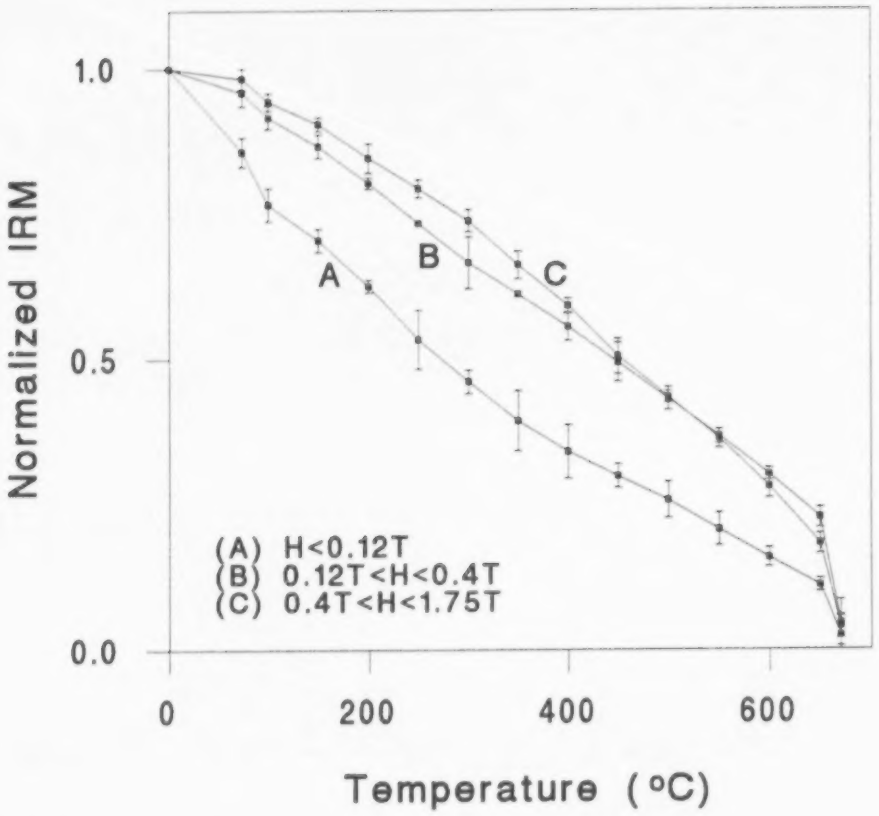

Figure 3.12. Thermal demagnetization of IRM for three distinct coercivity fractions. Each point corresponds to the average of the intensity values of 3 different siltstone samples, with the range represented by the bars. Corresponding NRM intensities range from 4.4 to 18.3x10^{-6} Am^2/kg.

magnetic carrier population. As in all preceding experiments no difference can be found between high and low NRM specimens.

3.4 Petrographic Analysis

Thorough petrographical observations on the Lodève Basin sequence have been reported by Laversanne (1976) and Odin (1986) , but they did not concentrate on the opaque mineralogy. Ten thin sections of representative lithologies were examined, both in transmitted and reflected light. In doing so we always had in mind the need to try to differentiate between high and low NRM samples and thin sections were obtained from both categories.

The main constituents are quartz and feldspar embedded in a clayey matrix more abundant in the finer grained members of the sequence. Diagenetic overgrowth of these two minerals is very common. The cement is mainly siliceous but sometimes carbonaceous. Red hematite pigment is found associated with the clay matrix that is thought to be detrital and is thus less abundant in the sandstone. The pigment is also observed coating quartz and feldspar grains and it can often be found between grain contacts, which indicates that it was formed before full compaction. Another occasional observation is the covering of the

pigment by a subsequent overgrowth of the host mineral, which again suggests an early formation of the coating. No crystalline structure can be observed optically in the pigment. These observations suggest that the pigmentary hematite was formed at a very early stage of the rock history and was possibly even deposited with the rest of the detrital fraction.

Larger hematite grains (specularite) can be readily observed in all members of the sequence. In the siltstone they take the form of tiny crystals, typically 1 to 5 μm in size, dispersed in the matrix (Fig.3.13, 3.14). They are either red or black with an apparent randomness in their relative proportion. Red and black grains can be observed in close proximity to one another, suggesting that the alteration indicated by the red colour did not take place in situ. Similar observations are reported by Elston and Purucker (1979) for the Moenkopi Formation of Arizona. A few much larger grains (20 - 50 μm) can also be found in the siltstone but make up only a small fraction (a few %) of the total hematite content (Fig.3.14). They generally show traces of in situ alteration and some of them may be authigenic although there is no unambiguous proof of this.

In the sandstone, the tiny grains are also present but range in size up to 10 μm. They are less abundant because of the less abundant matrix. The larger grains are more

numerous than in the finer rocks (Fig.3.15, 3.16) and roughly the size of the bulk of the detrital non-magnetic grains (40-120 μm). They may be responsible for the observed softer component in the IRM acquisition / destruction curves (Fig. 3.10). They vary from black to red with different degrees of alteration(Fig.3.15) and again an apparent randomness in the distribution of altered and non-altered grains. The amount of pigmentary hematite is much smaller in the sandstone but otherwise no differences are observed in the pigment structure.

Macroscopic examination of high and low NRM samples reveals no differences in colour or texture, and the microscopic analysis revealed no differences either. Systematic variations in amount and size of all types of hematite grains or differences in the degree of alteration were looked for but none were found, nor were differences in the amount or distribution of the pigment found.

The observations concerning the smaller grains strongly suggest that they are detrital. As mentioned earlier, it is now thought that the sediments filling the Lodève Basin have a volcanic origin. The small hematite grains found in our rocks may therefore have been formed as primary hematite and thereafter more or less altered within the parent rock and/or during transportation. Even the pigment, or at least a part of it, might have been brought into the basin associated with the clay matrix and

Figure 3.13. Photograph of a siltstone thin section in reflected light. Magnification=600, 1mm=1.6μm. The bright spots are small hematite grains (1-10μm).

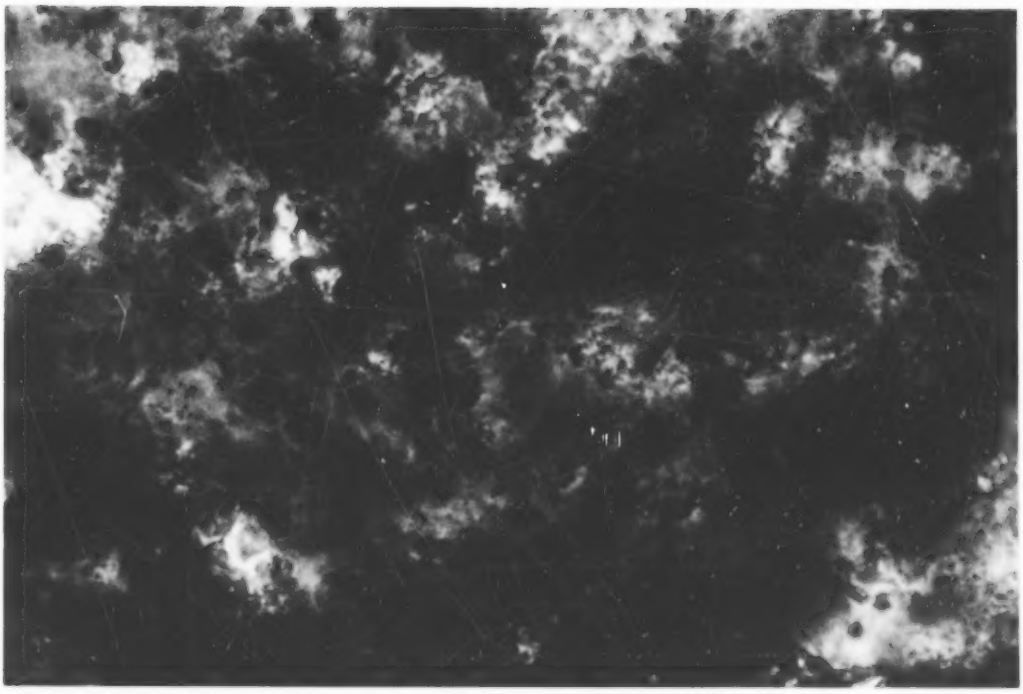

Figure 3.14. Photograph of a siltstone thin section in transmitted light. Magnification=600, 1mm=1.6μm. It shows a large hematite grain (~20μm) in the upper right center and smaller black and red grains. Dark red-brown colour is due to pigmentary hematite.

Figure 3.15. Photograph of a sandstone thin section in reflected light. Magnification=300, 1mm=0.8μm. Two large hematite grains are well visible. One (in the center) shows intense alteration whereas the one at the top is very fresh.

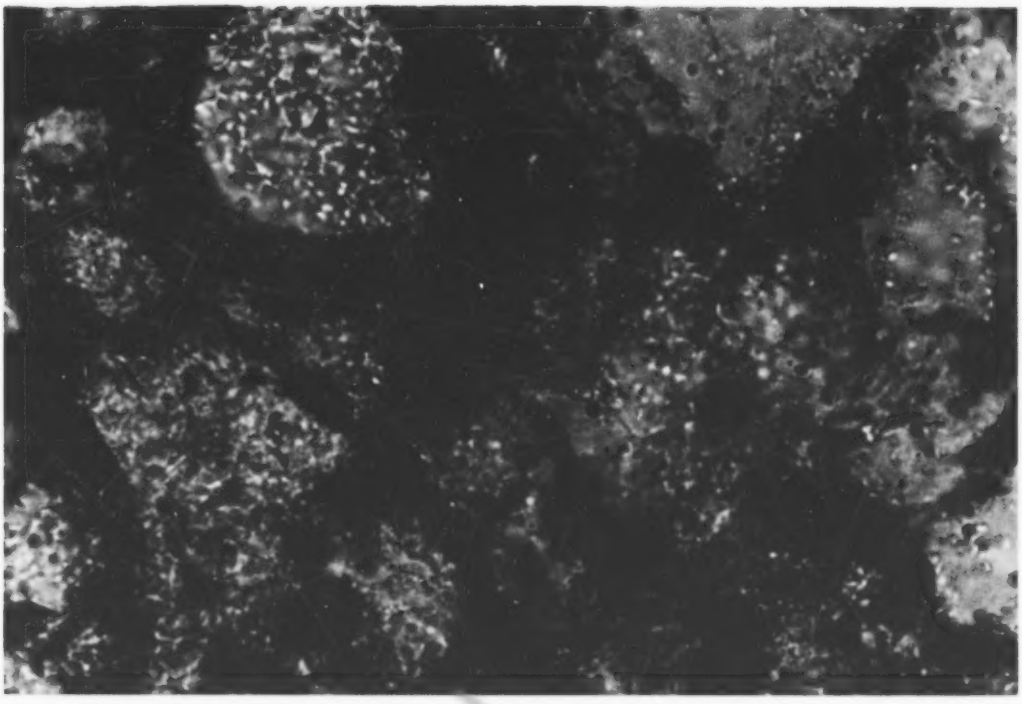

Figure 3.16. Photograph of a sandstone thin section in transmitted light. Magnification=300, 1mm=0.8μm. It shows a large hematite grain (opaque) and pigmentary coating around transparent grains (mostly quartz).

with grains coated in the parent area. The general nature of the rocks indicates that they are rather immature and have undergone a relatively short transportation. The origin of some larger grains might be similar; others could be authigenic or formed by overgrowth of secondary hematite.

3.5 Quantitative characterization of the intensity patterns

3.5.1 Statistical considerations

The asymmetric "saw-tooth" shape of the intensity peaks described in section 3.2 is a clear observational fact in a good number of cases. However, it is desirable to characterize this pattern in a more objective way, and to determine in a statistical sense if it is a feature of the whole intensity records and not only of particular, well chosen parts of them.

This was achieved by devising a simple statistical test designed to quantify the asymmetry of the curves. Let us consider an ideal model of a "saw tooth" pattern and define the following quantities using the notation of Fig.3.17:

$N^{(+)}$ = number of steps for which $\Delta_i > 0$

$N^{(-)}$ = " " " $\Delta_i \leq 0$

$\Delta_m^{(+)}$= average value of positive Δ_i

$\Delta_m^{(-)}$= " " negative Δ_i

We can now characterize the pattern by the two ratios:

$$R_N = \frac{N^{(+)}}{N^{(-)}} \quad \text{and} \quad R_\Delta = \frac{\Delta^{(+)}}{\Delta^{(-)}}$$

We immediately see that a "saw tooth" pattern with a flat side facing upwards will be distinguished by $R_N<1$ and $R_\Delta>1$. A symmetric or random pattern would tend to $R_N=R_\Delta=1$.

This test was performed on intensity data from site BLF, which provides the two longest available data sets. Result are presented in Table 3.2 below.

	# of steps	R_N	R_Δ
BLF1	91	0.82	1.22
BLF2	265	0.85	1.17

TABLE 3.2. Statistical parameters R_N and R_Δ

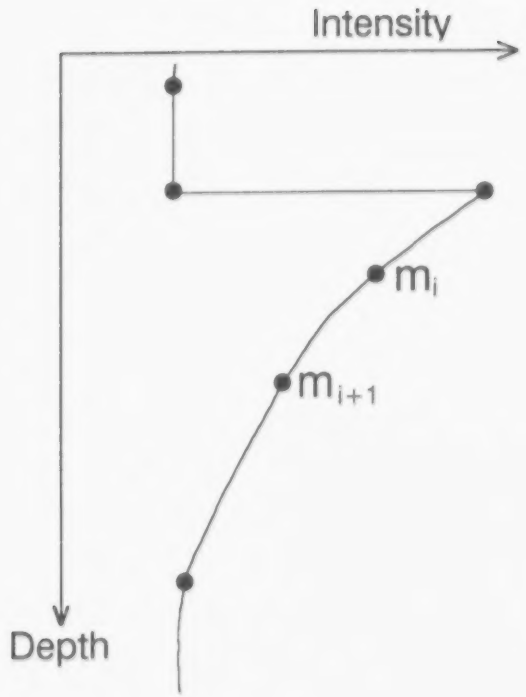

$$\Delta_i = m_{i+1} - m_i$$

Figure 3.17. Explanation of the notation used for statistical analysis of the intensity variations.

R_N values indicate that configurations in which consecutive points correspond to intensity decreases are more frequent than those corresponding to intensity increases. R_Δ values indicate a faster average intensity variation for intensity increases than for decreases (again with the sign conventions of Fig. 3.17). These results are therefore compatible with a predominance of the pattern that is claimed to be representative of the observed intensity variations. However, in order to know how significantly different from 1 these numbers are, one needs to compare them to a statistical distribution of R_N and R_Δ. This can be done using a Monte-Carlo approach to calculate a sample distribution of the two parameters. This is best achieved by randomizing the initial data series by permutations of its elements, and then re-calculating the values of R_N and R_Δ. By repeating this procedure a large number of times an empirical estimate of the distributions can be obtained. The advantage of this method over simple random drawing of numbers is that characteristics of the data set, such as mean and standard deviation, are easily preserved through the randomization process. Results obtained using 3000 permutations are presented in Fig.3.18 (BLF1) and Fig.3.19 (BLF2). R_N and R_Δ have, as expected, mean values very close to unity, and their distributions suggest that the values calculated from the initial data set are significant. The probability

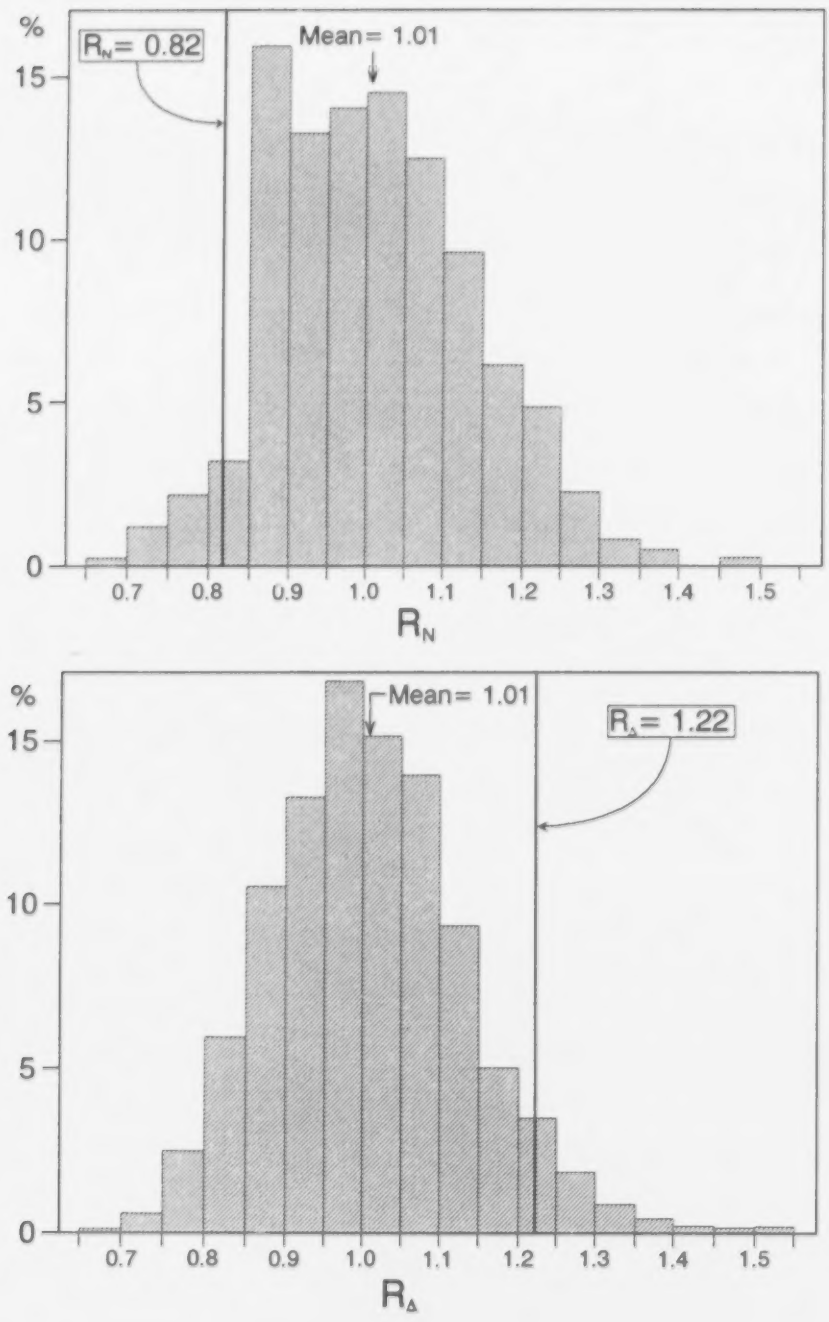

Figure 3.18. Histograms of R_N and R_Δ distributions for section BLF1; N=91.

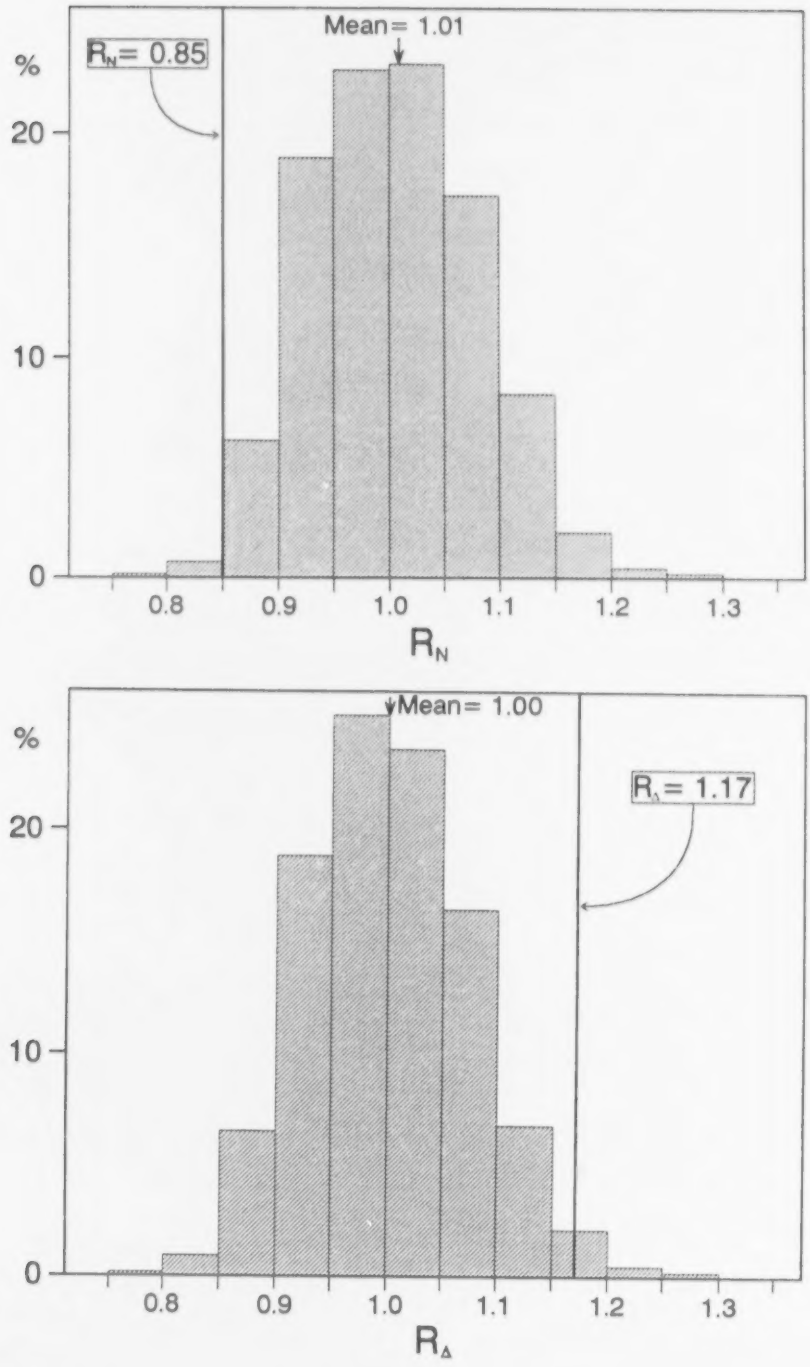

Figure 3.19. Same as Fig 3.18 for BLF2; N=265.

that the observed values of the two parameters be exceeded by chance can be estimated from the 3000 permutations. On the histograms, this number corresponds to the area extending beyond the line marking the actual values of R_N and R_Δ. In the case of BLF1, the probabilities for R_N and R_Δ are 0.035 and 0.055 respectively, for BLF2 the corresponding numbers are 0.010 and 0.015. This strongly confirms that a saw tooth pattern with flat side facing upwards is indeed a dominant feature of the observed intensity curves.

3.5.2 Trends in intensity variations

We have seen that intensity peaks are characterized by asymmetric "saw tooth" shapes, but it remains to look more closely at the way the intensity decreases with depth within each "saw tooth". It would indeed be interesting to discover if the intensity decay follows a definite law.

To do so, fourteen well defined intensity peaks were selected from the entire data set, retaining only the smooth, lower part, with the goal of comparing the trends to see if any common feature could be extracted. The selected decay curves are presented in Fig. 3.20, each with a different scale to emphasize their similarities. Six of them are sandstones, seven are siltstones, and only one example is a mudstone. They are all extracted from

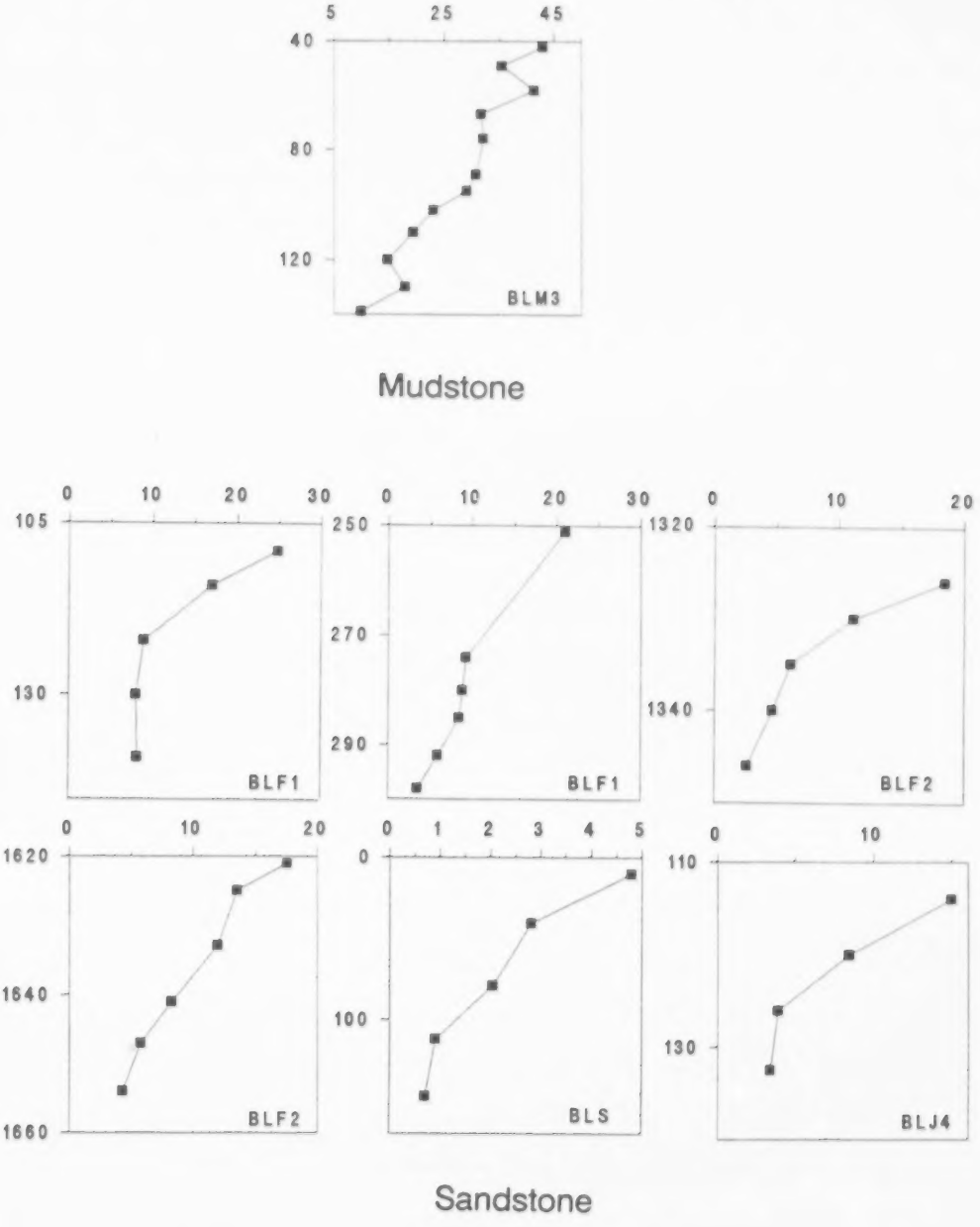

Figure 3.20. Fourteen examples of magnetic intensity decay patterns in different lithologies (continued next page). Depths (in mm) are the same as on the complete magnetograms that can be found in Fig.3.1 through 3.5. Intensities of magnetization are given in 10^{-6} Am^2/kg.

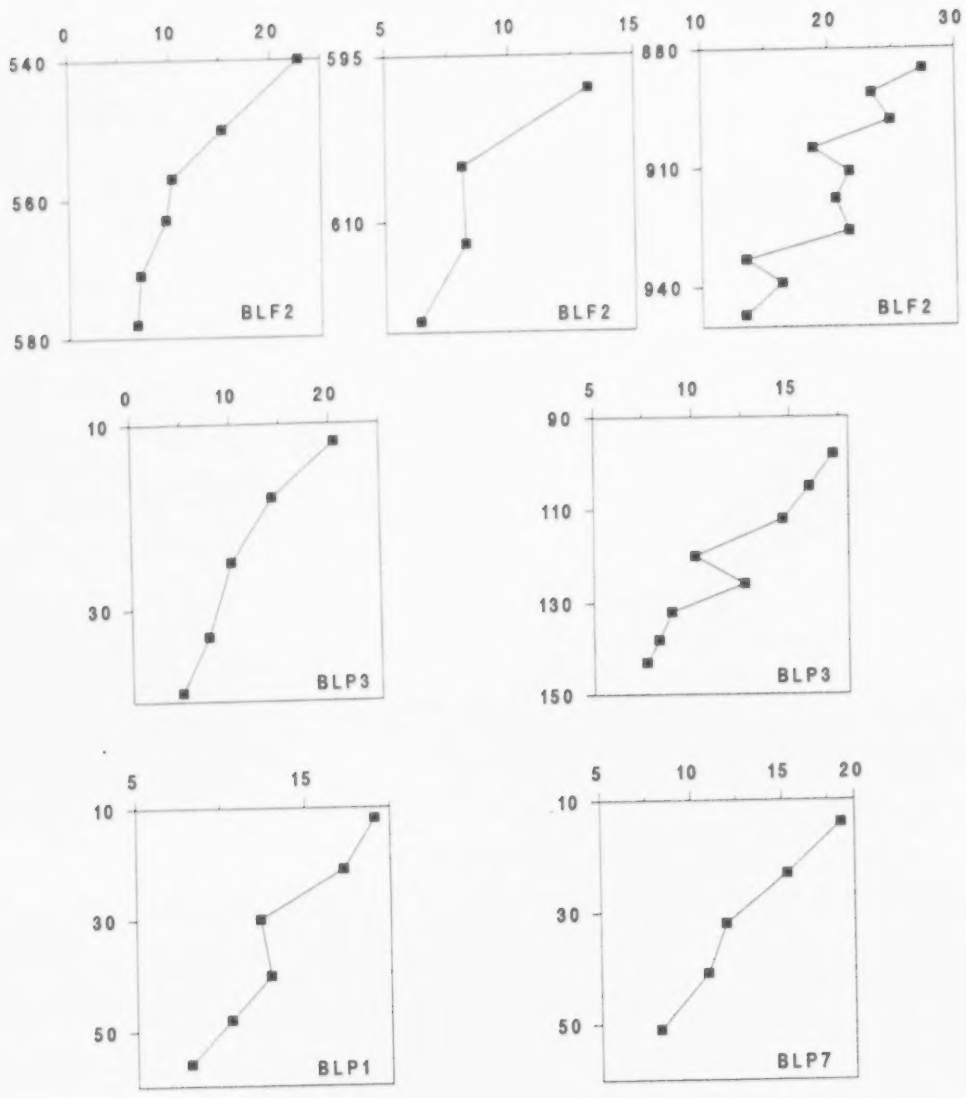
0
10
20
540
560
580
BLF2
5
10
15
595
610
BLF2
10
20
30
880
910
940
BLF2
0
10
20
10
30
BLP3
5
10
15
90
110
130
150
BLP3
5
15
10
30
50
BLP1
5
10
15
20
10
30
50
BLP7

Siltstone

data sets that can be found in their complete form earlier in this chapter.

In order to be able to compare these fourteen decay curves, it is necessary to normalize them, and to stack them together. This is done by normalizing maximum intensity and depth interval to unity, and plotting the data corresponding to each curve on the same graph. Fig.3.21 shows all the points from the fourteen examples. Fig.3.22 shows only the points corresponding to the simpler, monotonic curves, i.e. without BLF2 (880-940mm), BLP3 (90-150mm) and BLM3 (see Fig.3.20). Fig.3.23 and 3.24 show the same data divided in siltstone and sandstone respectively. In all cases, both a straight line and an exponential curve were fitted through the points, in order to see if a particular behaviour could be attributed to the intensity decay patterns. In all cases, the fit is better for the exponential due to the faster decrease of intensity in the first centimetre. No marked differences can be observed between sandstones and siltstones.

This analysis indicates that the observed intensity decay patterns do seem to possess certain common characteristics. They appear to be caused by a phenomenon characterized by a damping towards the bottom, and this damping seems to follow an exponential law. However the data are too scant to furnish sufficient information at

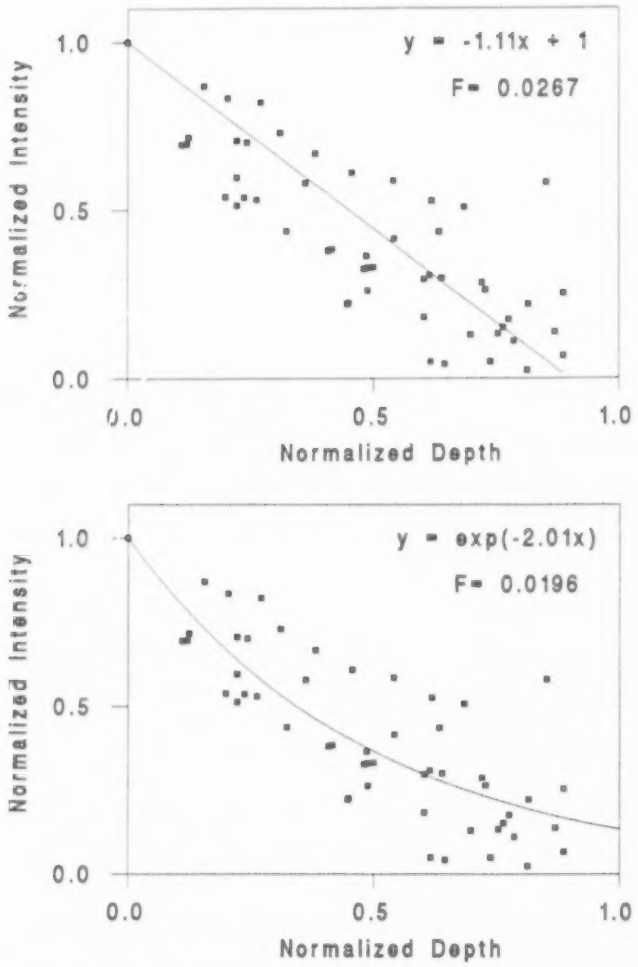

Figure 3.21. Stacked plot of data from Fig.3.20 after normalization (max. intensity range: 5-45x10^{-6} Am^2/kg; depth range: 25-130 mm). The straight line (top) and exponential curve (bottom) fitted through the data points are forced to pass through (0,1). The goodness-of-fit parameter (F) is simply $\frac{(y_i-y_f)^2}{N}$, where y_i is an observed intensity, y_f the corresponding value calculated according to the model (line or exponential) and N is the total number of experimental points. The better the fit, the smaller F.

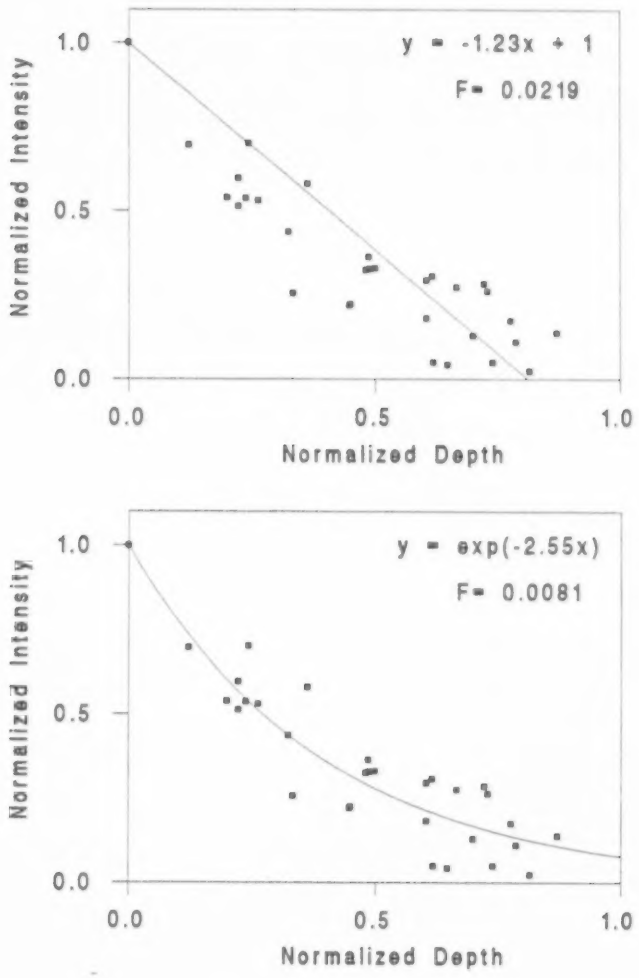

Figure 3.22. Stacked plot of data points from 11 monotonic intensity decay patterns. See Fig 3.21 for explanations.

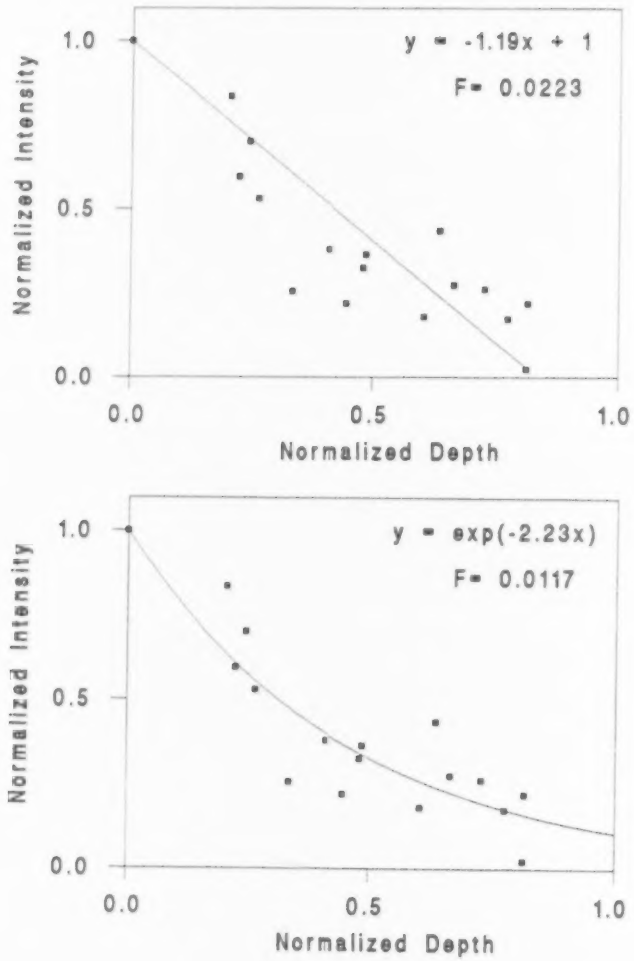

Figure 3.23. Stacked plot of data points from 5 intensity decay patterns in siltstones. See Fig 3.21 for explanations.

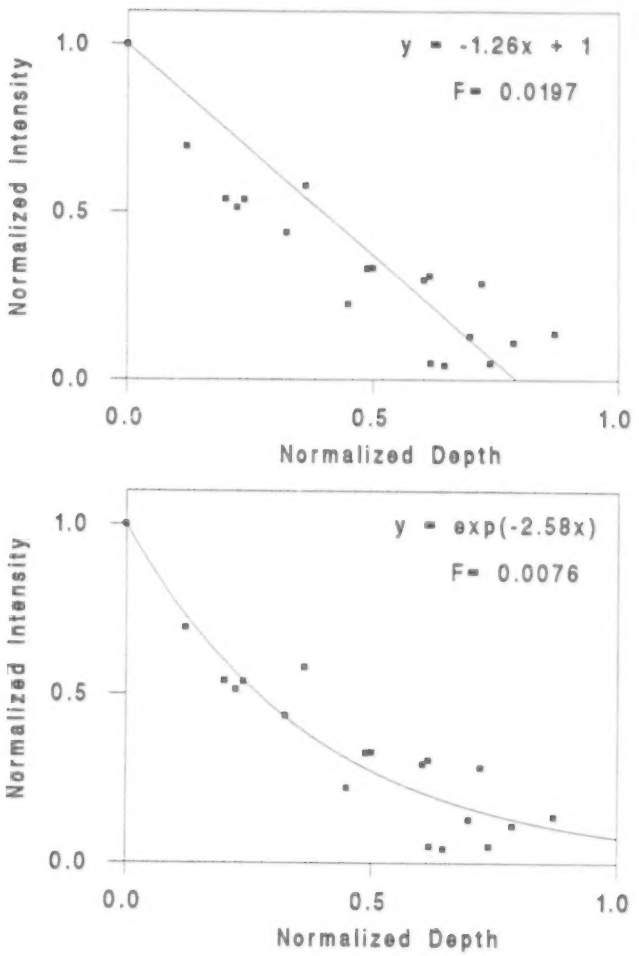

Figure 3.24. Stacked plot of data points from 6 intensity decay patterns in sandstones. See Fig 3.21 for explanations.

this preliminary stage to single out any particular physical or chemical cause.

3.6 Discussion

The experiments and observations described so far were meant to seek answers to three questions. What is the origin of the magnetization in the Lodève redbeds? What is the cause of the large, lithostratigraphically controlled, intensity variations? And finally, what is the interconnection between these two issues? All the magnetic and petrological observations must be brought together to see if any coherent picture emerges.

Fluctuations of the geomagnetic field intensity (Collinson, 1972) can be rejected because of the amplitude and frequency of the variations, but most of all because of the obvious lithostratigraphic control. The presence of antipodal components of magnetization with variable ratios (Larson et al., 1982) could also explain the observations. However, the total lack of normal polarities in the entire Lodève sequence and the simple behaviour of the specimens during stepwise demagnetization rules out the presence of widespread normal components. We are left with what can be called internal causes. The most obvious explanation is a simple variation of the amount of magnetic minerals present. Another possibility is a fluctuation of grain

size; small single-domain grains carry a stronger remanence than large multi-domain ones. Finally, one can also invoke a variation of *specific* remanence intensity of the magnetic grains, depending on their history.

Susceptibility and IRM results rule out total concentration variations as the cause of short range intensity variations. Petrographic observations confirm this conclusion since they show no significant fluctuations in the amount of pigmentary or specular hematite. The effect of grain size variation cannot be entirely rejected on the basis of IRM acquisition experiments because of the poor resolution of the method. However, the amplitude of the intensity variations makes it unlikely that a corresponding grain size variation could go unnoticed in the coercivity spectra. Furthermore, this effect should be optically observable, but is not seen. We are left with the possibility that the intensity variations are caused by different *specific* magnetization intensity in hematite grains. This eventuality cannot be investigated without the ability to measure the magnetization of individual grains. This was done by Collinson (1972) in his attempt to explain intensity variations in the Bonito Canyon quartzite and he found that specific intensity was not sufficiently variable to explain large NRM fluctuations. Of course this result is difficult to extrapolate to our case despite other

similarities. A last hypothesis is that the NRM is carried by only a fraction of the material capable of acquiring a magnetization. This is compatible with our results only if the non-magnetized fraction greatly overwhelms the magnetized one.

All the hypotheses examined so far involve properties of the grains and none is really satisfactory, but another possible interpretation is that intensity variations are due to a varying efficiency of the process of magnetization acquisition. The magnetic grains could be all the same everywhere but the way by which they record the geomagnetic field could vary in efficiency.

At this point it is appropriate to see what can be deduced about the actual origin of the magnetization. As is well known, the magnetization in redbeds can be either chemical or depositional. The thin section analysis shows that three possible hematite remanence carriers are present in the sandstone - the large grains, the small crystals dispersed in the matrix, and the pigment. In the siltstone, this number is effectively reduced to two because of the scarcity of large grains. The similarity of sandstone and siltstone NRM in all respects and especially under AF demagnetization suggests that the large hematite grains do not play any significant role in the NRM, although they are probably responsible for the low coercivity component present in the sandstone IRM. The

role of the pigment is more difficult to assess but the very small size of its constituents coupled with the relatively low coercivity of the NRM suggests that its role is subordinate. The best candidates as main NRM carriers are thus the small hematite crystals dispersed in the matrix. Their size (1-5 μm) puts them in the range of single-domain crystals and the most likely to acquire a strong magnetization (Dekkers and Linssen, 1989). As already seen these grains are probably detrital and this would suggest a similar origin for the NRM.

We can now examine which process, chemical or depositional can best explain lithologically controlled intensity variations. CRM has often been invoked for redbeds and in the particular case of the Lodève Basin, the presence of important uranium mineralizations indicates that large fluid migrations must have occured. However, these mineralizations took place in the Jurassic (Lancelot et al., 1984), and since no remagnetization of this age is found, it is very unlikely that they could be associated with magnetization processes.

It is difficult to imagine a chemical process producing large intensity variations on a short range through the subtle changes permitted by the experimental results. On the other hand, depositional processes can easily create such variations through the more or less efficient alignment of magnetic particles along the

Earth's field direction. Then no fluctuations are needed in grain properties but only in the depositional and post-depositional conditions prevailing before consolidation of the rock. Indeed experimental studies have demonstrated how the intensity of magnetization can be enhanced by perturbations of the still unconsolidated sediments (Tauxe and Kent, 1984; Ellwood, 1984). They show that intensity variations of an order of magnitude between perturbed and unperturbed sediments can be created by this process. Furthermore, in a continental, semi-arid environment like the one in which the Thuringian rocks of Lodève were formed, the deposition is essentially discontinuous – periods of rapid sedimen-tation alternate with stages of no deposition. Therefore, the magnitudes of post-depositional processes are likely to vary stratigraphically, and maxima at bed tops can be expected since they correspond to longer periods of exposure. The good correlation over small distances of a few tens of centimeters, as opposed to the poor correlations over distances of several tens of metres, indicate that the amplitude of the phenomenon varies locally, as would be expected with surficial perturbations. The nature of potential perturbations is unknown; bioturbations and water currents are possibilities that need to be considered. Their effect would be to loosen the magnetic grains, allowing them to rotate more freely and to become

better aligned in the direction of the ambient field. In the case of perturbations acting from the surface, it is natural to expect a diminishing effect towards the bottom of the unconsolidated sedimentary column. The actual degree of saturation (i.e. water content) can also influence the grain realignment; however, some studies have shown that its role is not as critical as that of perturbations (Verosub, Ensley and Ulrick, 1979; Payne and Verosub, 1982). In the case of fine sediments deposited in a continental environment, a sufficient water content is necessary but probably not enough to ensure that the magnetic carriers will realign themselves.

3.7 Conclusions

The magnetization of the Lodève redbeds is characterized by large, lithostratigraphically controlled intensity variations with peaks near the top of individual strata. Variations of similar or even larger amplitudes have been reported in several other redbed formations but without stratigraphic control (Collinson, 1969; Irving and Runcorn, 1957; Larson et al., 1982). In this study, the sharp intensity variations could only be noticed because of the unusual size of the samples (5 to 7 mm thickness); had they been regular 25mm cores most, if not all, of the peaks would have been smoothed out.

Rock magnetic experiments and petrographic observations suggest that no variation of intrinsic properties of the magnetic grains can be convincingly invoked. Therefore the intensity changes can be explained by a difference in the effectiveness of the remanence acquisition process. This can more readily occur when depositional magnetization is involved, and since other evidence tends to confirm this, it is suggested that intensity changes are due to more or less effective alignment of the magnetic grains in the direction of the ambient field. Because of the clear lithological control, the applied field intensity cannot be the factor governing the efficiency of the particle alignment. Therefore, the most likely controlling factor is the grain mobility depending on the magnitude of mechanical perturbations occasioned either by organisms or hydraulic phenomena.

It is proposed that the NRM is carried mainly by small hematite grains that are deposited with the rest of the detrital material. When deposition stops, post-depositional processes act to improve the alignment of the magnetic grains. They are most effective near the surface of the unconsolidated layer and their effect diminishes downwards. The characteristic magnetic intensity decrease from top to bottom is produced by a combination of the decreasing impact of perturbations and of the increasing load that tends to hinder grain movements. This can

account for the exponential shape of the downward side of the intensity peaks. The larger peaks correspond to major sedimentation discontinuities during which organic and hydraulic activities have more time to act. When deposition resumes, the bottom of the new layer (less influenced by surficial perturbations and therefore more weakly magnetized) comes in contact with the top of the underlying bed, hence the sharp intensity change at sedimentation discontinuities.

It is felt that the combined weight of all the evidence presented above indicates that the remanence carried by the Lodève strata is primary, having been acquired during and very shortly after deposition. Furthermore, there is a suggestion that the process of magnetization is essentially discontinuous, individual beds being magnetized as a unit. If this is so, each bed can be regarded as a "spot" reading of the geomagnetic field. The proposed model is certainly not the only possible one but it is the simplest, and most likely to describe the conditions prevailing during the acquisition of the magnetization in the Lodève redbeds.

CHAPTER 4

DIRECTION OF MAGNETIZATION

4.1 Introduction

In the previous chapter we have examined in detail certain magnetic properties of the Lodève Basin strata that are the subject of this investigation. In order to gain some insight into the origin of the magnetization, scalar properties like bulk susceptibility and magnetic intensity were used. It is now time to turn our attention to the directional magnetic properties.

This chapter will deal with the detailed analysis of the direction of magnetic remanence carried by the Lodève rocks. It is well known that the direction of Natural Remanent Magnetization (NRM) can result from the combination of several magnetization directions reflecting different episodes of the rock history. It is therefore essential to identify all the components of the NRM in order to be able to decipher a potentially complicated history. This is done through stepwise demagnetization of selected samples, which will be the object of the first section of this chapter.

Luckily it is known that the Lodève Basin has undergone little tectonic disturbance since its formation and previous studies have shown that the magnetization is simple and composed of a primary Permian magnetization and a secondary overprint in the direction of the present day Earth's magnetic field (Kruseman,1962, Evans & Maillol, 1986, Merabet & Guillaume, 1988). However, these studies have been confined to the lower part of the Permian sequence and thus have not dealt with the mudstones. More detailed work on the mudstone magnetization was therefore needed.

When pilot demagnetizations have been performed, one can choose a standard treatment to be applied to the bulk of the specimens, in order to remove undesirable secondary magnetizations. The result is a data set consisting of magnetization directions that, in the cases where the magnetization history is simple, represent the oldest, characteristic remanent magnetization first acquired by the rock. These results, coming both from the Basin Traverse and the closely sampled sections, will be presented in later sections of this chapter. Their meaning and how they can be exploited for geophysical purposes will be discussed in Chapter 5.

4.2 Pilot demagnetizations

4.2.1 Alternating field (AF) demagnetization

This technique (see e.g. Collinson (1983) for a description) has the advantage of leaving the rock intact, as opposed to thermal and chemical treatments which always present the potential risk of alteration of the minerals. Unfortunately, it is generally ineffective with red sediments because of the high coercivity of hematite which is usually the magnetic carrier in these rocks.

This technique was nevertheless applied to 8 pilot specimens, 6 disks and 2 cores from the basin traverse. Results concerning the intensity decay have already been presented in Chapter 3 (section 3.3.2, Fig.3.7), and it was seen that the maximum peak field available is insufficient to destroy all the magnetization. Two examples of the effect on directions are represented in Fig 4.1. They show some removal of the modern overprint, but at the maximum field the direction are still not typical Permian ones. Subsequent thermal demagnetization of the same samples showed that indeed a good part of the overprint had been left after AF treatment.

These results were expected since, as we have seen in Chapter 3, the magnetization is carried by hematite. Therefore, the method preferred for "cleaning" the samples appeared to be thermal treatment.

Figure 4.1. a) and b). Stepwise AF demagnetization of two pilot specimens. The top diagram is a an equal area projection of the vector remanence at different demagnetization steps.
The middle one is an orthogonal component Zijderveld plot. Solid lozenges represent the magnetization component in the horizontal plane (axes labelled N,W). Empty lozenges represent the component in a N-S vertical plane.
The bottom diagram is an intensity decay curve showing the decrease of magnetization intensity during progressive demagnetization.
Intensities are normalized and magnetic fields are in Tesla.

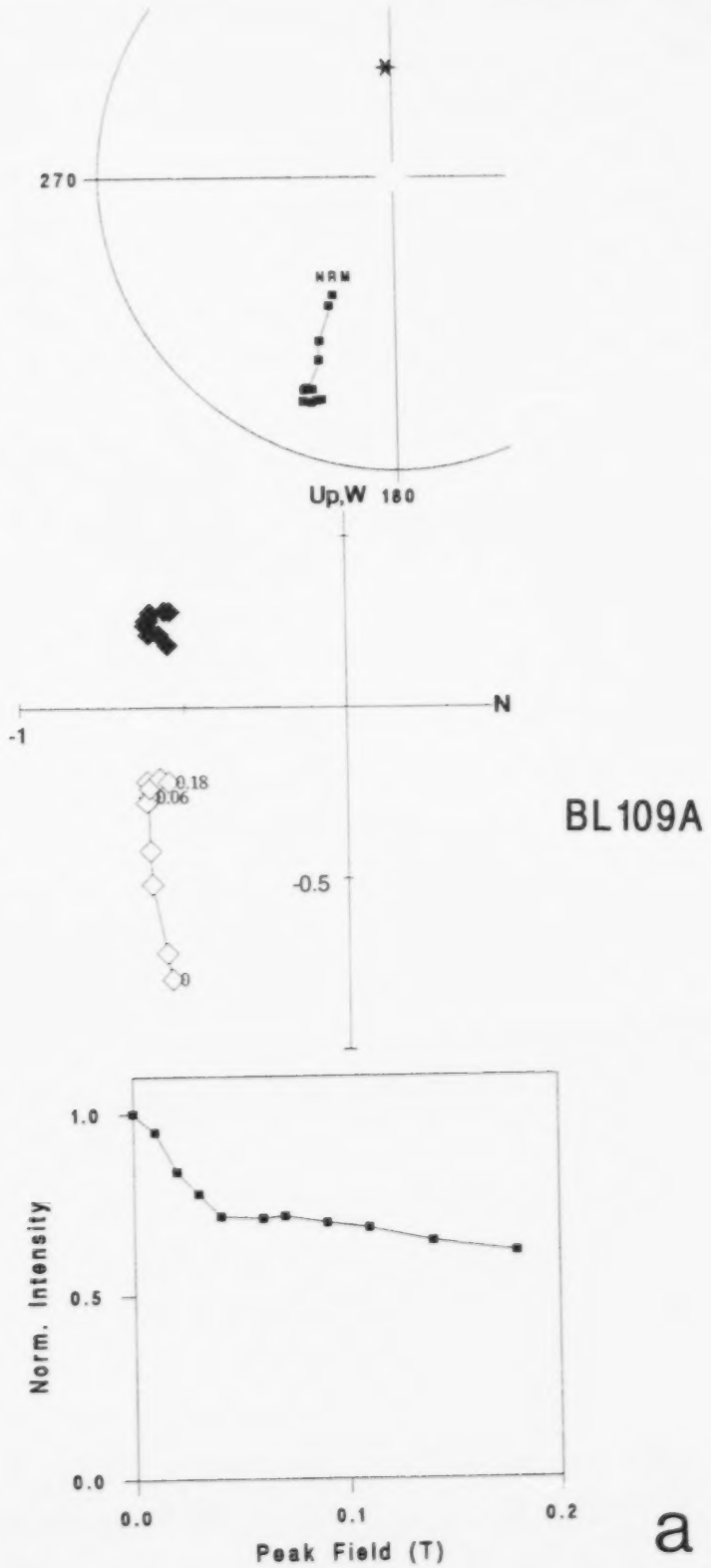
270
NRM
Up,W 180
N
-1
0.18
0.06
-0.5
0
BL109A
1.0
0.5
0.0
Norm. Intensity
0.0
0.1
0.2
Peak Field (T)
a

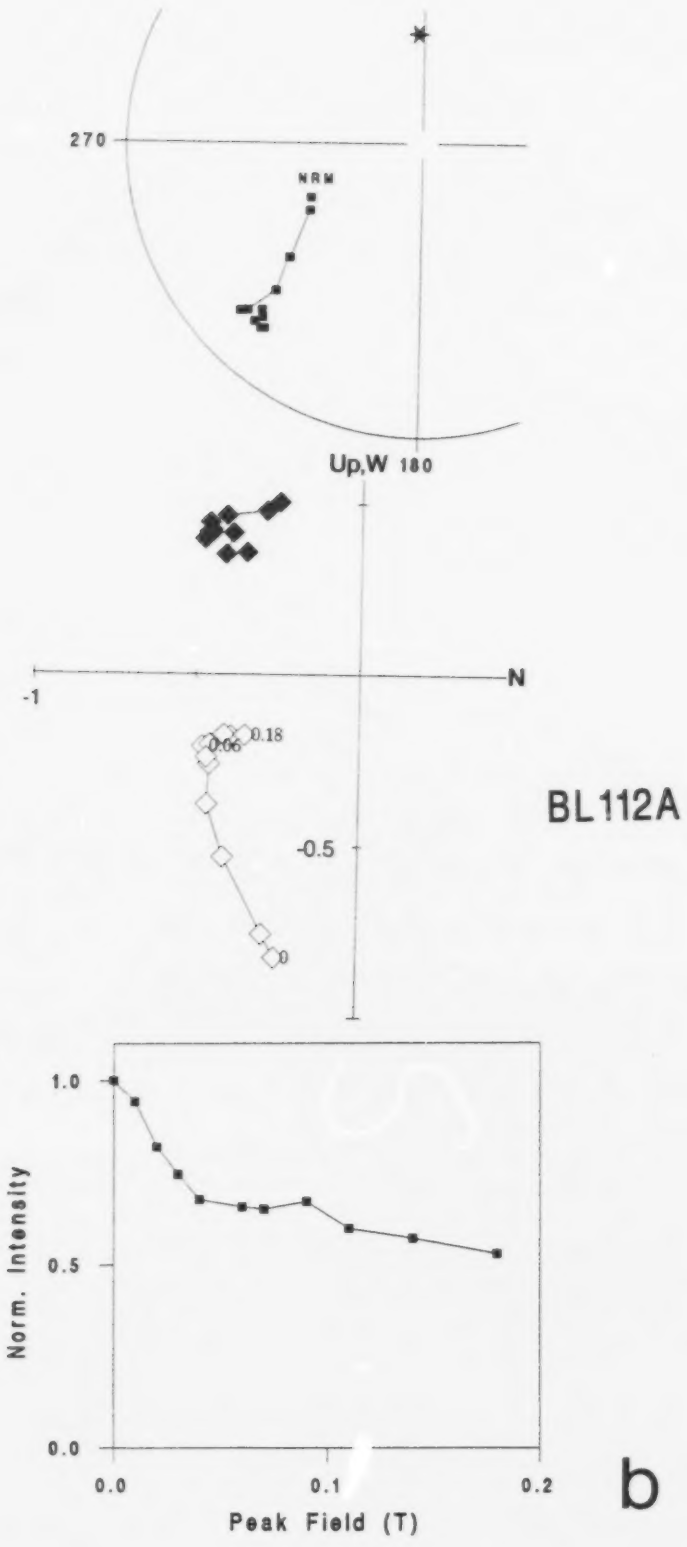
270
NRM
Up,W 180
N
-1
0.06
0.18
-0.5
0
BL112A
1.0
0.5
0.0
Norm. Intensity
0.0
0.1
0.2
Peak Field (T)
b

4.2.2 Thermal demagnetization

A total of 15 samples from the basin traverse were selected, so as to represent the different categories involved in this study, namely cores and plastic tops, representing the three lithologies (sandstone, siltstone, mudstone). In addition to these, 10 disks from the closely sampled sections were also subjected to the same treatment, mainly to monitor the intensity decay since in these samples the overprint is small. These last results have been presented in Chapter 3 and only two examples, with corresponding directional data, will be repeated here.

A list of the different specimens used in this section is given in Table 4.1. The pilot specimens were subjected to progressive heating up to a maximum of 670°C in a computer controlled furnace located in a magnetically shielded room (see Appendix 2 for details of the equipment).

Complete results of the thermal demagnetization are given in a series of figures (Fig.4.2 a to q) in the form of three different types of diagram. For each sample a equal area projection indicates the way the direction of magnetization changes in space during progressive heating. An orthogonal component plot (Zijderveld, 1967) is also given, as well as an intensity decay curve.

The most immediate observation is that the sample behaviour varies during the heating, but always with the common feature of two components of magnetization. One is in the direction of the modern field (Dec=3°W, Inc=59°), the other in the direction of the Permian field (Dec=200°, Inc=5° on average, taking into account the tectonic tilt). The differences are due to the variable magnitude of the modern overprint. In some specimens it is very reduced, and the direction barely changes (e.g. Fig.4.2a and b), in others it is very important and in those cases the initial NRM is close to the direction of the present field (e.g. Fig.4.2 o and p).

The intensity decay curves show a range of variations between concave and convex. The concave ones are always associated with large overprints. This is explained by the fact that the secondary component has lower blocking temperatures than the primary component. When the latter is predominant, most of the magnetization is destroyed at high temperature and the rate of destruction increases with temperature, thus giving a convex shape to the decay curve. The opposite behaviour occurs when the secondary component prevails. The curvature of the intensity decay curves, as well as that of the vector paths in the Zijderveld plots indicate that primary and secondary components have, in fact, overlapping blocking temperature

spectra. The characteristic magnetization begins to be destroyed before the overprint is totally eliminated.

It is rather difficult to classify the different pilot specimens into distinct classes according to their behaviour during thermal demagnetization, but one can discern general trends. The magnitude of the overprint is generally smaller in coarser grained specimens than in mudstones, and it is also smaller in cores than in plastic tops. Actually, the major factor governing the magnitude of the overprint seems to be the amount of weathering that the samples have undergone. The lithology by itself does not seem to be a predominant factor since the mudstone samples obtained from the deep mining core segments showed only a small overprint. Moreover, the disks cut from the very fresh rocks sampled for the small scale study have a very small overprint (Fig4.2 a, b), while samples of exactly the same lithology but from less fresh outcrops exhibit more substantial direction changes during heating (Fig.4.2 d, f). However, lithology may be an indirect factor since very compact sandstones and siltstones are much less alterable than easily cracked mudstones. The difference between methods of sampling can also be tied to a difference in weathering. The plastic top method was devised for the very reason that it allows sampling of more surficial rocks (and reduces the amount of digging). As a result, the specimens collected were likely to have

undergone more severe weathering than cores drilled in compact rock.

The main goal of stepwise demagnetization experiments is of course to determine if a primary, characteristic direction of magnetic remanence can be isolated, and if so, what is the standard treatment to be applied to the bulk of the sample collection. In this respect, all the pilot samples show that indeed thermal treatment is successful in isolating a characteristic direction. Zijderveld plots show that after 500°c, and in many cases, after only 400°c the tips of remanence vectors follow approximately straight paths going through the origin, which indicate that only one component remains. Equal area projections give another point of view by showing that after the given temperatures the remanence directions change very little. Several examples show some irregularities at high temperature (above 600°c), but they are due to measurement uncertainties that become important in heavily overprinted specimens when the intensity of magnetization decreases to levels approaching the limits of sensitivity of the instrument.

The component removed before 500°c is in the direction of the modern geomagnetic field; it is very common in redbeds and gives rise to the so called "streaking" (Creer, 1959) where NRM directions are spread in a plane passing through the direction of the present field and the

characteristic direction. This effect becomes much more apparent when the complete sample collection is considered in the next section.

In some cases (e.g. Fig.4.2 c, o) a third, very low blocking-temperature component is revealed, below 100°C. It can be attributed to a "storage component", possibly a viscous remanent magnetization acquired during preliminary storage and transport of the samples, before they could be safely stored in the magnetically shielded room.

The results of the progressive thermal demagnetization show that heating at 500°C or more effectively removes the overprint and leaves a well defined characteristic magnetization. This result, in accord with previous studies of the Lodève redbeds, led me to choose a temperature of 510°C as a standard for treatment of the rest of the samples. This temperature seemed a safe compromise between the requirement of being as certain as possible of the complete removal of secondary components, and the need to preserve as much as possible of the magnetization to ensure accurate measurements.

Name	Sampling type	Lithology	Fig.4.2
BLF2FM	disk	SiSt	a
BLF2IB	disk	SiSt	b
BL44I	core	SSt	c
BL50	core	SSt	d
BL64	core	SiSt	e
BL73	core	SSt	f
BL88C	core	MSt	g
BL97A	core	SSt	h
BL121B	plast. top	MSt	i
BL126B	plast. top	MSt	j
BL131B	plast. top	MSt	k
BLA51A	plast. top	MSt	l
BLA40A	plast. top	MSt	m
BLA37B	plast. top	MSt	n
BLA33A	plast. top	MSt	o
BLA22A	plast. top	MSt	p
BLA12C	plast. top	SiSt	q

Table 4.1. List of specimens used for pilot thermal demagnetization experiments represented in Fig4.2. (SSt=sandstone, SiSt=siltstone, MSt=mudstone)

Figure 4.2 a) to q). Stepwise thermal demagnetization of 17 pilot samples. See Fig.4.1 for explanation of the diagrams.
Intensities are normalized and temperature are given in °C.

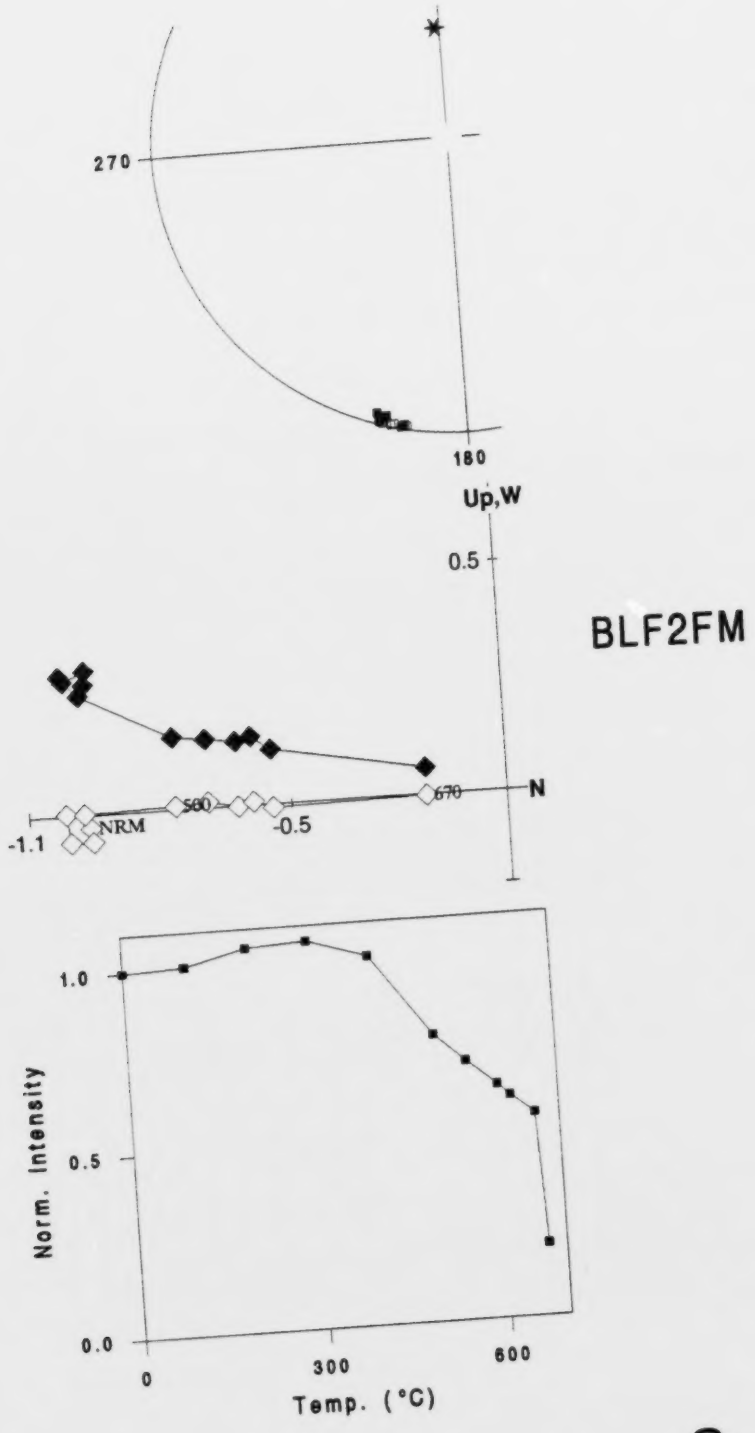
270
180
Up,W
0.5
BLF2FM
N
580
670
NRM
-0.5
-1.1
1.0
0.5
0.0
Norm. Intensity
0
300
600
Temp. (°C)

a

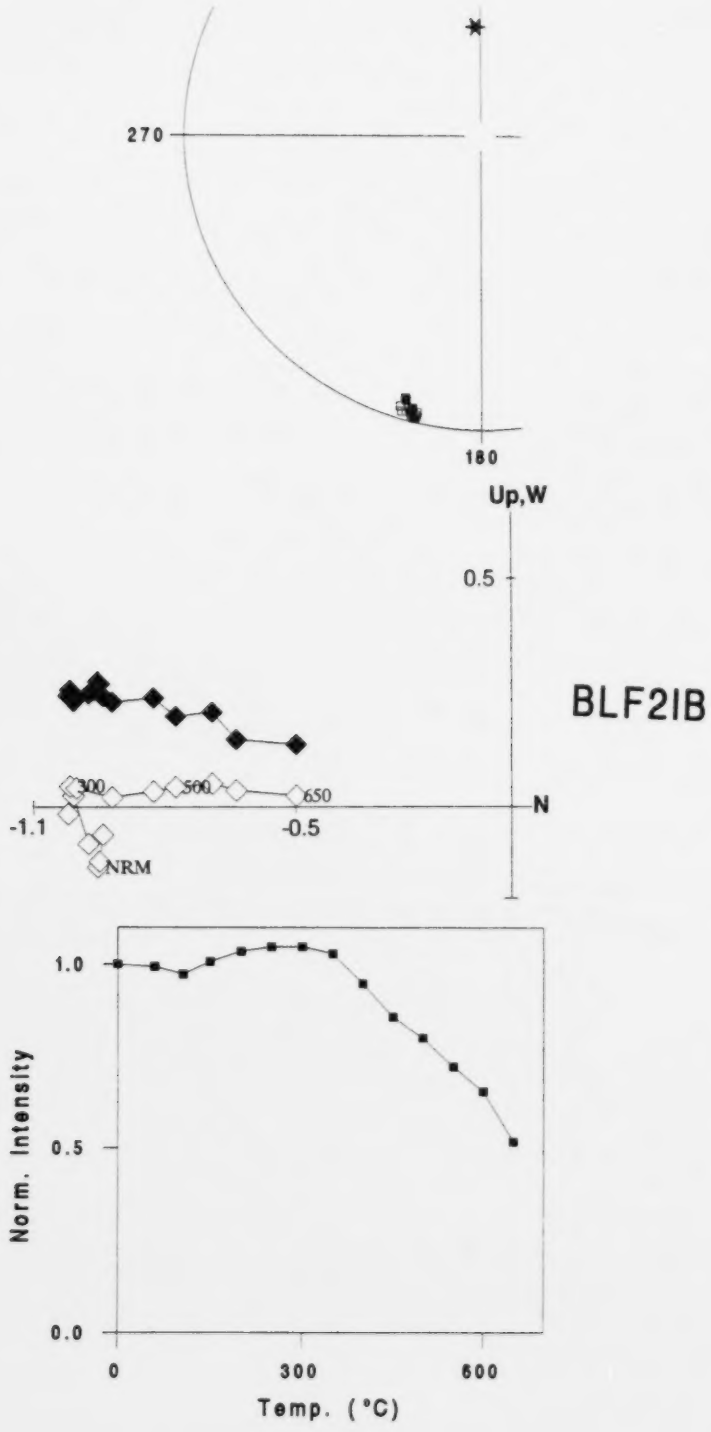
270
180
Up,W
0.5
BLF21B
300
500
650
N
-1.1
-0.5
NRM
1.0
0.5
0.0
Norm. Intensity
0
300
600
Temp. (°C)

b

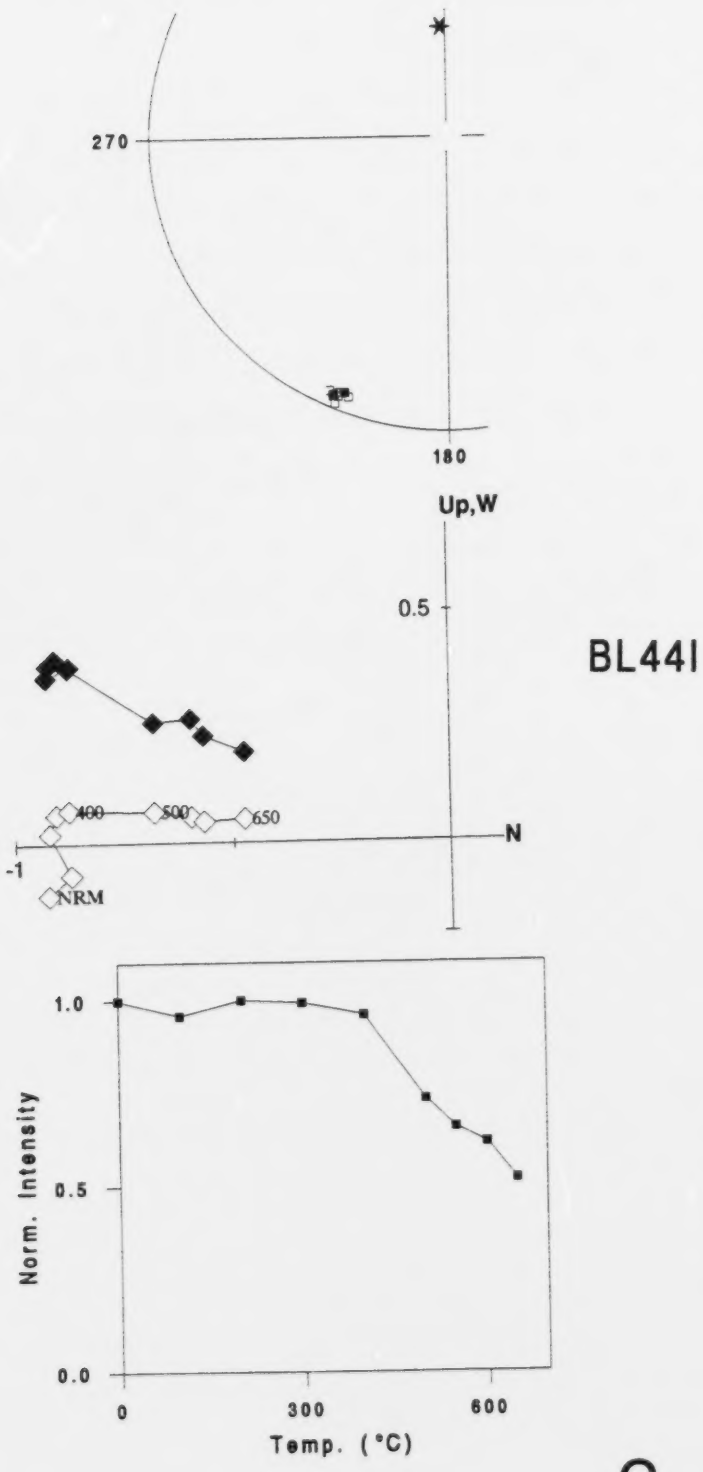
270
180
Up,W
0.5
400
500
650
N
-1
NRM
1.0
0.5
0.0
Norm. Intensity
0
300
600
Temp. (°C)

BL441

C

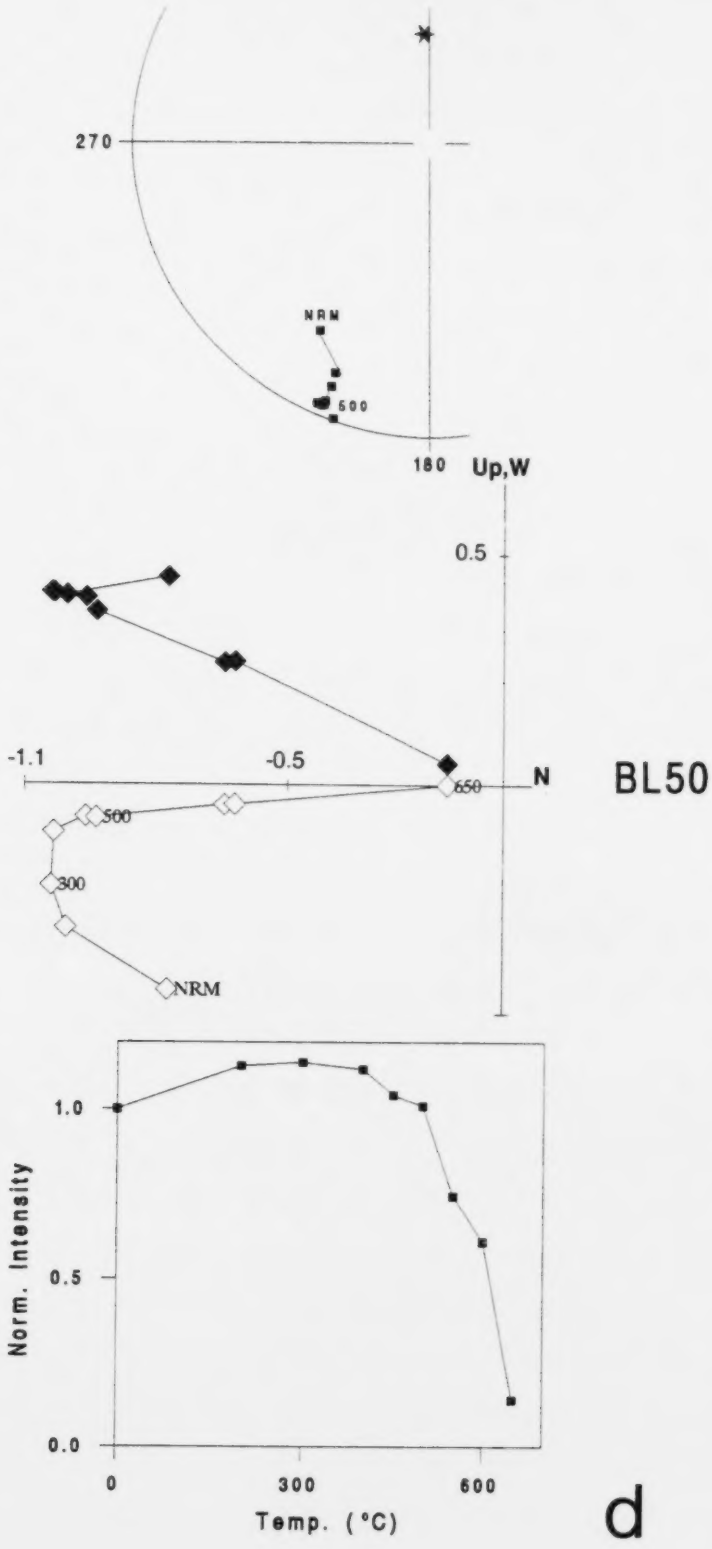
270
NRM
500
180
Up,W
0.5
-1.1
-0.5
N
650
500
300
NRM
1.0
0.5
0.0
Norm. Intensity
0
300
600
Temp. (°C)

BL50

d

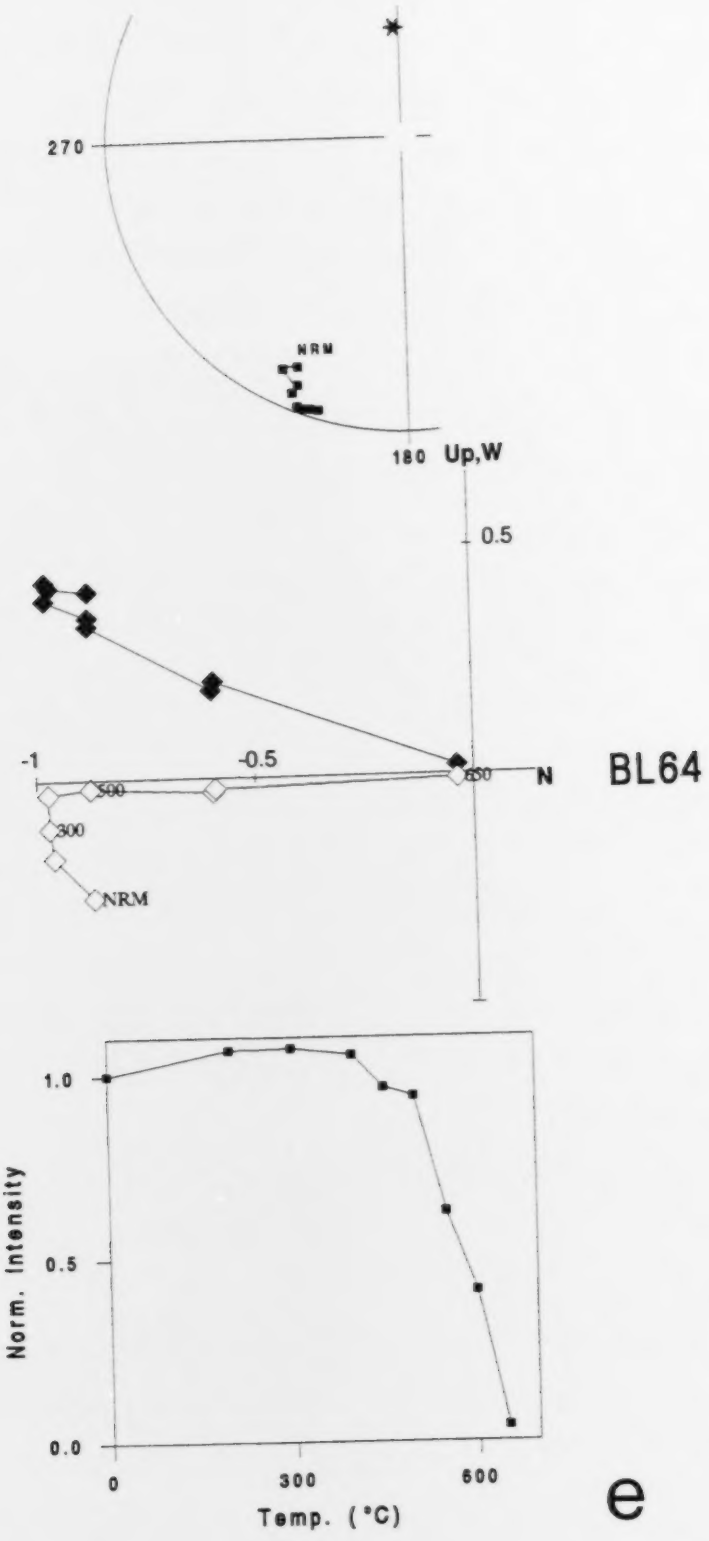
270
NRM
180
Up,W
0.5
-1
-0.5
N
BL64
500
300
NRM
1.0
0.5
0.0
Norm. Intensity
0
300
600
Temp. (°C)
e

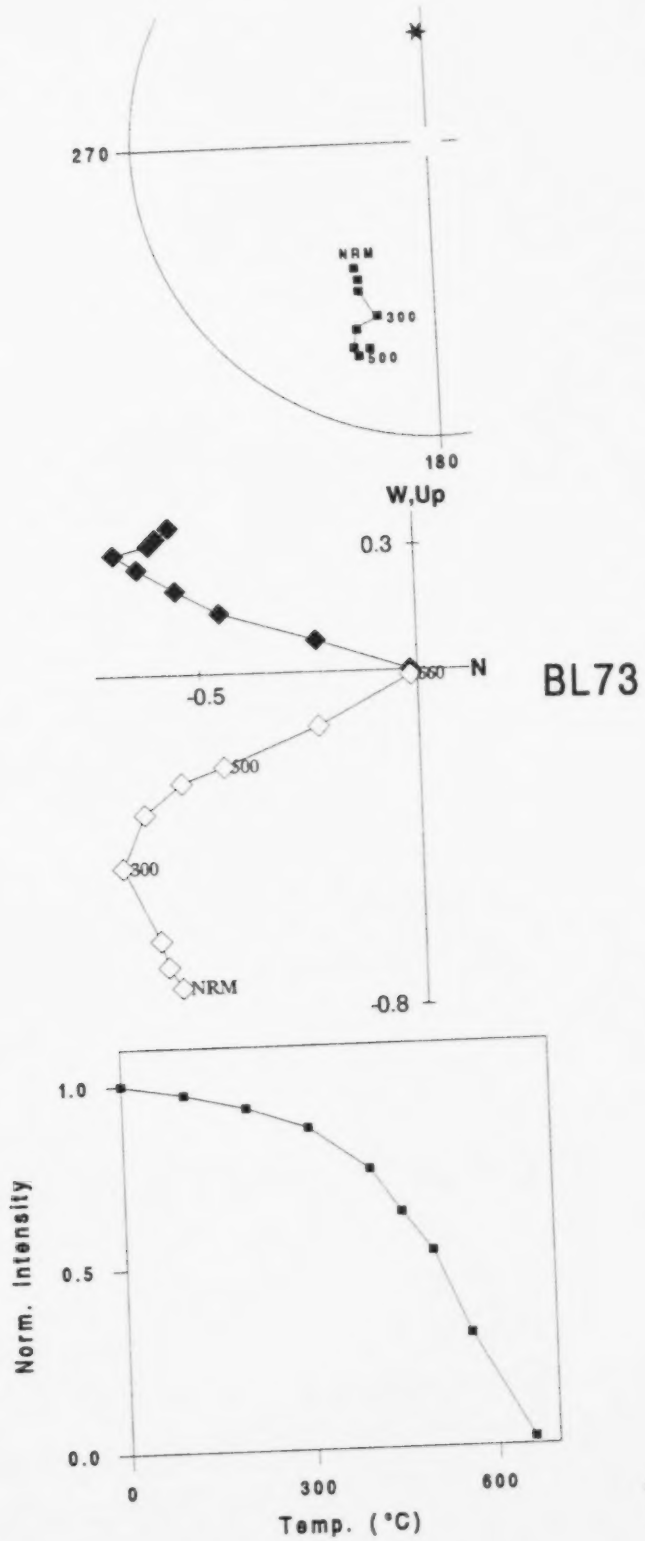
270
NRM
300
500
180
W,Up
0.3
-0.5
660
N
500
300
NRM
-0.8
1.0
0.5
0.0
Norm. Intensity
0
300
600
Temp. (°C)

BL73

f

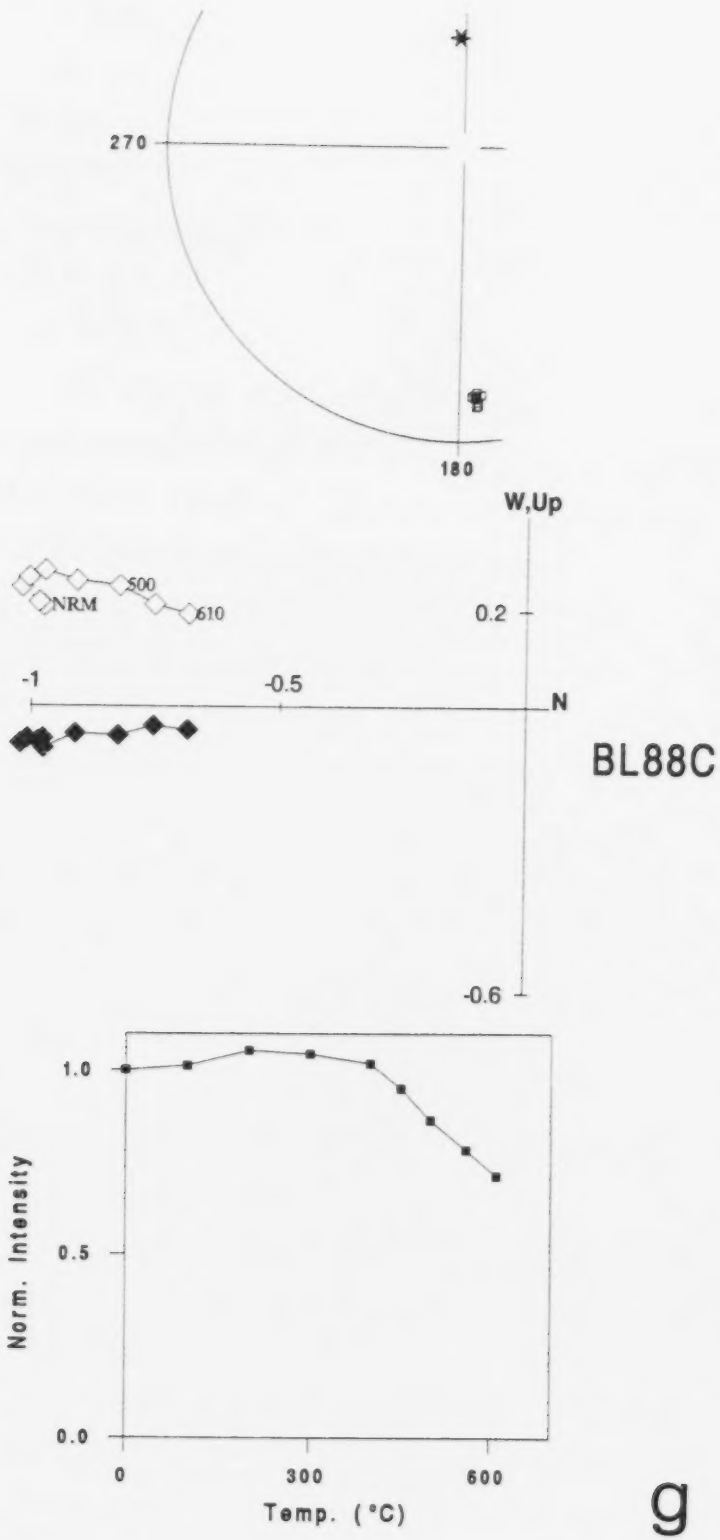
270
180
W,Up
NRM
500
610
0.2
-0.6
-1
-0.5
N
BL88C
1.0
0.5
0.0
Norm. Intensity
0
300
600
Temp. (°C)

g

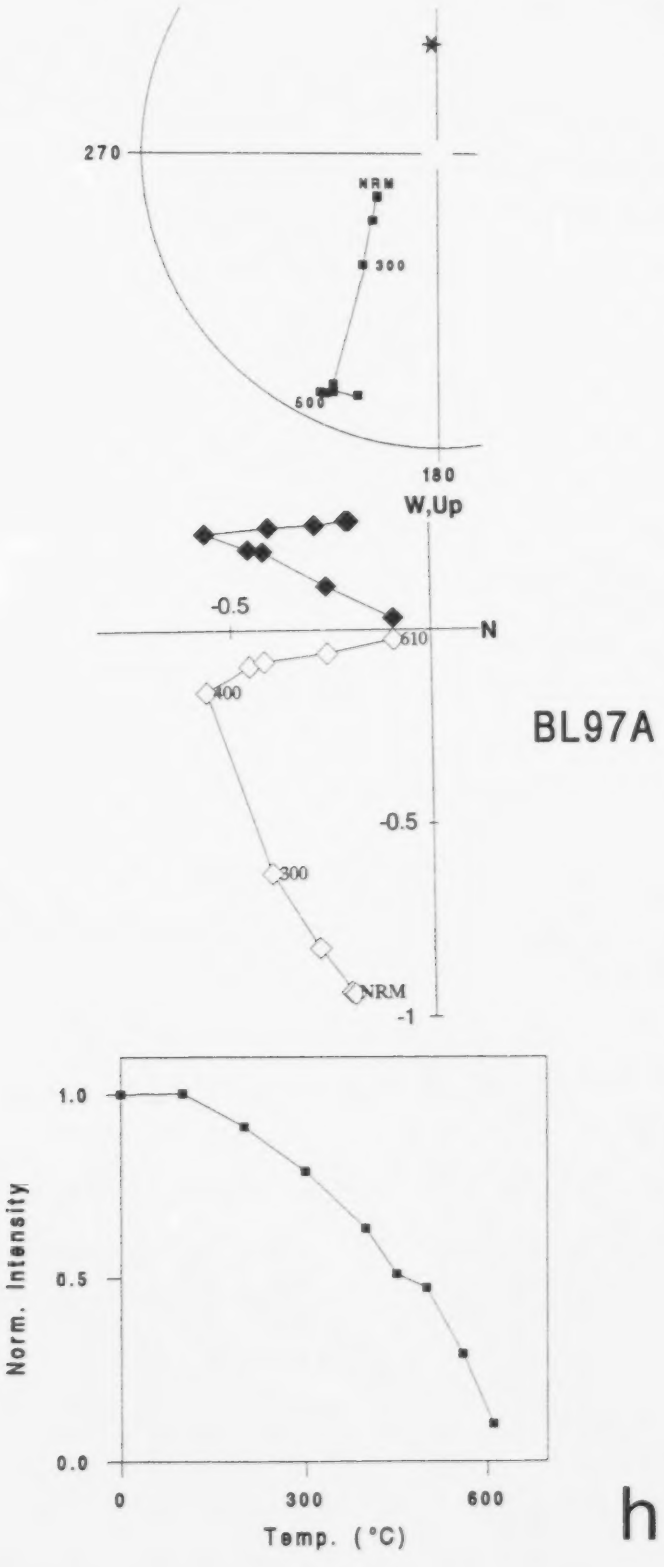
270
NRM
300
600
180
W,Up
-0.5
N
610
400
-0.5
300
NRM
-1
BL97A
1.0
0.5
0.0
Norm. Intensity
0
300
600
Temp. (°C)
h

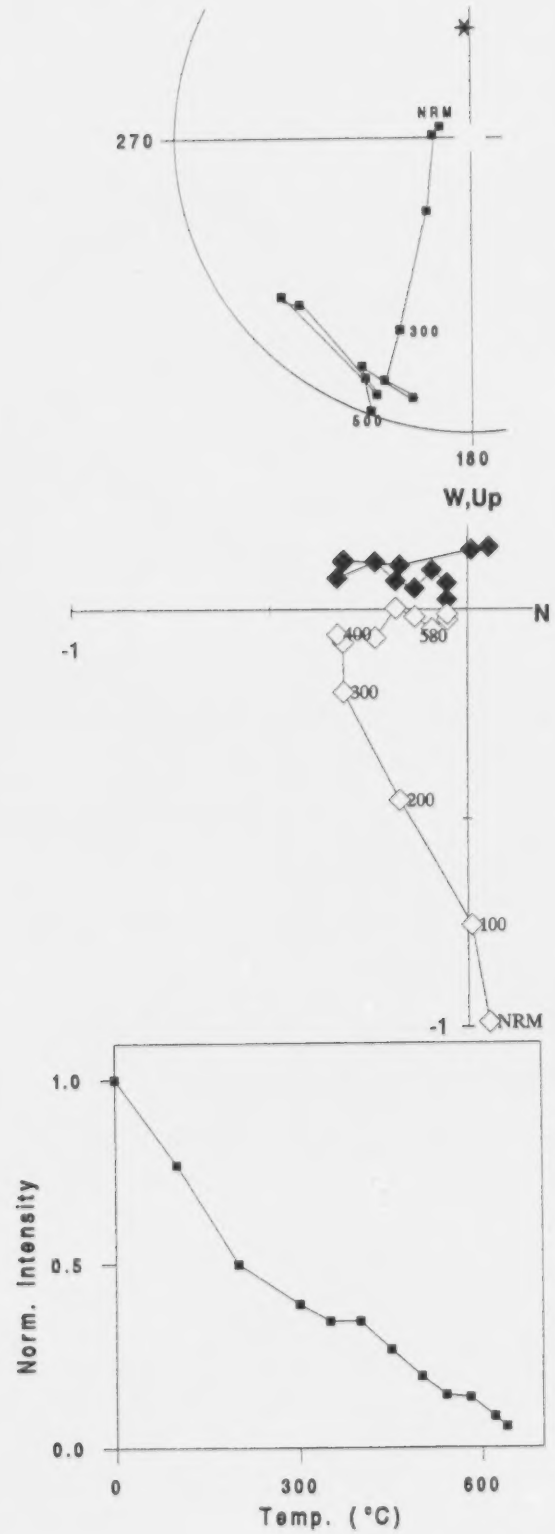
NRM
270
300
600
180
W,Up
N
-1
400
580
300
200
100
-1
NRM
1.0
0.5
0.0
Norm. Intensity
0
300
600
Temp. (°C)

BL121B

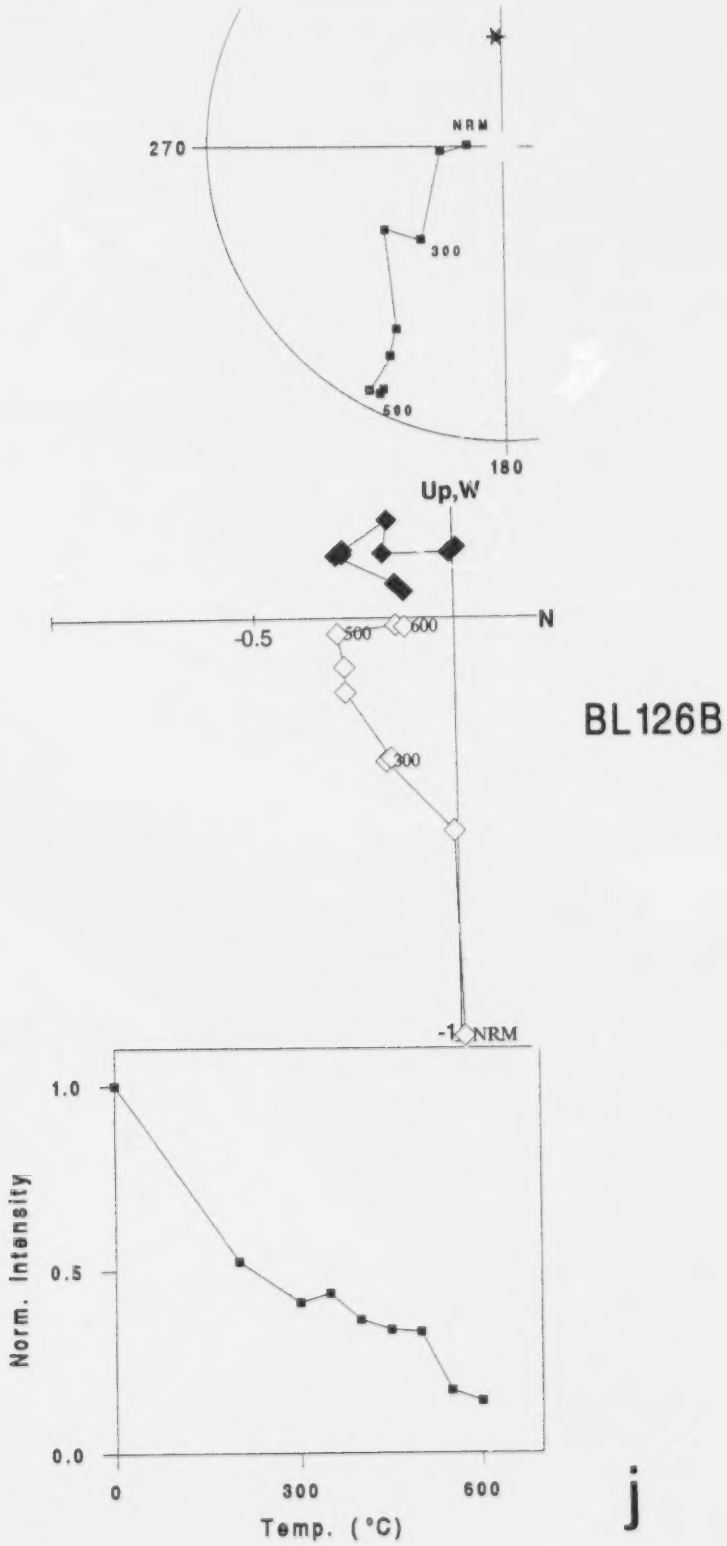
NRM
270
300
500
180
Up,W
N
-0.5
500
600
300
-1
NRM
1.0
0.5
0.0
Norm. Intensity
0
300
600
Temp. (°C)

BL126B

j

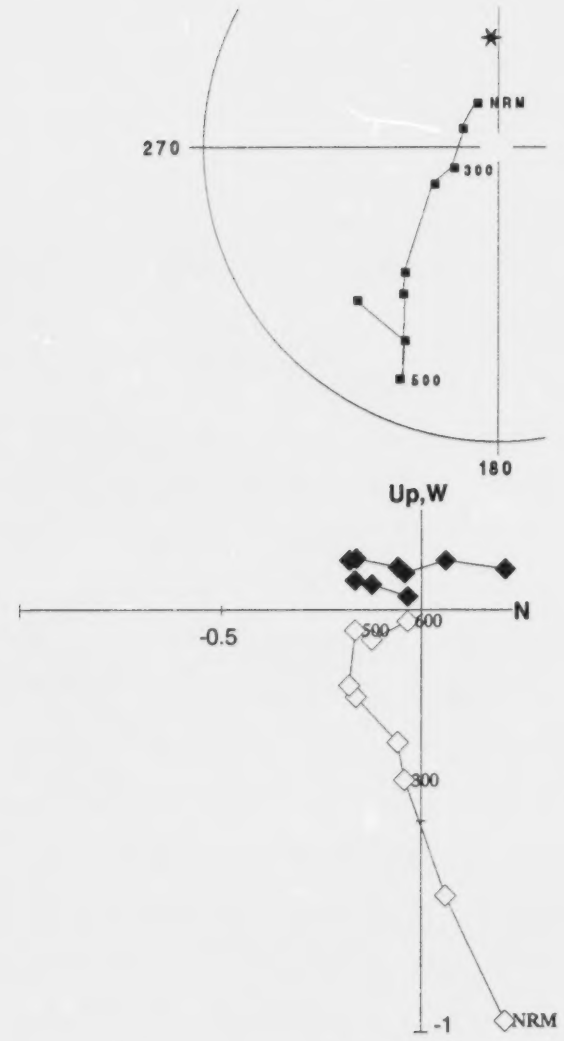
NRM
270
300
500
180
Up,W
N
-0.5
500
600
300
-1
NRM

BL131B

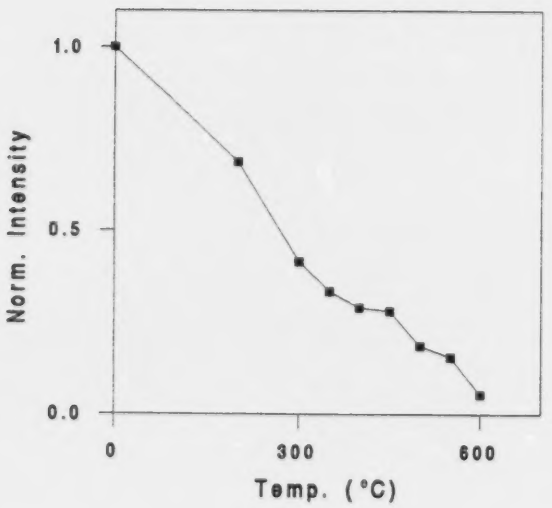
1.0
0.5
0.0
Norm. Intensity
0
300
600
Temp. (°C)

k

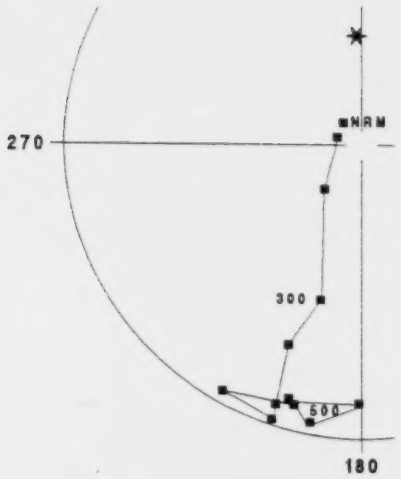
NRM
270
300
500
180

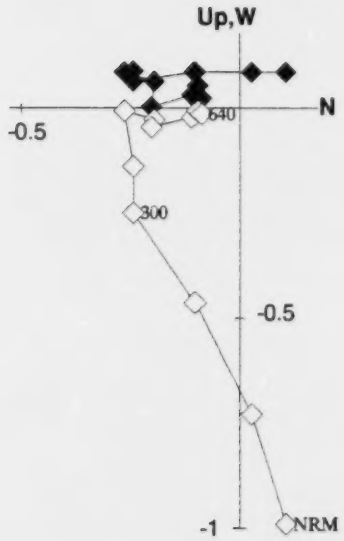
Up,W
N
-0.5
640
300
-0.5
-1
NRM

BLA51A

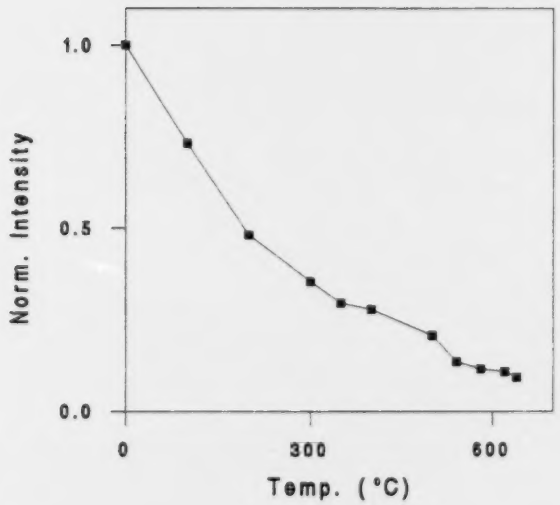
1.0
0.5
0.0
Norm. Intensity
0
300
600
Temp. (°C)

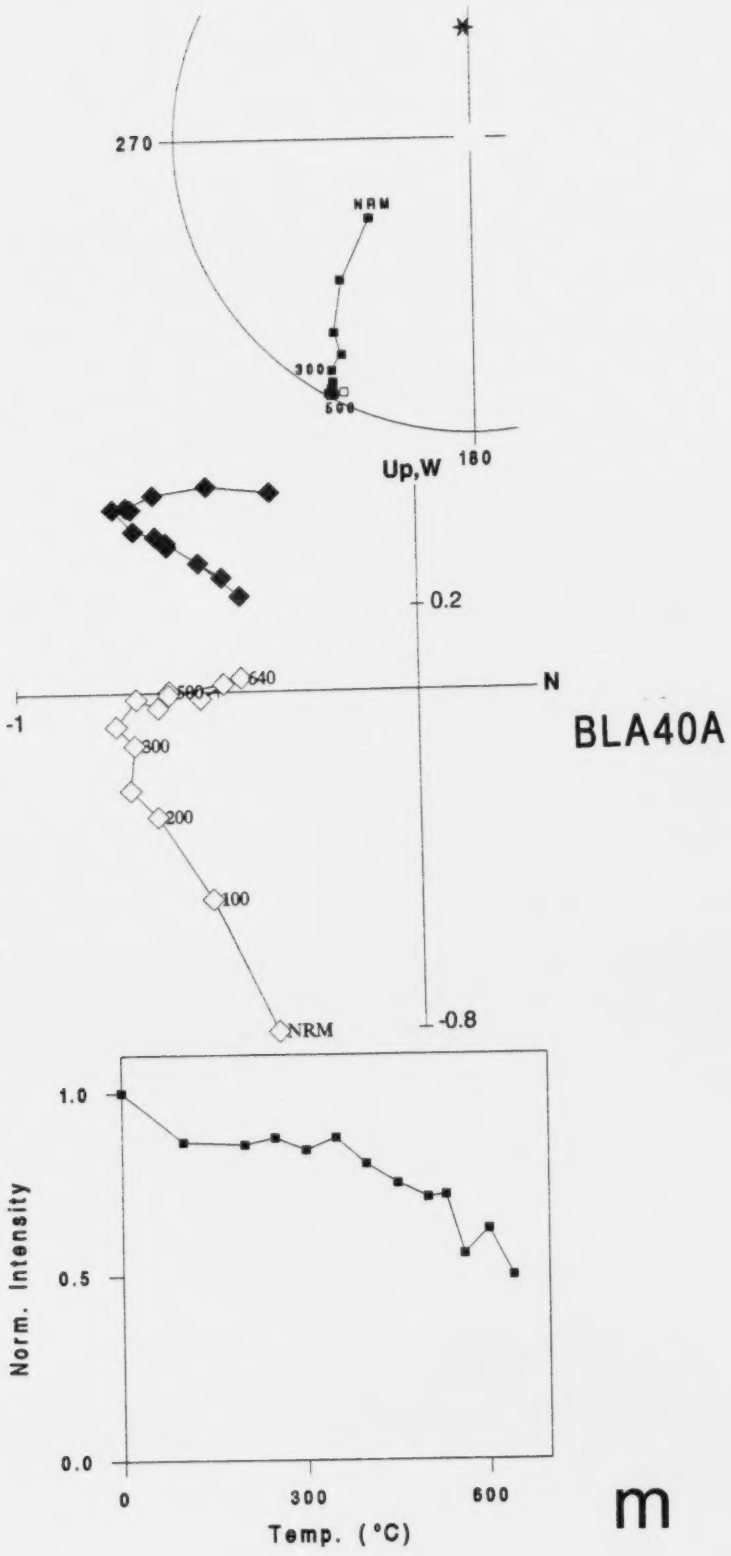
270
NRM
300
500
Up,W
180
0.2
N
-1
640
500
300
200
100
NRM
-0.8
BLA40A
1.0
0.5
0.0
Norm. Intensity
0
300
600
Temp. (°C)
m

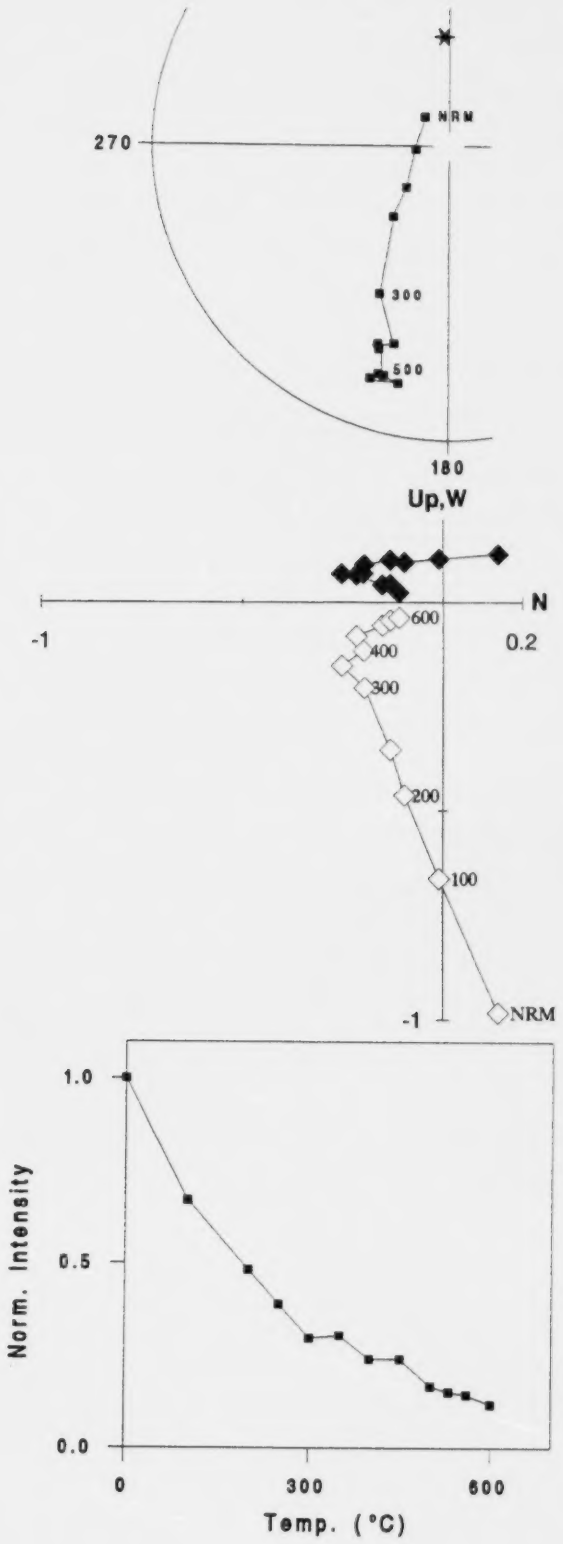
NRM
270
300
500
180
Up,W
N
-1
0.2
600
400
300
200
100
NRM
-1
1.0
0.5
0.0
Norm. Intensity
0
300
600
Temp. (°C)

BLA37B

n

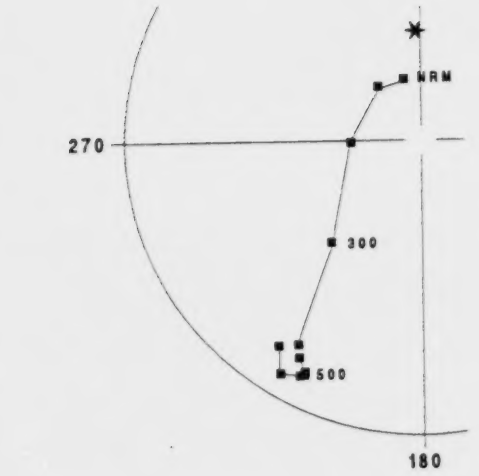
NRM
270
300
500
180

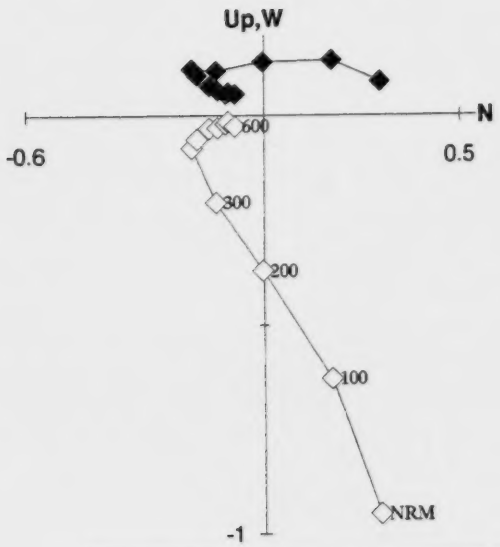
Up,W
N
-0.6
0.5
600
300
200
100
NRM
-1

BLA33A

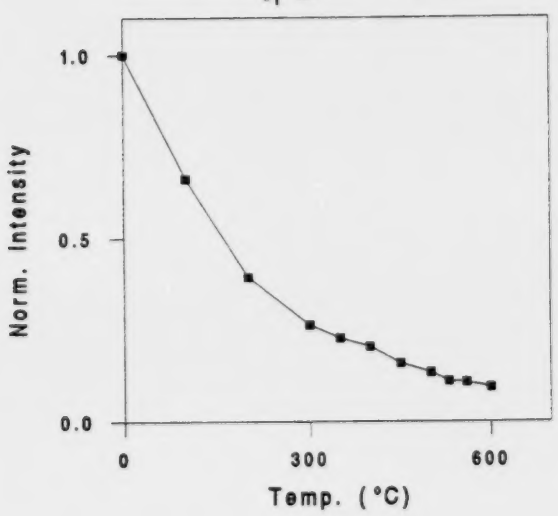
Norm. Intensity
1.0
0.5
0.0
0
300
600
Temp. (°C)

O

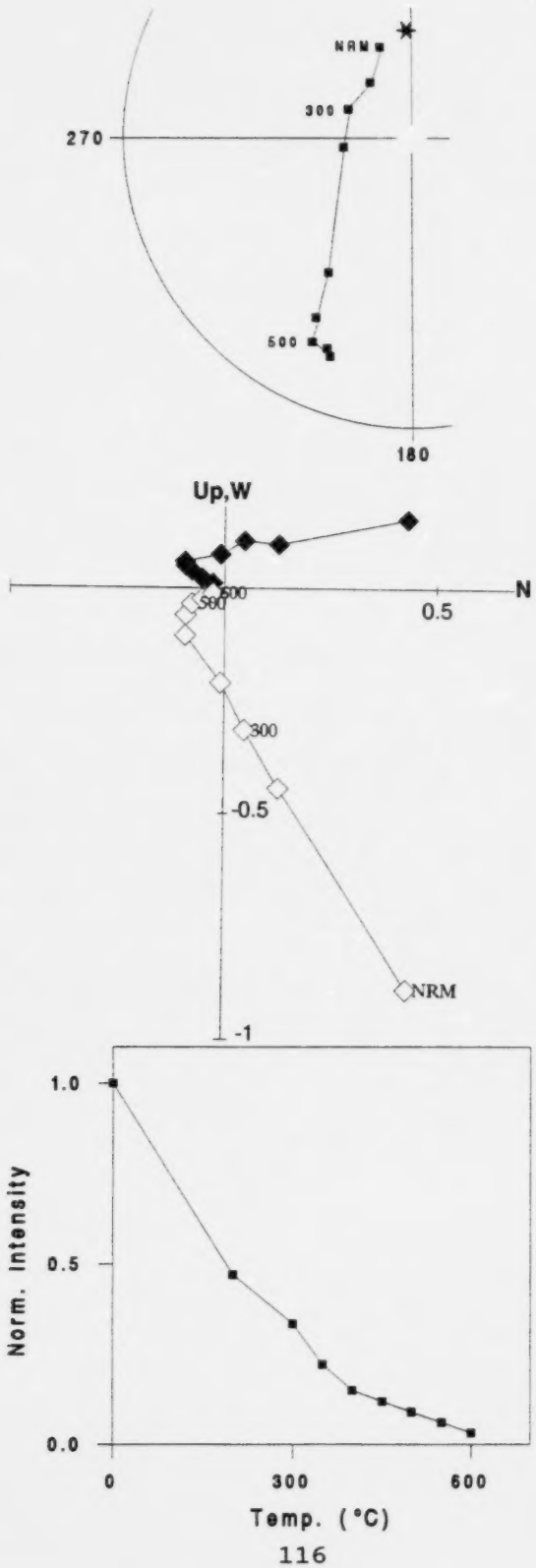
NRM
300
270
500
180
Up,W
N
600
580
0.5
300
-0.5
NRM
-1
1.0
0.5
0.0
Norm. Intensity
0
300
600
Temp. (°C)

BLA22A

p

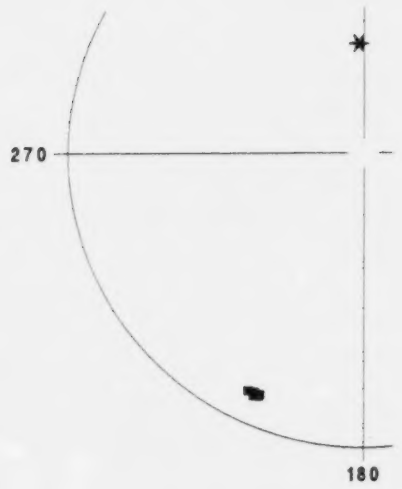
270
180

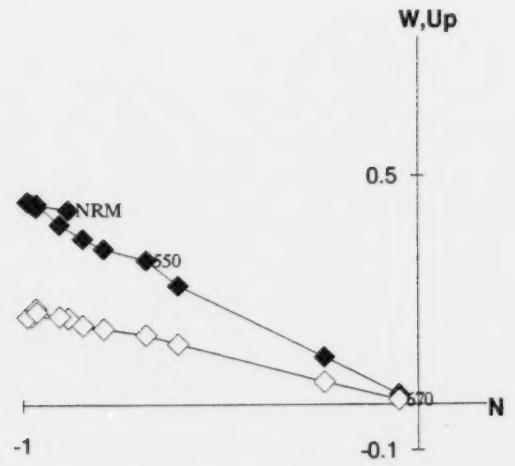
W,Up
0.5
NRM
550
670
N
-1
-0.1

BLA12C

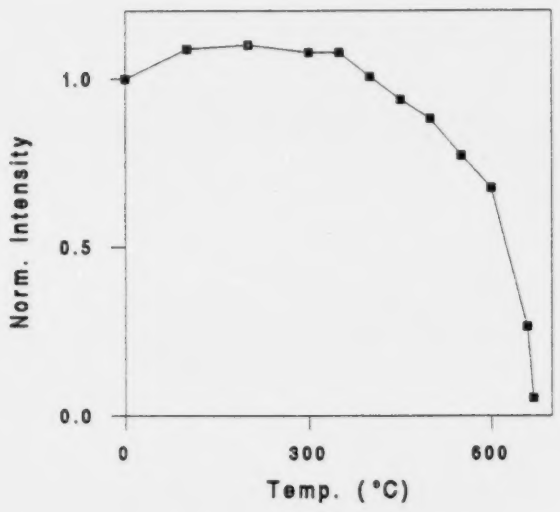
1.0
0.5
0.0
Norm. Intensity
0
300
600
Temp. (°C)

q

4.3 Presentation of directional data

4.3.1 Basin Traverse

From the initial collection, some specimens were destroyed during transportation despite the care taken in packaging; others did not survive the first trials of preparation described in section 2.5.1. As a result, there remained 201 specimens representing 108 sites separated by 1 to 20 m of stratigraphic distance. Fig.4.3 shows a polar equal area projection of the individual samples NRM's from the Basin Traverse. The "streaking" effect is very apparent, with data points scattered close to a great circle passing through the directions of the present and Permian fields. Fig.4.4 shows the directions after cleaning at 510°C, in a polar (Fig.4.4a) and equatorial projection (Fig.4.4b).

All the results shown up to this point were directions obtained in the geographical reference frame, i.e. without bedding correction. However, we have seen that the Lodève strata have a uniform dip towards the south and all directions must be corrected accordingly. Bedding planes were measured at regular intervals along the traverse and each result was corrected individually. Since the bedding variations are very small (typically less than a few degrees in strike and dip), there is no real possibility for a fold test. However, the simple fact than mean directions after bedding corrections are closer to the

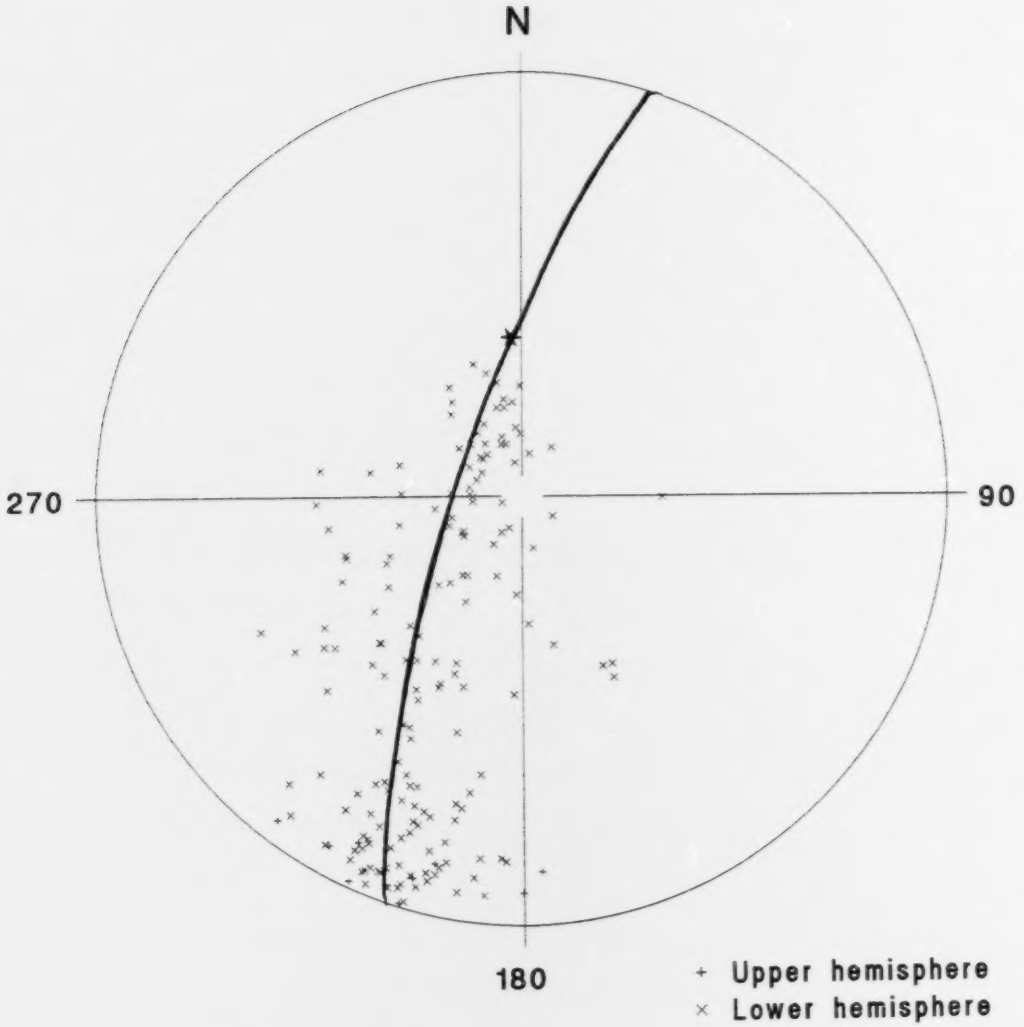

Figure 4.3. Polar equal area projection of NRM directions of individual samples from the Basin Traverse (no bedding correction). The star indicates the present day geomagnetic field, and the great circle represents the plane passing through the present and Permian field directions.

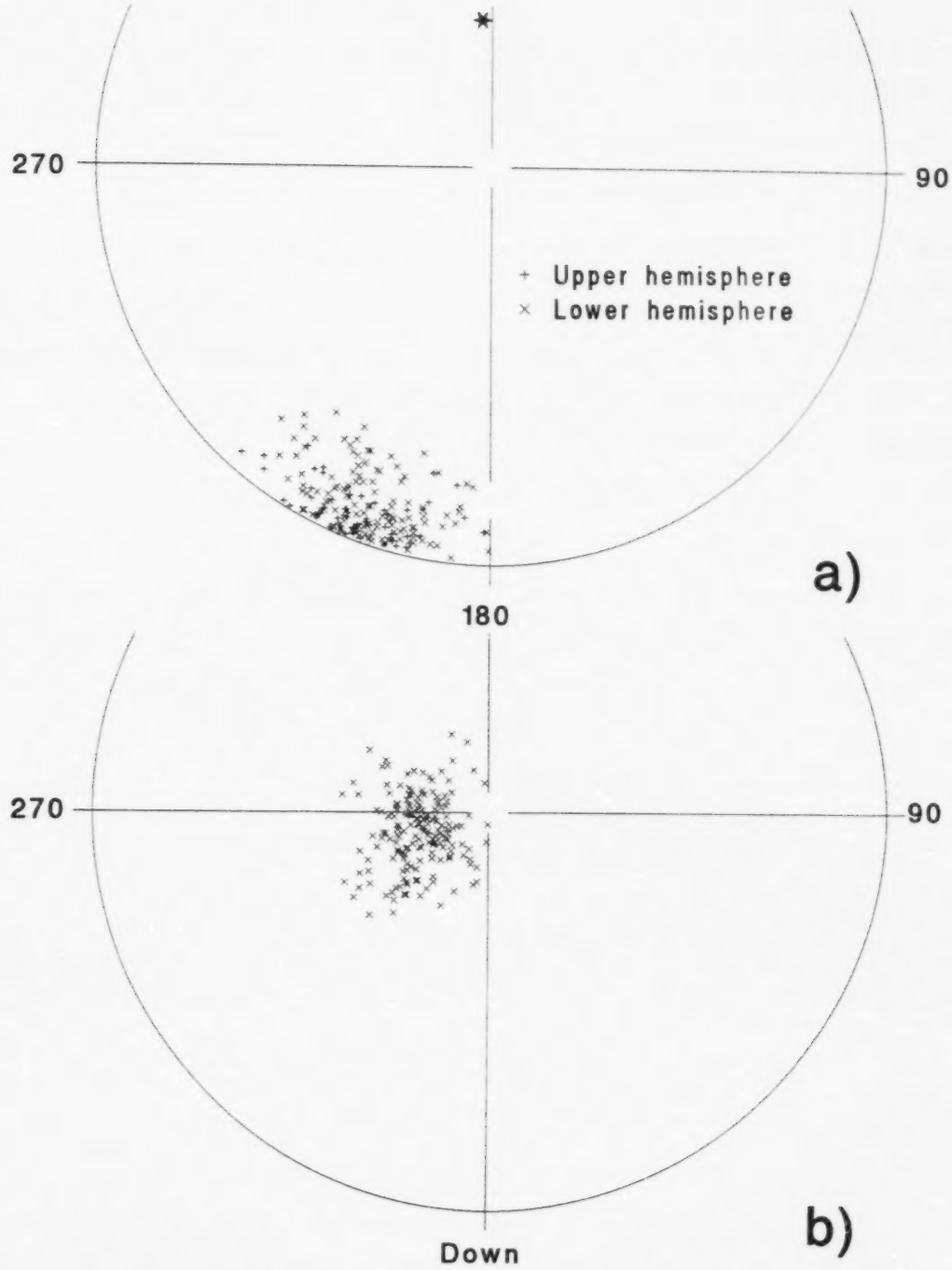

Figure 4.4. Polar (a) and equatorial (b) equal area projection of remanence directions of individual samples from the Basin Traverse after thermal treatment (no bedding correction). The star indicates the present day field.

well known Permian field than before correction is a good indication that the structural dip was acquired after acquisition of the remanence. This is further substantiated by the results presented in Chapter 3 that indicate a very early acquisition of the remanence. The standard paleomagnetic statistics (Collinson, 1983) calculated using Fisher's statistics (Fisher, 1953) are given in Table 4.2 below. Their significance will be discussed in Chapter 5.

	D	I	N	k	α_{95}
Individual samples	199.8	-5.7	201	31.5	1.8
site means	200.3	-3.8	108	35.4	2.3

Table 4.2. Statistics of directional data from the Basin Traverse.
D=declination of mean vector; I=inclination of mean vector; N=number of samples or sites; k=estimate of Fisher's precision parameter, α_{95}= semi-angle of the 95% confidence cone.

Although in most cases only the NRM and the remanence at 510°C were measured, it is tempting to use the whole data set to gain some more insight into the recent remagnetization (the modern overprint). An easily calculated parameter which gives a measure of the magnitude of the overprint is the angle (α) between the NRM vector and the characteristic remanence vector after

demagnetization. The greater the angle, the greater the overprint. A histogram of its distribution is shown in Fig.4.5. The sample population was split into two categories according to lithology and one can clearly see the difference between mudstones and coarser grained rocks. As explained earlier the greater overprint in mudstones is most likely due to more intense surface weathering.

A complication is caused by the fact that the magnetization vectors rarely move exactly along a plane passing through the present and Permian field directions. The discrepancy can be quantified by calculating another angle (β), this being the angle between a vector normal to the ideal plane defined by the present/Permian field directions, and a vector normal to the plane defined by the NRM/demagnetized remanence directions. This was done using a convention giving a positive sign to the angle β when the demagnetization plane projection is located East of the ideal plane in Fig.4.3. The distribution is shown in Fig.4.6. It is seen that a majority (78%) of the demagnetization planes are within 20° on either sides of the ideal plane, but that some discrepancies are substantial. This can best be explained by the presence of the third, low temperature component that was revealed below 100°C during stepwise demagnetization (see section 4.2), and that tends to scatter the demagnetization planes

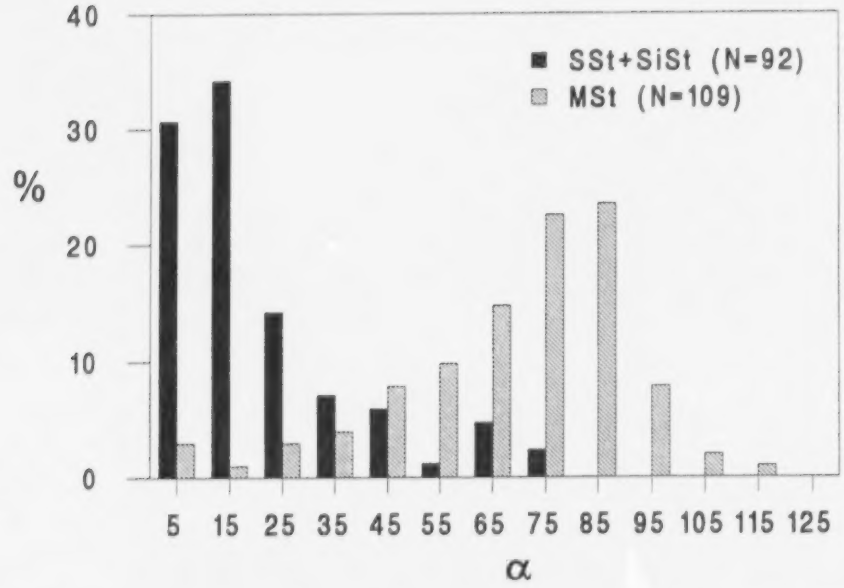

Figure 4.5. Histogram of the angle α betwee NRM and cleaned directions calculated for each specimen.

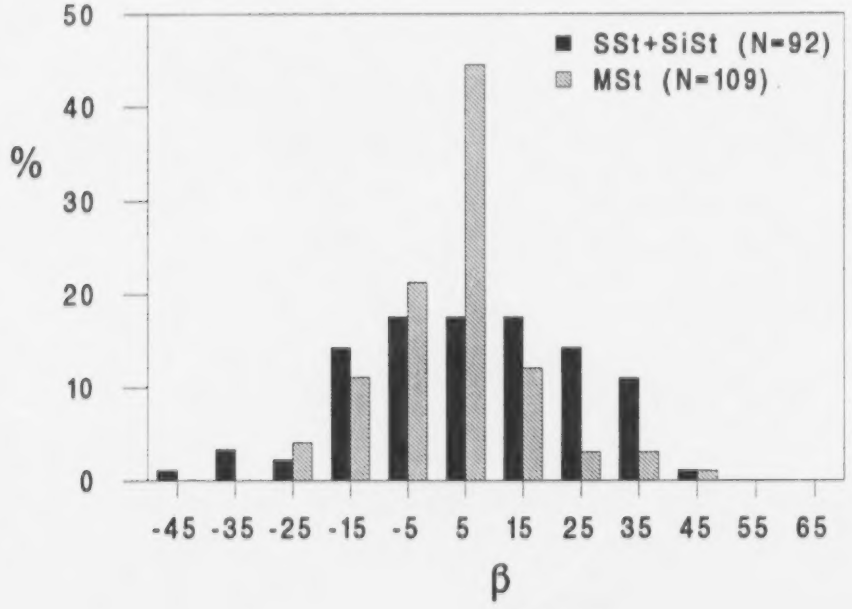

Figure 4.6. Histogram of the angle β between the normal to the plane defined by the present-day/Permian field directions and the normal to the plane defined by NRM/cleaned directions of each specimens.

away from the ideal plane. In this case one does not observe a clear distinction between sandstones/siltstones and mudstones, except for a tendency of the former to have a broader distribution. This can be simply explained by the smaller modern overprint and thus a comparatively greater effect of the third component.

After examining the Basin Traverse data set as a whole it is now time to see how the results are organized stratigraphically. Indeed the main goal of this study was to recover information about the time variations of the magnetization directions, and as described previously, the sampling scheme was designed so as to know precisely the stratigraphic distribution of the sampling sites. The complete data series is shown in Fig.4.7 where each point represents an individual sample. Fig 4.8 represents the site means obtained by calculating the vectorial average when more than one sample is available at the same stratigraphic horizon. A complete listing of the data with the number of samples at each site can be found in Appendix 1b. On Fig.4.8 is also represented a smoothed variation curve (thick line) obtained by spline interpolation of the data to regular 5 m intervals and smoothing using a 20 m sliding window. Despite the initial large intervals between sites, a simple examination reveals marked, coherent oscillations in most parts of the record. The amplitude of these variations can reach 25° in

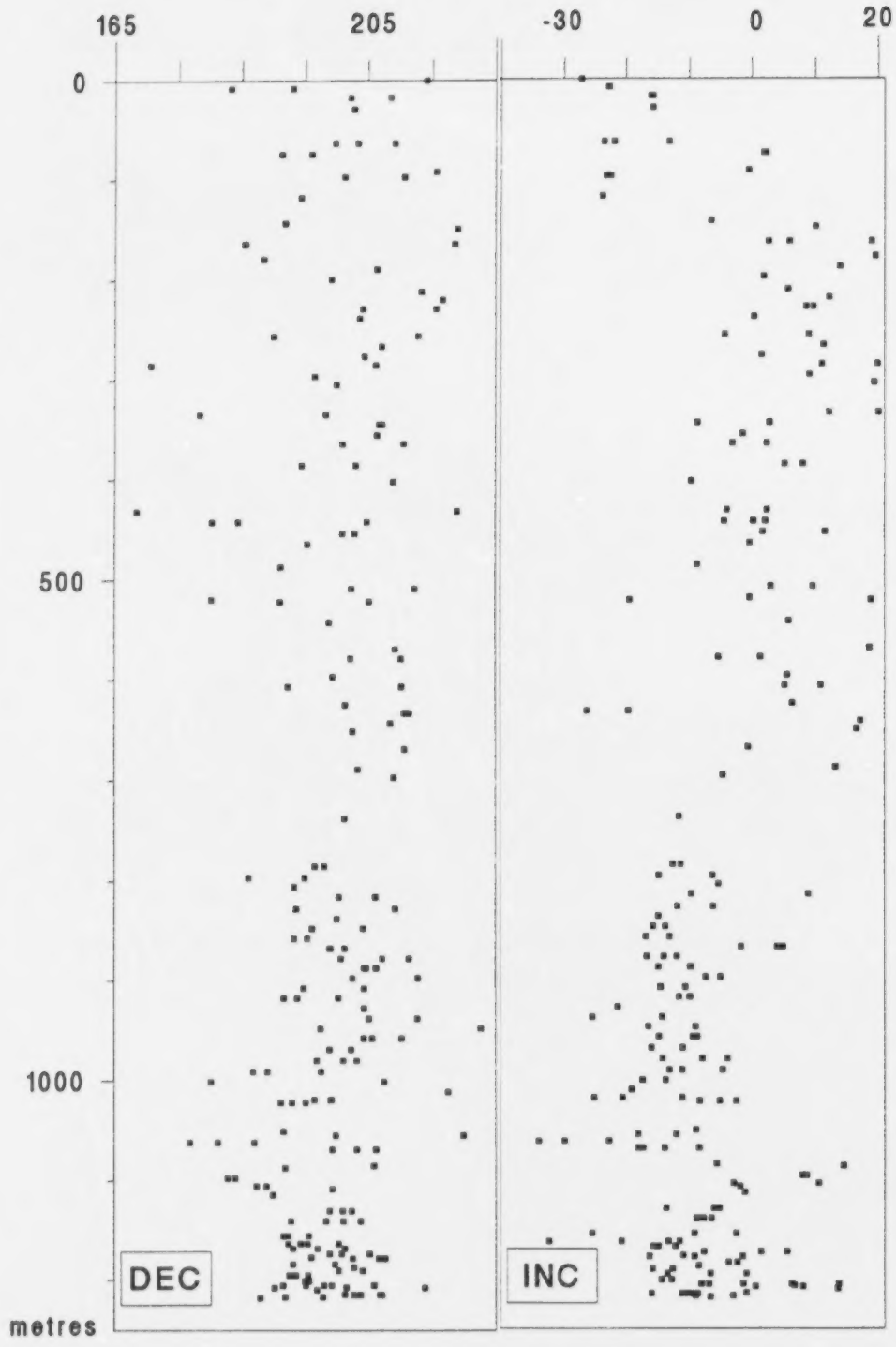

Figure 4.7. Declination (DEC) and Inclination (INC) magnetograms for the 201 samples of the Basin Traverse.

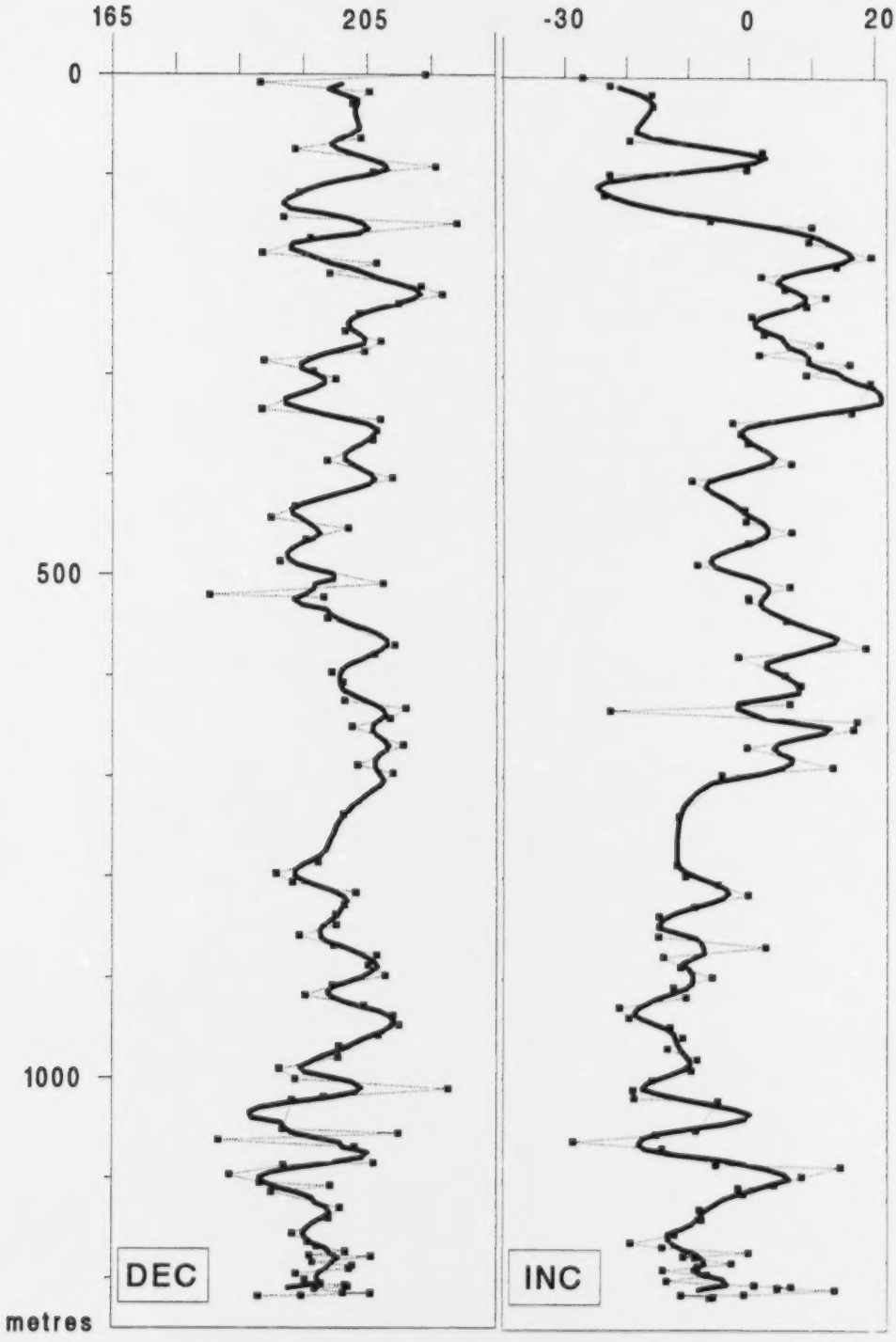

Figure 4.8. Declination (DEC) and Inclination (INC) magnetograms for the 108 site means of the Basin Traverse. The thick line is obtained by smoothing of the data using a 20m sliding window.

both declination and inclination. The significance of these oscillation patterns will not be examined here except to point out that they are similar to observations reported by Baag and Helsley (1974) and Van den Ende (1977) in other redbed formations, which were interpreted as paleosecular variation records. A full account of the analysis performed on the Lodève data will be given in Chapter 5.

4.3.2 Closely spaced samples

After the encouraging results obtained from the widely spaced samples, it became evident that more information was needed on the small scale behaviour of the magnetization. The interesting results obtained for the intensity of magnetization have been reported in Chapter 3, but the corresponding vectorial data still remain to be described.

The most important finding is that variations of magnetization directions are indeed present even at the much smaller scale used in this part of the study. In addition, the oscillation patterns appear to be coherent and seem to be the expression of a definite, underlying physical process. At three locations, several sections of the same horizon could be sampled, and this allows correlations between records. In all cases, fairly convincing correlations can be made between main features of the magnetograms. These comparisons often show vertical

shifts of the main features between equivalent sections that can be explained by bed thickness variations, very common in continental deposits.

All results are displayed in a series of figures (Fig.4.9 through 4.14) that show declination and inclination magnetograms obtained at all the sites already described in Chapter 3 (see Table 3.1). Again the meaning of these fine scale variations will be examined in the next chapter.

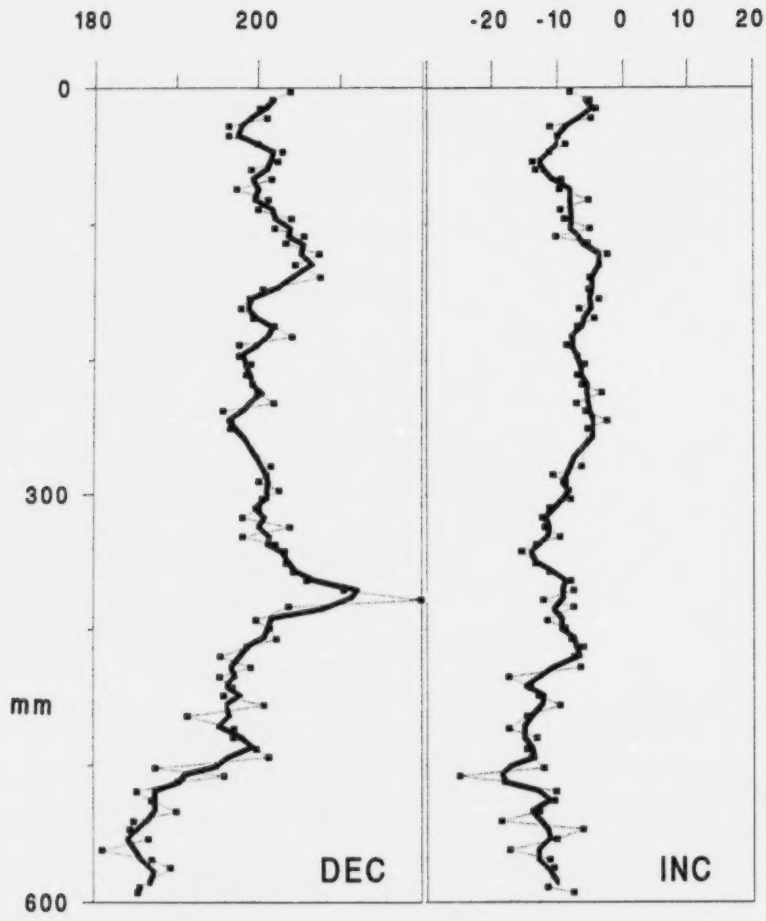

Figure 4.9. Declination (DEC) and Inclination (INC) magnetograms for section 1 of site BLF. Depths are in mm. The thick line is obtained by smoothing of the data using a 3 point moving average.

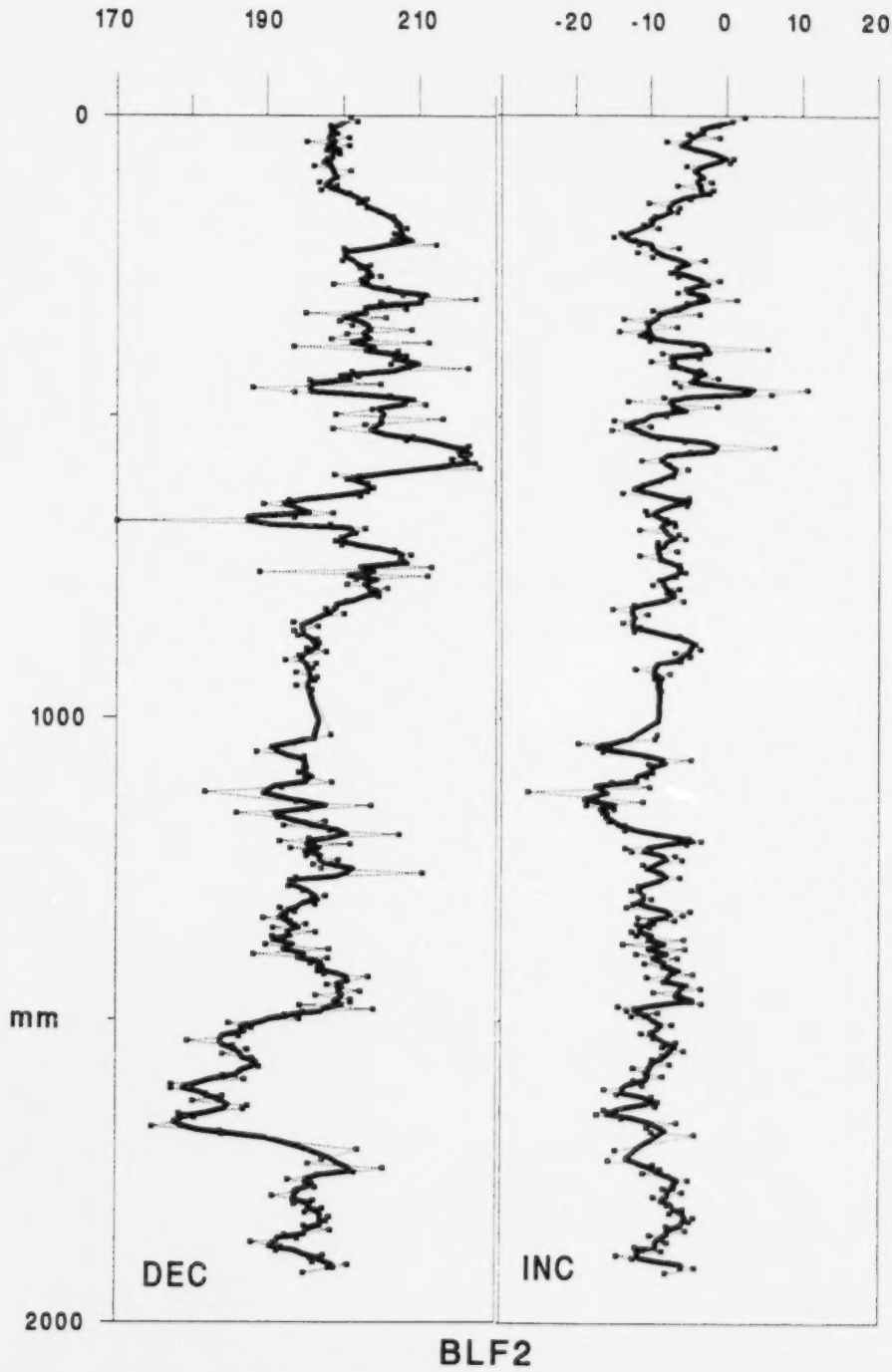

Figure 4.10. Declination (DEC) and Inclination (INC) magnetograms for section 2 of site BLF. Depths are in mm. The thick line is obtained by smoothing of the data using a 3 point moving average.

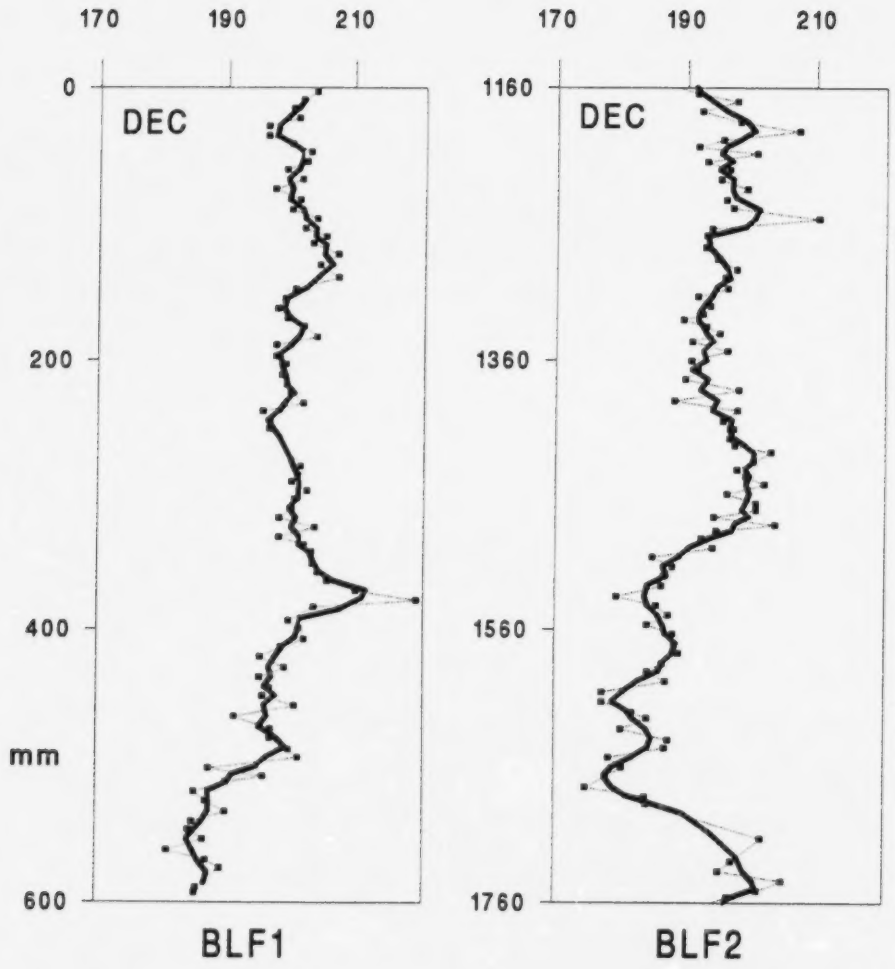

Figure 4.11. Compared declination records of the two sections sampled at site BLF. The top of BLF1 corresponds to a depth of 1160mm in BLF2 (determined by stratigraphic correlation in the field). Similarities can be found in both records, particularly the westward motion of the direction present in the lower parts of both declination curves. Vertical shifts are expected and can be easily explained by thickness variations very noticeable over the 30m separating the two sections. Depth in mm.

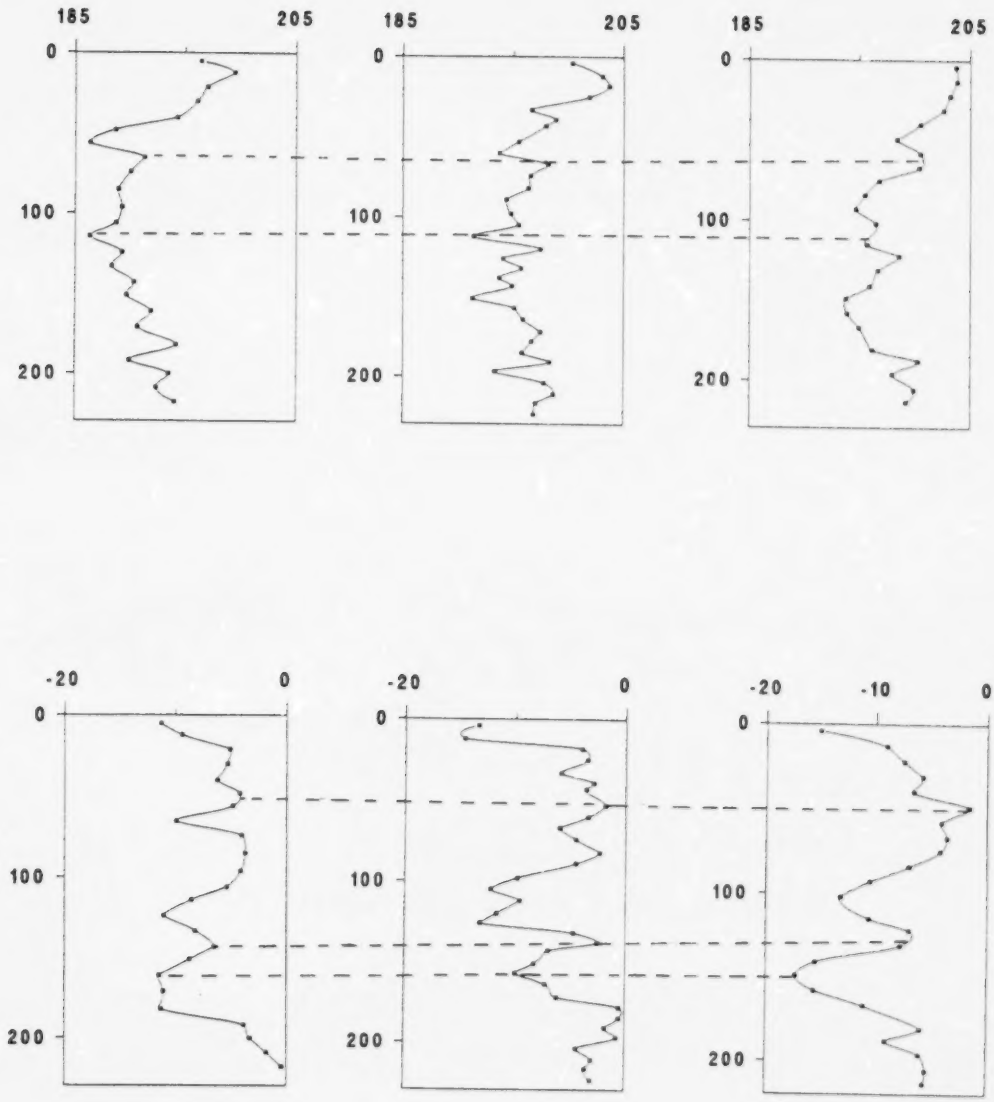

Figure 4.12. Compared declination (top) and inclination (bottom) records for 3 cores collected at site BLP (intercore distances 40 and 50cm). Dashed lines indicate tentative correlations of certain features. Depth in mm.

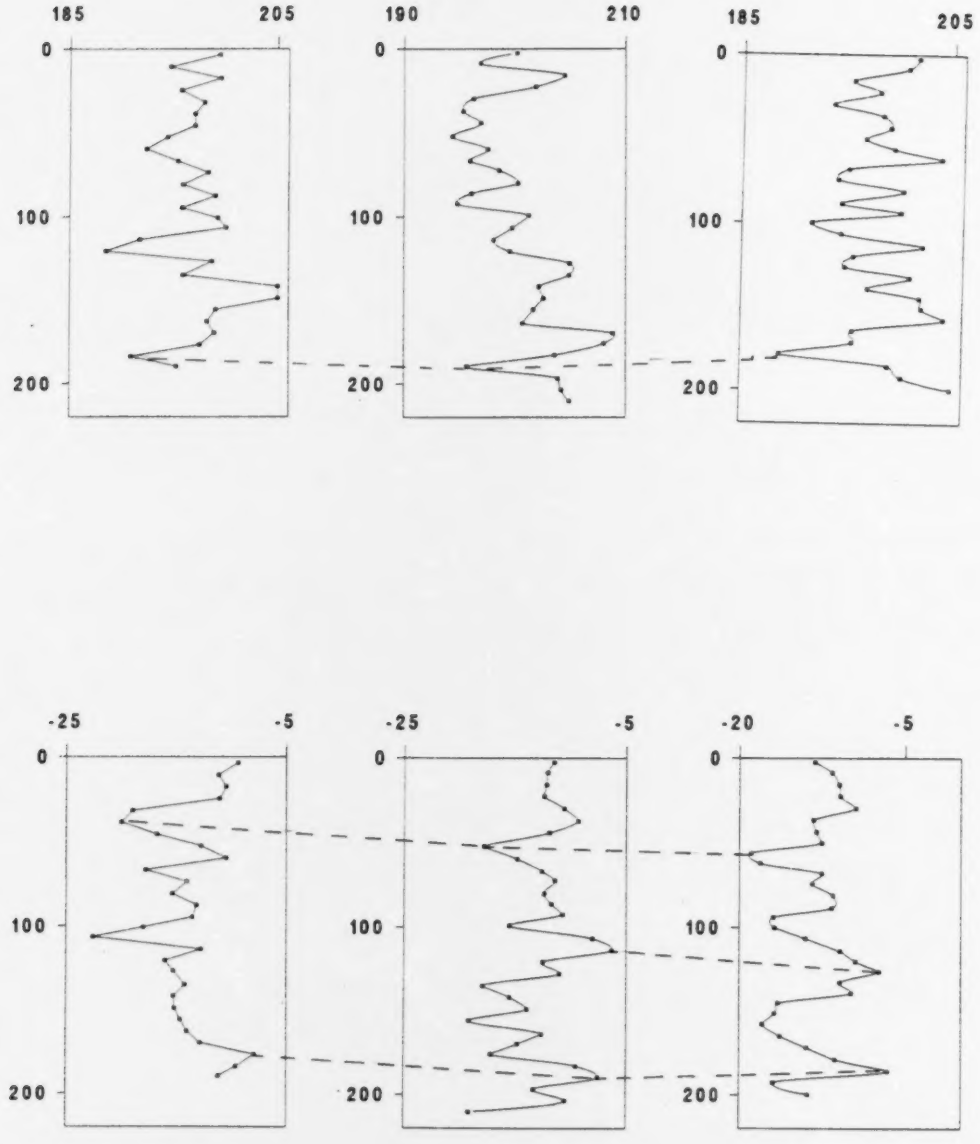

Figure 4.13. Same as Fig.4.14 for site BLJ; intercore distances 30 cm.

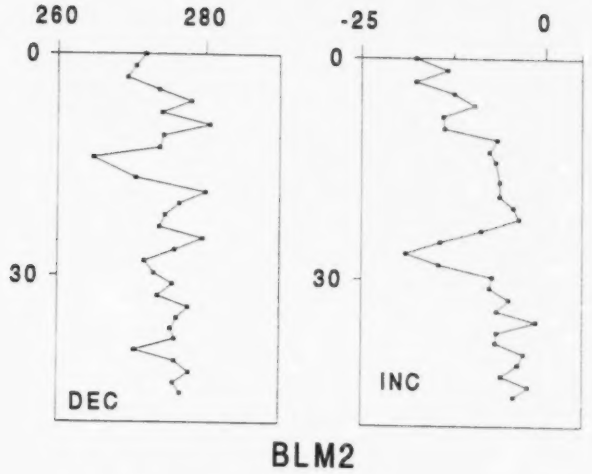

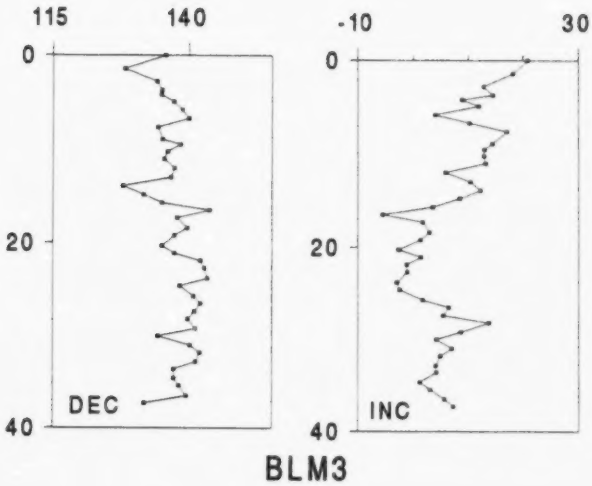

Figure 4.14. Declination and inclination records for 2 mining core segments. Declinations are with respect to an arbitrary origin. Depth in mm.

CHAPTER 5

GEOPHYSICAL INTERPRETATION OF DIRECTIONAL DATA

5.1 Introduction

We have seen in the previous chapter that directional variation patterns are observed in the Lodève strata, at scales ranging from several hundreds of metres in the Basin Traverse to a few centimetres in the closely sampled sections. No definite interpretation of these patterns has been made so far in order to first present only observational facts, without the possible subjectivity associated with interpretation. It is now time to see what exploitation of these observations can be made within a geophysical framework.

Obviously, the main question is whether or not these variations are indeed the expression of geomagnetic phenomena, and more specifically whether they constitute a record of paleosecular variation during the late Permian. This issue will be addressed first with all precautions required by the study of material dating back several hundreds of millions of years. We will then see what can be learned from these data by analyzing its angular dispersion, which is the most widely used approach in PSV

studies since it can be calculated for all data sets regardless of the stratigraphic/time relationship between individual results. However, the present study went one step further since the actual stratigraphic position of each sample is known. This offers, at least in principle, the possibility of analyzing the data sets as real time series and thereby obtaining more information than the mere amplitude of the variation.

5.2 Interpretation of directional variations

Declination and inclination magnetograms from the Basin Traverse and the closely sampled sections (see Fig.4.7 to 4.14) indicate that non-random directional variations are found in all data sets. This property is suggested by the fact that in several parts of the records, sequential variations are indicated by several data points organized in coherent patterns. In other words, directions from adjacent horizons are more alike than those from different elevations. This feature can be quantified by analyzing the short-range or *serial* correlation of directions.

A statistical test was devised by Watson and Beran (1967) to accommodate paleomagnetists' need for a way to quantify serial correlations between directional data. Suppose that $X_1,\ldots,X_N$ represent the direction of

magnetization at N successive points in a magnetogram. If there is a strong nearest neighbor correlation, the angle between successive vectors will be much smaller than the angle between vectors with very different serial numbers. If the cosine of the angle between successive vectors is used, it will be large. They therefore propose, as a statistic, the sum (L) of the cosines of the angles between directions at adjacent points in the sequence, with large L indicating significance. This parameter, also called path length is given by:

$$L=\sum_{i=1}^{N-1} X_i . X_{i+1}$$

In order to assess the significance level, a distribution is needed to compare the observed L with, to determine if it is improbably large. This can be done by selecting at random a large number of permutations (P) of the original data set and calculating L(P) for each P. The significance level can then be determined from the fractions of the L(P) distribution above and below the observed L.

This test was performed on site means of the Basin Traverse as well as on data from site BLF2, the longest closely sampled section. In both cases a serial correlation is detected with significance level better than 99%. Results are given in Table 5.1 below.

	N	L	p
Traverse	108	103.66	99.3
BLF2	265	259.65	99.7

Table 5.1. Results of Watson & Beran's test.
N: number of data points; L: observed path length;
p: % of $L(P) \leq L$.

This strongly suggests that the magnetic direction variations are indeed the recording of a definite physical process. As in all studies of this kind, the exact nature of the process is impossible to prove, but there is no reason to suppose that the remanence direction variations are not due to geomagnetic fluctuations at the time of acquisition of the magnetization.

One legitimate concern is that direction fluctuations are caused in some way by geological phenomena. Even if the magnetization is detrital, it is difficult to imagine how mechanical causes intervening during the deposition could produce coherent variations both in declination and inclination with the observed amplitude. This becomes even more unlikely if, as was suggested in Chapter 3, the orientation of the magnetic grains was acquired by early post-depositional processes. Diagenetic effects could also be invoked. Early chemical reactions could cause a partial remagnetization or acquisition of secondary magnetizations in directions differing from the primary remanence. This would indirectly produce variations in the resultant

remanence vector. It is possible that such secondary magnetization would be resistant to magnetic cleaning. However, if chemical processes affected the magnetization direction, it is very likely that they would also affect magnetic properties like susceptibility and intensity. One would therefore expect to detect correlations between vectorial and scalar variations. This eventuality was tested using the 265 measurements from site BLF2 where both kinds of variations are substantial. As shown in Fig.5.1 and 5.2 no hint of a correlation is observed.

In addition to the considerations mentioned above, it was seen that the average direction of magnetization is coincident with the Permian field direction determined in other studies. Furthermore, there are good reasons to believe that the remanence was acquired shortly after deposition, possibly by (post-)depositional phenomena (see Chapter 3). Finally, it was seen in Chapter 4 that directional patterns are well correlated for laterally equivalent sections. All this suggests that what is observed in the Lodève strata is a record of paleosecular variation during the Permian. Consequently, the remainder of this chapter will deal with the utilization of the data to learn more about the Permian geomagnetic field.

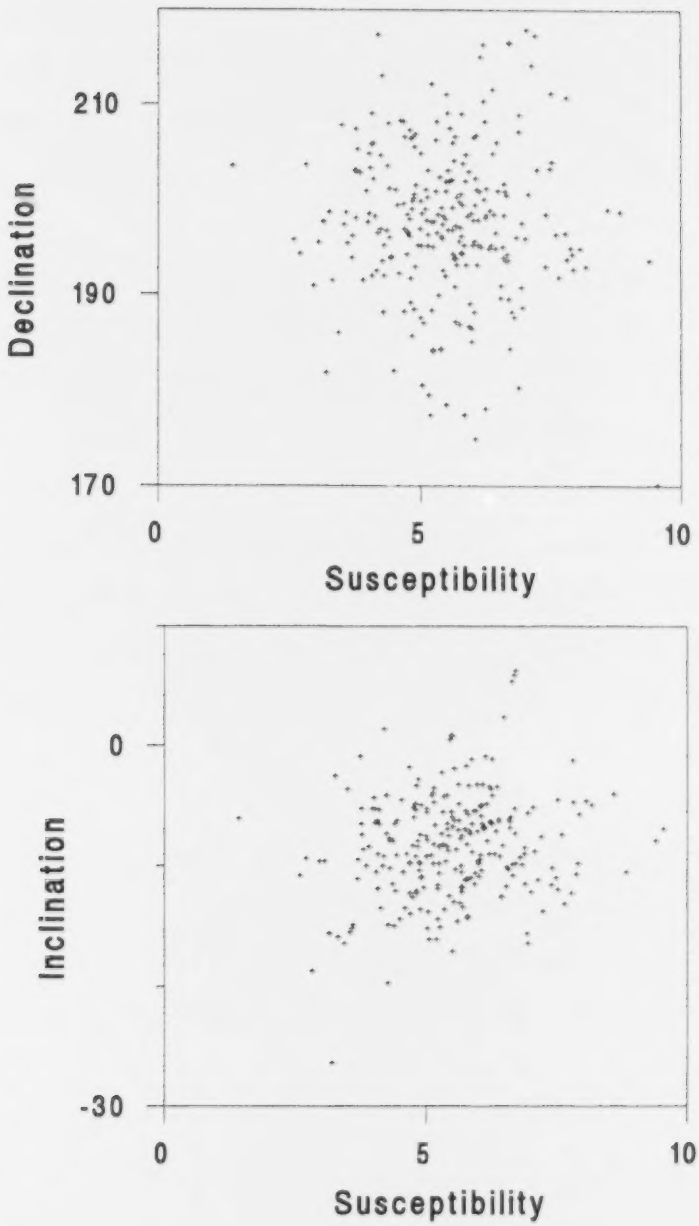

Figure 5.1. Plots of Declination (top) and Inclination (bottom) vs. susceptibility for section BLF2. No trend or correlation is apparent. Angles in degrees and susceptibility in 10^{-8} m^3kg^{-1}.

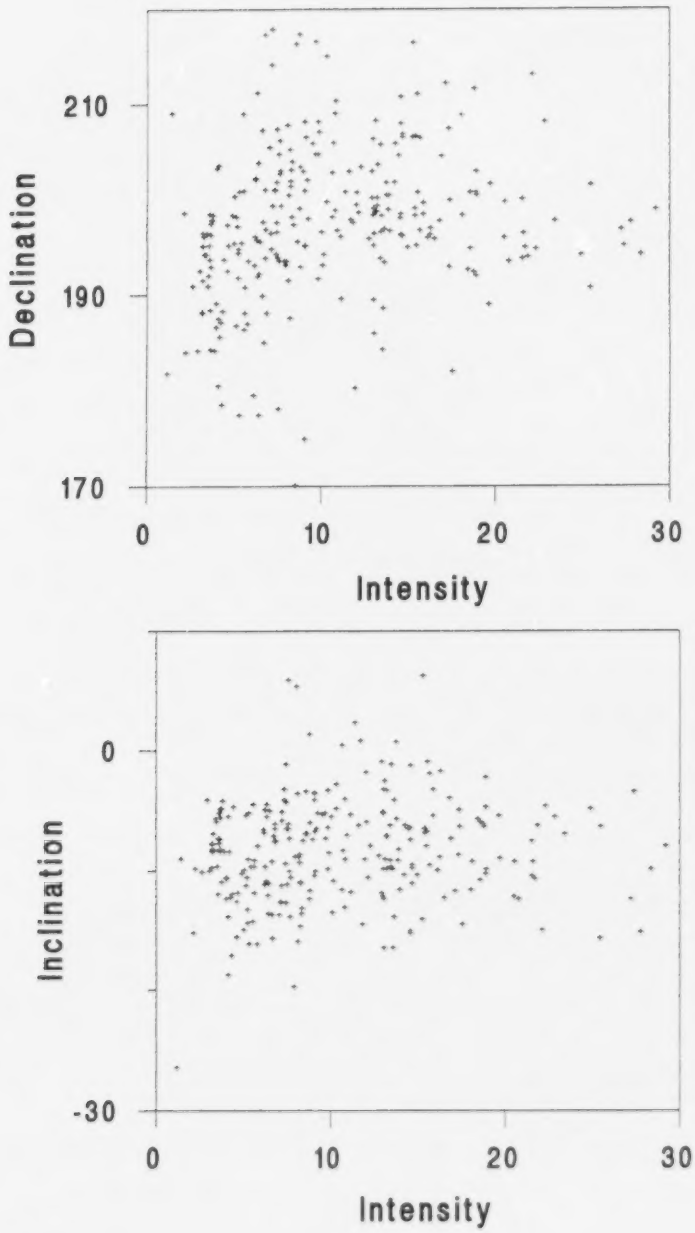

Figure 5.2. Plots of Declination (top) and Inclination (bottom) vs. intensity for section BLF2. No trend or correlation is apparent. Angles in degrees and intensity in 10^{-6} Am^2kg^{-1}.

5.3 Angular dispersion

5.3.1 Existing paleosecular variation (PSV) models

Angular dispersion of the geomagnetic field over long time periods is the aspect of geomagnetic secular variation most accessible to paleomagnetic studies. If one is reasonably satisfied that the observed magnetic direction variations are due to PSV, one can obtain an estimate of the amplitude by calculating the angular dispersion of the directions. There is no need to know the exact time sequence of the data but only an estimate of the corresponding total time span, and this makes this method applicable to nearly all paleomagnetic studies.

Two approaches can be taken by finding the dispersion of either field directions or virtual geomagnetic poles (VGP), calculated as shown in Appendix 3. It is now well known that the dispersion is a function of latitude. We have seen in section 1.3 that it is convenient to separate the contributions of the dipole and non-dipole field when attempting to model the latitude variation, and since VGP dispersion resulting from any motion of the main dipole is latitude invariant, the approach using VGP dispersion is generally favored.

This approach has been used in several PSV models enumerated in section 1.3 and summarized by McElhinny and Merrill (1975) and McFadden and McElhinny (1984). These models have been compared to actual data from the present

day geomagnetic field and to paleosecular variation data at various latitudes. Since the contribution of the dipole part of the field is latitude invariant, fitting of the models to real data allows one to calculate the relative contributions of dipole and non-dipole components to the VGP dispersion (see Merrill and McElhinny, 1983).

More recently, McFadden et al. (1988) developed a new model (model G) in which the VGP scatter is divided into contributions from the primary (dipole) and secondary (quadrupole) dynamo families. Roberts and Stix (1972) have shown that under certain conditions, the magnetic field solutions for a spherical dynamo separate into two completely independent families, which they refer to as the dipole and quadrupole families. Details of the theoretical basis can be found in Lee and Lilley (1986). With the notation usually used in geomagnetism (see Appendix 3), spherical harmonic terms of degree n and m belong to the dipole family if (n-m) is odd and to the quadrupole family if (n-m) is even. This leads to some confusion in the nomenclature since the geomagnetic dipole has terms (equatorial dipole, Gauss coefficients g^1_1, h^1_1) in the quadrupole family, whereas the quadrupole has terms (g^1_2, h^1_2) in the dipole family. This is why the terms primary and secondary family are preferred (Merrill and McFadden, 1990). Using this basis, McFadden et al. (1988) separate the VGP dispersion into two contributions, one

due to the primary dynamo family, the other due to the secondary dynamo family. They use the coefficients from the International Geomagnetic Reference Field 1965 (IGRF65) to calculate these contributions in the modern field and their result is shown in Fig.5.3. It can immediately be seen that all the scatter at the equator is due to the quadrupole family terms, and that the latitudinal variation comes from the dipole family. Moreover, below 70° this variation in latitude is linear. These observations lead them to propose the very simple model expressed by:

$$S = \sqrt{A^2\lambda^2 + B^2}$$

where S is the VGP angular dispersion, λ is the latitude and A, B are constants. They find a very good agreement of the model with data for the last 5 Ma (Fig.5.4).

The improvement of model G over previous models is that the separation between primary and secondary dynamo families has a theoretical justification - the decoupling of the two families under certain conditions- unlike the distinction between dipole and non-dipole components of the field as used in earlier work. Although this rationale is valid only under particular specifications, it has proved a powerful tool for modelling the PSV, independent of its validity. In addition, it can be shown (Merrill and McFadden, 1988) that, if valid, this rationale takes on an

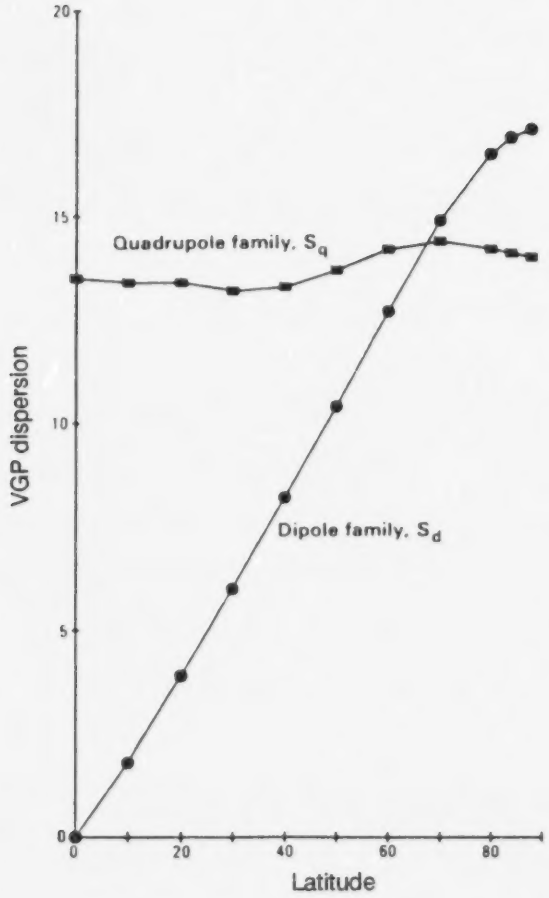

Figure 5.3. Angular dispersion of VGP for IGRF65 separated into the contributions from the quadrupole (secondary) dynamo family (S_q) and the dipole (primary) dynamo family (S_d). From McFadden et al.(1988). Both axes in degrees.

even greater meaning in the context of field reversal mechanisms.

Several authors have proposed models of field polarity reversals in which the reversal rate is dependent on the amplitude of secular variation (Cox,1968; Mazaud et al,.1989; Constable, 1990). These models are statistical or phenomenological and do not provide a physical basis to the underlying mechanism. On the other hand, dynamo theory cannot yet provide a complete model that is satisfactory. Nevertheless, Merrill and McFadden (1988, 1990) have proposed a model involving interactions between the primary and secondary dynamo families. Both families would be decoupled most of the time but a strong coupling would occur during polarity transitions. The most important prediction of this model is that low reversal rates would be accompanied by a reduced relative contribution of the secondary family to the field. This prediction is confirmed by a study of paleosecular variation from lavas dating back to 190Ma (McFadden et al.,1991). In particular a very small contribution of the secondary family is found during the Cretaceous Long Normal Superchron (KN, 124-83Ma)(see Fig.5.5). There lies the link between PSV and reversal studies and more data especially from older periods of the Earth's history are increasingly needed.

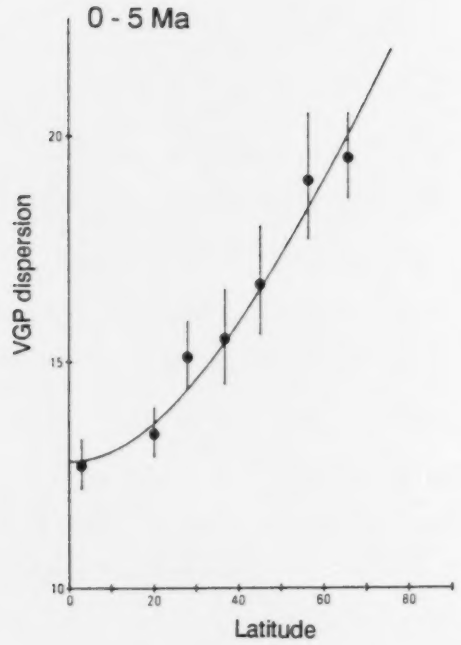

Figure 5.4. Fit of model G to combined polarity data for the past 5Ma. From McFadden et al.(1988). A=0.23±0.02; B=12.8±0.4.

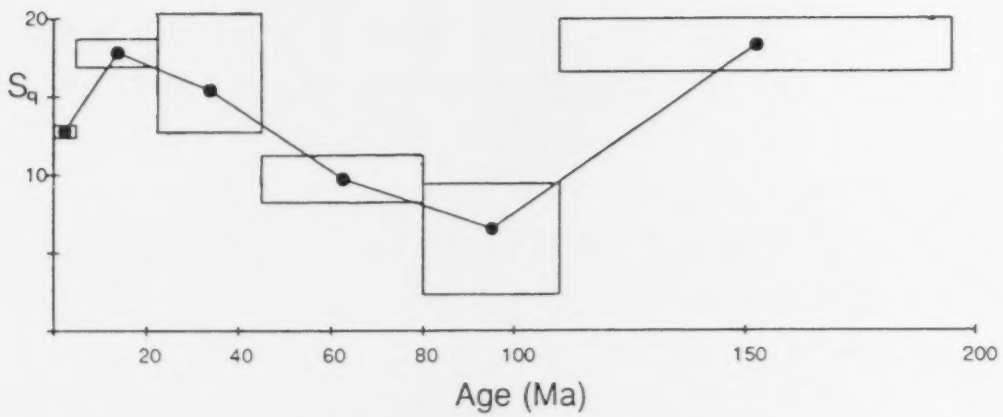

Figure 5.5. Variation of VGP dispersion due to the quadrupole family for the last 190Ma (S_q). The boxes around the plotted points indicate the age ranges contributing to the estimated parameter and the 95% confidence limits on the estimate. Modified from McFadden et al. (1991).

5.3.2 Lodève results

In view of the considerations presented above, the present study is interesting for several reasons. The strata involved were formed during the Permo-Carboniferous Long Reversed Superchron (PCR, 320-250Ma), which is the longest known interval of constant polarity, and during which observations similar to the ones reported for the KN are much needed. Although the data come from sedimentary rocks, evidence was presented that the magnetization acquisition was a rapid, intermittent process, very much like in a cooling lava flow, and therefore probably provides an accurate recording of field variations. The data set covers 1220 m of Thuringian sediments and, despite the difficulty of assessing magnetization rate, stratigraphic evidence indicates that this represents several million years (Odin, 1986). This duration is well sufficient to ensure a complete representation of PSV. Finally, the present study, though it provides only one value of angular dispersion, is located at a site near the Permian equator (paleo-latitude=2°), which is the only way to estimate the relative contribution of the secondary family without possessing dispersion values at several distributed latitudes. Indeed it has been shown (see section 5.3.1) that at zero latitude the primary family does not contribute to the geomagnetic angular dispersion

and consequently, that an estimate of the dispersion is an estimate of the secondary family contribution.

The angular dispersion or angular standard deviation of VGPs about the axis of rotation that will be used throughout is given by:

$$S_T = \left(\sum_{i=1}^{N} \frac{\theta_i^2}{N-1} \right)^{1/2}$$

where θ_i is the angle between the i^{th} VGP direction and the axis of rotation, and N is the number of VGP's (Cox, 1970).

The quantity calculated from paleomagnetic data is of course only an estimate of this variation since the true position of the spin axis is not known. However, following the basic hypothesis of the paleomagnetic method, it is assumed that when data span a sufficiently long time, the paleomagnetic pole coincides with the Earth's rotation axis. The total dispersion is given to a good approximation by:

$$S_T^2 = S_B^2 + \frac{S_W^2}{n}$$

where S_B and S_W are contributed by the between site and within site dispersion respectively, and n is the average number of samples per site. The within site dispersion is due mainly to experimental causes while the between site dispersion is due to geomagnetic field variations (McElhinny and Merrill, 1975). The latter is of course the

only one of geomagnetic interest but in order to determine it, we need to estimate the within site dispersion.

In the present study it is not possible to calculate S_w for each site of the Basin Traverse because for some of them only one sample is available and for the majority of the others the samples were not taken from exactly the same sedimentary units and cannot therefore be considered precisely contemporaneous. It would seem thus that the only accessible parameter would be S_T which is an overestimate of the VGP dispersion since some scatter must be due to experimental causes. However, it is possible to try to estimate a likely value for S_w by examining the possible sources of errors in the experimental procedure. A component that can be isolated and directly evaluated is the error due to measurements of the magnetization. By repeatedly measuring the same sample with the same instrument, one can calculate a good estimate of the standard error. This was done for 4 cores and 2 plastic top samples; each of them was measured 10 times over a period of 2 hours. In the VGP reference frame, the result is an average angular dispersion of 1.6° for the cores and 3.8° for the plastic top specimens. The larger value for the latter was expected and may be due to the difference in the measuring sensor (lower signal/noise ratio in the large head), or to a greater heterogeneity in the large plastic top samples. Since both types of specimens are

roughly equally represented the average of the two numbers, 2.9° (calculated by averaging the variances), provides a lower limit for S_w. Another possible source of error is the orientation of the samples in the field and from mechanical considerations it is generally thought not to exceed 2° (see e.g. Doell and Cox, 1963; Butler, 1992). Another 1° might be introduced by the preparation of the samples in the laboratory. If all the contributions that can be evaluated are added, a total angular dispersion of 3.7° is obtained, which may be safely rounded off to 4° since it is likely to be a lower limit. This number, although only an estimate, should provide a reasonable lower bound for S_w.

Because most of the samples at each site were collected at vertical distances of several tens of cm, it is preferable to calculate the total angular dispersion from individual VGP's rather than from site means. To use the means might yield an artificially low dispersion because of the averaging of direction variations due not only to experimental errors but also to PSV. In other words, an unknown fraction of S_B would be wrongly attributed to S_w. The total dispersion for the 201 samples of the Basin Traverse is 10.7°. By applying the estimate of the correction due to within site dispersion (4°), this number is reduced to 9.9°, which probably remains a

slightly overestimated value of the between site dispersion.

So far we have considered causes that can increase the angular dispersion and thus must be subtracted to obtain a estimate of the dispersion due to geomagnetic phenomena. However, in sedimentary paleomagnetism, other causes can decrease the dispersion by their smoothing effect. The mechanism of acquisition of the magnetization itself can produce a smoothing of the geomagnetic variations. The variations with quasi-periods of the order of the time constant of the remanence locking mechanism will be smoothed out, thus reducing the total angular dispersion. This effect can be important with CRM or DRM in very slowly deposited sediments, and is often most difficult to assess. However, we have seen that there are reasons to believe that the remanence in the Lodève strata is a pDRM, and that is was acquired rapidly, in a high sedimentation rate environment. As a result it is reasonable to think that this effect is limited here.

Another cause of smoothing is the very size of the samples themselves. If substantial magnetic direction variations can occur over a few centimetres, as was observed in the closely sampled sections (see Chapter 4), the simple fact of measuring a specimen 2 to 3 cm thick will introduce some smoothing. This effect can be evaluated by using the disk-shaped specimens of the small

intervals sections. To measure a 2.54 cm core or a 3cm thick plastic top sample is equivalent to measuring 4 disks at once. By calculating a 4 point moving average along short section magnetograms and calculating at each step the angular dispersion for the four points involved in the average, one can obtain an estimate of dispersion "lost" because of the size of the bigger samples. This calculation was performed on data from close sampling sites representative of the three lithologies (see Chapter 3 for a description), and the results are summarized in Table 5.2.

Sites	BLF	BLJ	BLP	BLM	Average
Average dispersion	4.3	3.6	2.2	2.7	3.3

Table 5.2. Average angular dispersion in degrees for 4 successive specimens, in VGP reference frame.

An average of 3.3° is found but we must remember that a part of this dispersion is again due to experimental errors. The disk samples were measured in the small head of the Molspin magnetometer and, as explained previously, a correction of at least 1.6° must be made, reducing the observed value of 3.3° to 2.9°. This value is probably only a crude approximation of the real effect of the sample size, but it constitutes an estimate of the correction that should be added to previously calculated VGP

dispersion. Applying it increases the value of S_B from 9.9° to 10.3°.

After all these considerations, one is left with a value of VGP angular dispersion that is essentially equal to 10°, possibly a little smaller since the within site dispersion has been underestimated. The exact value cannot be determined but it is very likely <10°. If we remember that the area investigated lay near the equator during the Permian, and if model G is valid, this dispersion is almost entirely due to the activity of the secondary dynamo family. We can now compare these results to those given by McFadden et al. (1991) for similar latitudes, keeping in mind that our study occurs during a period of zero reversal rate. For the past 5 Ma, corresponding to a relatively high reversal rate, a fit of model G to experimental values yields a dispersion of 12.9° for a latitude of 2°, significantly higher than the Lodève result. For the period 80-110 Ma, approximately corresponding to the KN, they find a dispersion of 6.5°. The Lodève results indicate a somewhat reduced activity of the field during the PCR, and are therefore compatible with a link between reversal rates and PSV. However, the difference between the value obtained in the present study (≤10°) and the value for a high reversal rate period (~13°) is not large enough to be really compelling.

cannot, at this stage, be regarded as settled.

5.4 Time series

5.4.1 Basin Traverse

The present data set should in principle provide more information than the mere statistical dispersion of measurements. Indeed, we have seen that the series of paleomagnetic directions are strongly serially correlated and thus potentially offer a way to investigate the PSV in greater detail, in particular its frequency content. Here we face two major difficulties. Firstly, in the absence of any absolute time marker it is impossible to know with any precision the actual rate of magnetization acquisition. Estimates can be inferred from average sedimentation rates for this kind of rock and from stratigraphic considerations, but the accuracy of these estimates are unlikely to be better than an order of magnitude. Secondly, the problem is further complicated by the sedimentation environment in which the rocks sampled in the basin traverse were deposited. In a continental environment with conditions changing from deltaic to playa-like, the deposition is an essentially discontinuous process and rates can be expected to vary dramatically. Consequently, even if we believe that the remanence was acquired shortly after deposition, it is illusive to

ascribe a definite and constant rate to the magnetization acquisition. All this makes it very difficult to change from a depth scale to a time scale in the data analysis. However, over a long section like the Basin Traverse and with the large sample intervals, it is possible that, on average, the rate of remanence acquisition remained constant enough to allow some long period information to be recovered. Thus, despite the unpromising outlook, frequency analysis was performed on the basin traverse data.

The complex maximum entropy method (MEM) was chosen mainly because it is the most suitable for directional data since it provides information on the type and direction of the motion, in addition to frequency information; the conventions used here are explained in Fig.5.6. This method was introduced to paleomagnetic research by Denham (1975) and a derivation of the equations used was published by Smylie et al. (1973). A general discussion of the MEM can be found in Kanasewich (1981). In order to compensate for the widely variable sampling intervals, the data were interpolated and resampled at 5m intervals by fitting a cubic spline through the experimental points. This was done on the X, Y, and Z components of the remanence vectors. The analysis was first performed on the entire 1220m series (complete

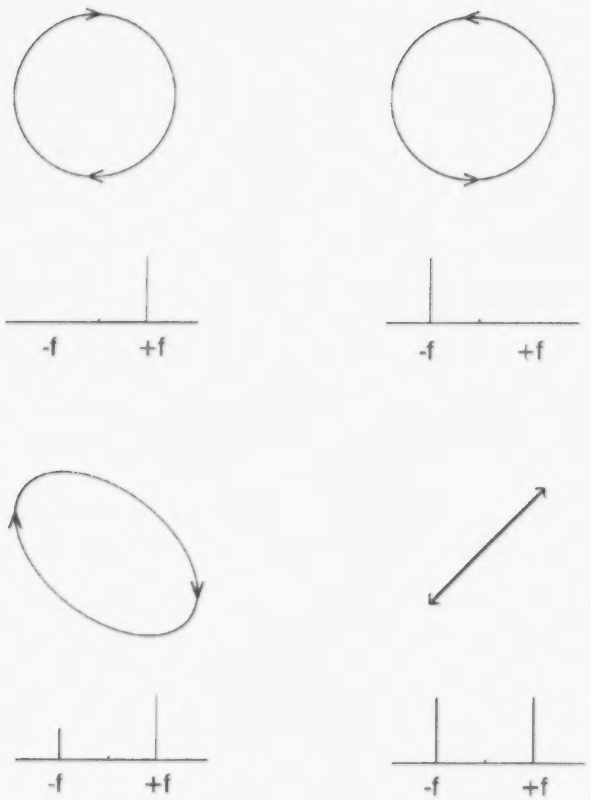

Figure 5.6. Illustration of various remanence direction variation patterns and corresponding complex MEM spectra. Positive (negative) frequencies correspond to clockwise (counter-clockwise) motion.

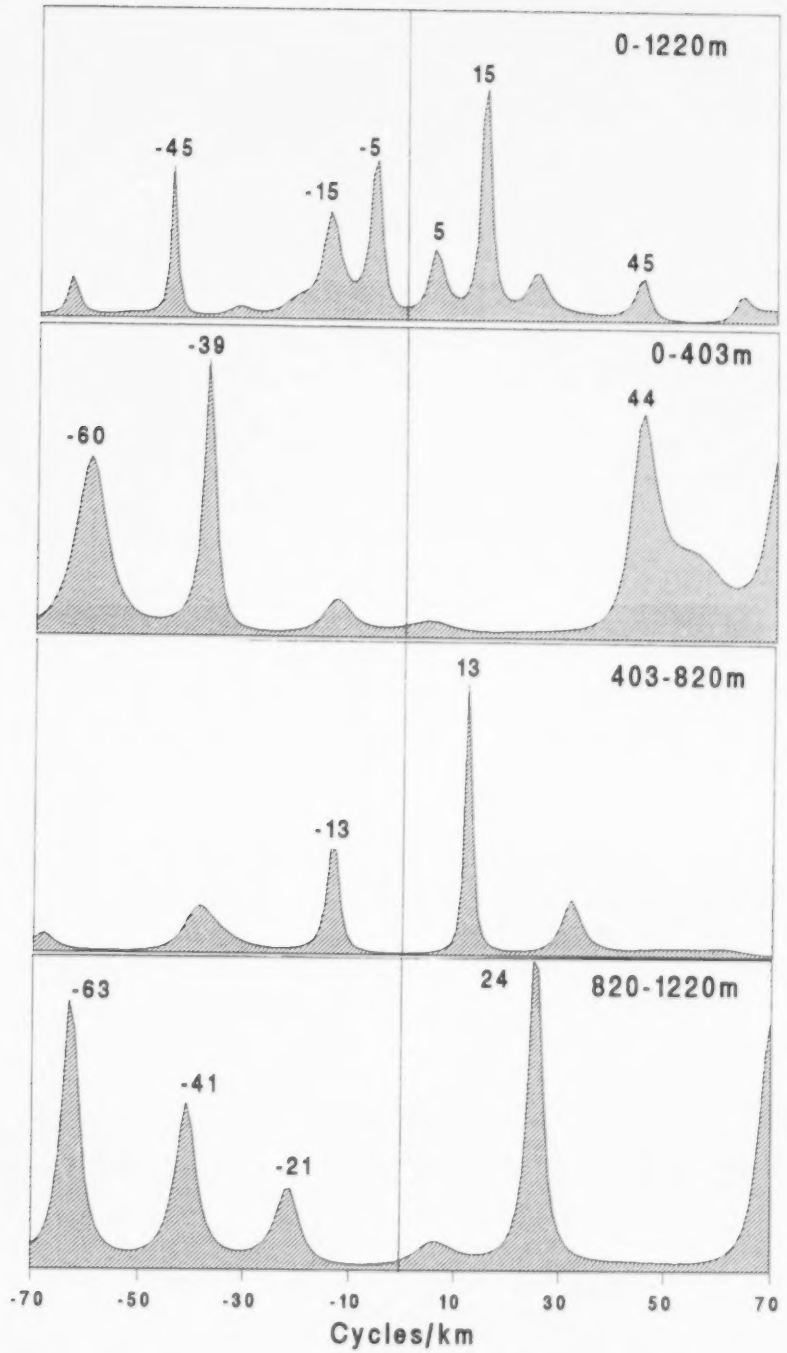

Figure 5.7. Complex MEM spectra for the Basin Traverse; complete data (top) and three subsets. All spatial frequencies are in cycles/km.

depth-series are shown in Fig.4.8), and the resulting spectrum is shown in Fig.5.7 (top). The most prominent features of this spectrum are, as expected, in the low frequency range. It is dominated by elliptic patterns, clockwise at 15 cycles/km and counter-clockwise at 5 cycles/km. A higher frequency (45 cycles/km) almost circular, counter-clockwise component also seems to be present. However, one has to be very careful in assessing the reality and meaning of such frequency spectra. To further investigate the frequency content, the record was subdivided in 3 equal parts, each about 400 m long, and MEM spectral analysis was carried out independently on each of them. The results (Fig.5.7) show that the spectrum is not stationary and that in fact the frequency content varies for different part of the record. Again this could be expected, and in view of the problems concerning the magnetization acquisition rate, it is not possible to attribute the non-stationarity to either geomagnetic or sedimentological causes alone.

The spectrum appears to be dominated by the central part of the record (403-820m, Fig.5.7) where a 13 cycles/km clockwise, elliptical component is strongly present. However this part of the record corresponds to the smallest density of data points, which weakens all results coming from it. The lower frequency component (around 5 cycles/km), well marked in the complete series

spectrum, is hinted in the upper and lower parts only. This is probably due to the series being too short to allow detection of such a low frequency. Higher frequencies (between 20 and 70 cycles/km) are predominant in the upper and lower parts of the record. The lower part (820-1220m) is where the greatest density of data point is available, and it should provide the most reliable results. Clockwise looping with frequency around 24 cycles/km, and counter-clockwise, nearly circular motion at 41 cycles/km are the main features of the spectrum. These features are clearly apparent on Bauer plots (inclination vs declination) of the corresponding parts of the Basin Traverse magnetograms, as shown in Fig.5.8.

All this indicates that no really precise results can be obtained about the exact frequency content of paleosecular variation recorded in this material. Nevertheless, clear, coherent variation patterns can be detected, and at least a crude evaluation of their frequency can be made. In order to see what these results translate into in terms of time, an estimate of the average rate of magnetization acquisition must be made. Based on stratigraphic and sedimentologic considerations, Odin (1986) gives an average sedimentation rate of 0.12 mm/yr for the Thuringian. This leads to a plausible 10 Ma for the time span corresponding to the Basin Traverse. If we assume that on average, the rate of magnetization

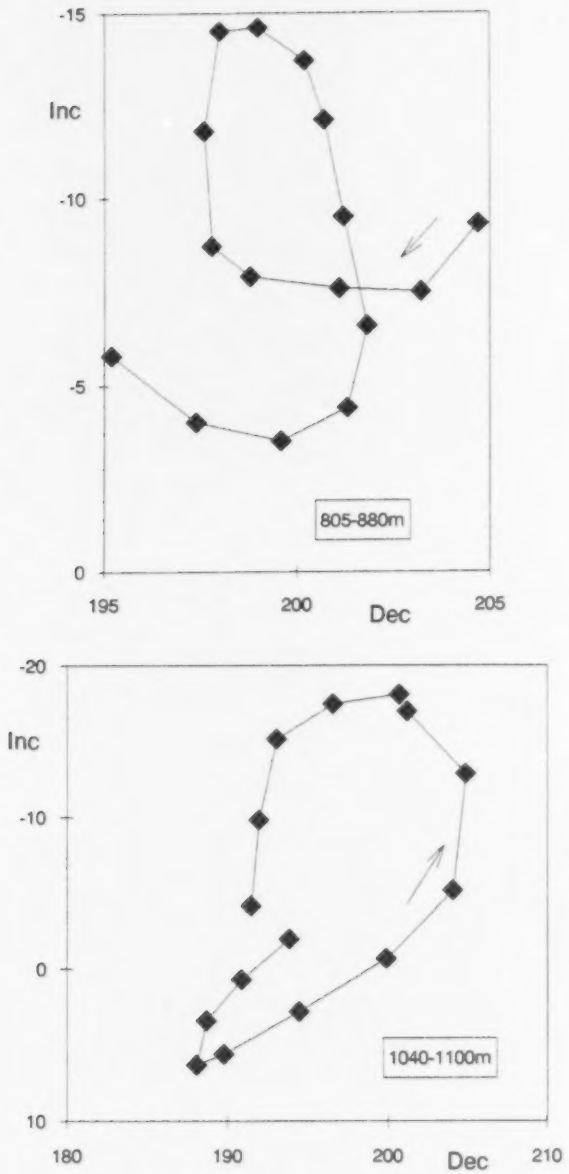

Figure 5.8. Smoothed Bauer plots of two parts of the Basin Traverse showing clockwise (top) and counter-clockwise (bottom) looping. Angles in degrees.

acquisition is the same as the rate of accumulation this provides a basis for translating the results into a time frame. Again it must be stressed that this in only an estimate of the *average* accumulation rate and that actual sedimentation rates during deposition periods can, and must, have been much higher. If we now apply these estimates to the 15 cycles/km component described above, we obtain a period of 0.55 Ma; the spatial frequency of 41 cycles/km gives a period of 0.2 Ma. These are only very crude estimates but the order of magnitude is likely to be right. This indicates that a major part of the paleosecular variation recorded in the Lodève redbeds is due to a slow variation of the geomagnetic field. It is impossible to attribute this variation to any particular feature of the field since the results are from a single location on the globe. However, periods of the order of 10^5 years are often proposed for the elusive dipole wobble (see e.g. Merrill and McElhinny, 1983).

5.4.2 Closely sampled sections

It is natural to try to perform a spectral analysis on some of the closely sampled sections since they possess direction variations similar to those of the Traverse. The best candidate is, as always, section BLF2 with its 265 very regularly spaced data points. The same technique as

for the Basin Traverse was used and the resulting spectrum appears in Fig.5.9. Its main feature is an almost linear looping pattern at 8 cycles/m. The linear character could be predicted from the magnetogram (Fig.4.10) that shows more variation in the declination than in the inclination. A Bauer plot of a portion of the data series shows the best example of this linear pattern (Fig.5.10).

With the closely sampled sections, the passage from space domain to time domain is even more problematic than for the Basin Traverse. In the latter, the very large sampling interval and the very size of the record made it legitimate to use an average deposition rate. However, in a small section like BLF2, that consists of 3 beds of distinct lithology but clearly part of the same unit, things are more complicated. During active deposition the rate was very likely higher than the average 0.12mm/yr, an estimate of 1mm/yr, possibly more, is reasonable for this kind of environment (Turner, 1980). However, the problem is that the deposition was certainly an essentially discontinuous process, with numerous periods of no deposition alternating with periods of rapid accumulation. How the rate of acquisition of the magnetization relates to all this is even less clear, but there are reasons to believe (see Chapter 3) that it was also discontinuous. Nevertheless, it is interesting to try to obtain at least the order of magnitude of the time scale of the observed

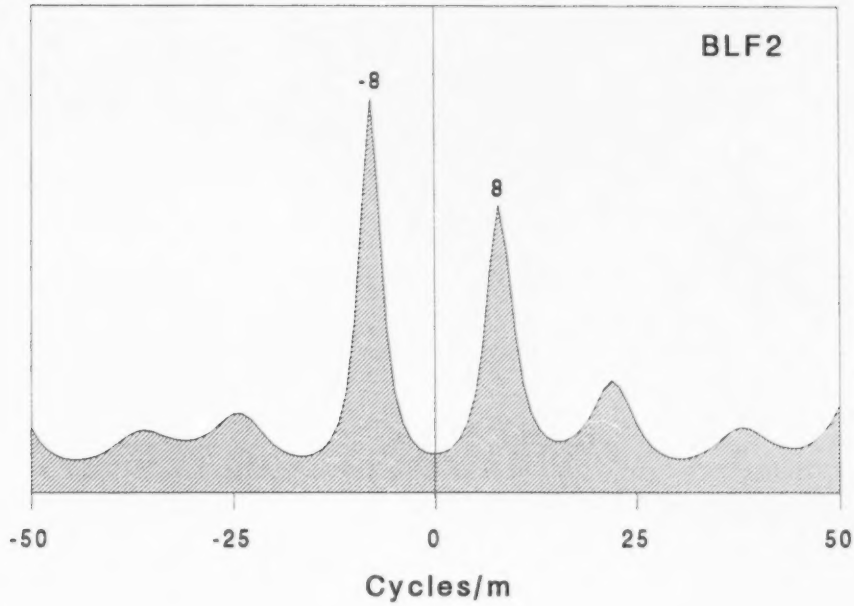

Figure 5.9. Complex MEM spectrum for section BLF2. Spatial frequencies in cycles/m.

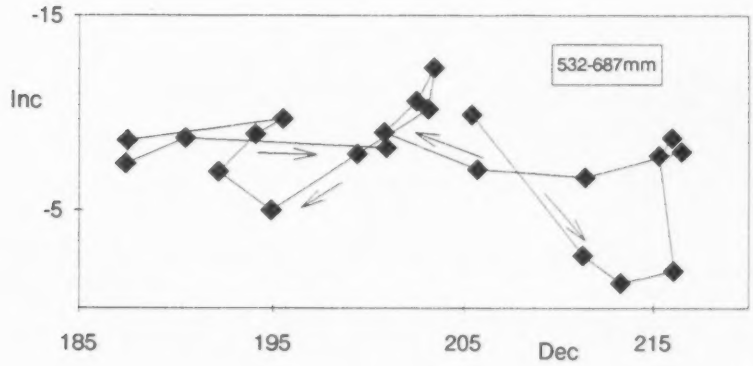

Figure 5.10. Smoothed Bauer plot for a part of section BLF2.

variations. With an average rate of 1 mm/yr, section BLF2 would correspond to approximately 2000 yr, and the linear pattern detected in the frequency spectrum would have a period of 125 yr; with the average 0.12 mm/yr this period becomes ~1000 yr. The significance of these numbers with regard to the Permian geomagnetic field is very difficult to assess within the confines of the present knowledge, and extreme caution is advised. However, these frequencies are certainly within the range of typical secular variations of the field in the recent past (see e.g. Merrill and McElhinny, 1983)

5.5 Paleogeographic considerations

The Permian paleogeographic controversy has been reported in the introductory chapter (see section 1.4). Although the present study relates to only one particular location on the surface of the globe, it is interesting to see how the results fit into a more general framework.

The main problems that affect reconstruction of Pangea are the discrepancies between Permian and late Triassic paleomagnetic data. This can be solved by considering different configurations for these two periods like in the Pangea A and B models of Irving (1977), (Fig.5.11). However, a new problem arises since these different configurations require dramatic readjustments of the

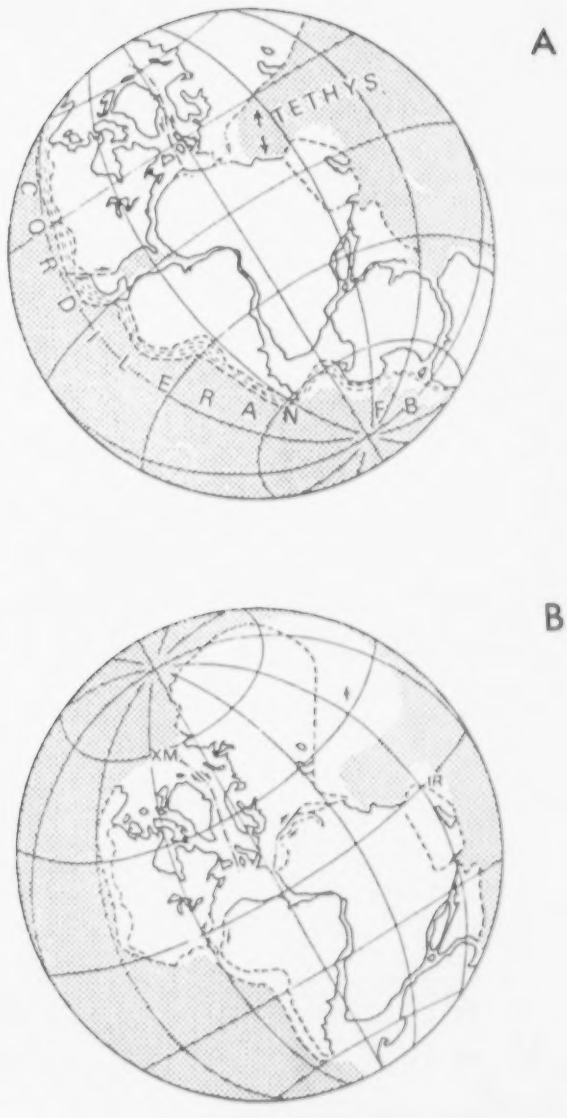

Figure 5.11. Maps of Pangea A and B reconstructions, from Irving (1977).

continental masses during the Late Permian - Early Triassic, unsupported by geologic evidence. The Lodève data cannot help distinguish between the different models, but since they cover 10 million years at the end of the Permian it is interesting to look for a long term trend that could reveal details of plate motions. An examination of the Basin Traverse magnetograms (see Fig.4.8) reveals that indeed a trend toward more positive inclination does exist in the data. To further investigate this, the data series was divided into two approximately equal length segments and the average poles were calculated for each (Table 5.3).

	Long.	Lat.	A_{95}
Complete Traverse	154.1	44.6	1.6
0-607m	154.1	42.0	2.8
607-1220m	154.2	46.3	1.9

Table 5.3. Virtual geomagnetic poles from the Basin Traverse (A_{95} is the semi-angle of the 95% confidence cone).

To compare these results with other poles one needs a reference frame. According to Van der Voo (1990), such a reference can be provided by the common apparent polar wander path (APWP) of Europe and North America for

Paleozoic to Early Jurassic times. In the Bullard et al. (1965) reconstruction, these two continental masses are joined together and their paleopoles can be combined. The mean poles relevant to the present study are given in Table 5.4 and are plotted on Fig.5.12 along with the Basin Traverse poles.

Time Interval (Ma)	Long.	Lat.	A_{95}
Lower Triassic (233-245)	149	50	2.7
Upper Permian (246-266)	159	49	5.0
Lower Permian (267-281)	163	45	2.1
Upper Carboniferous (282-308)	167	39	1.7

Table 5.4. Combined mean paleopoles for Europe and North America in European coordinates; from Van der Voo (1990).

The pole from the lower half of the Traverse is not significantly different from the mean Upper Permian paleopole as shown by the overlapping confidence circles. The pole from the entire Traverse and its upper half show a greater discrepancy. There is a definite trend towards more southerly latitudes, which is almost at right angle to the Carboniferous to Triassic APWP. The angular difference between the lower (B) and upper (T) poles is 4.3°, which would correspond to a displacement of the Basin

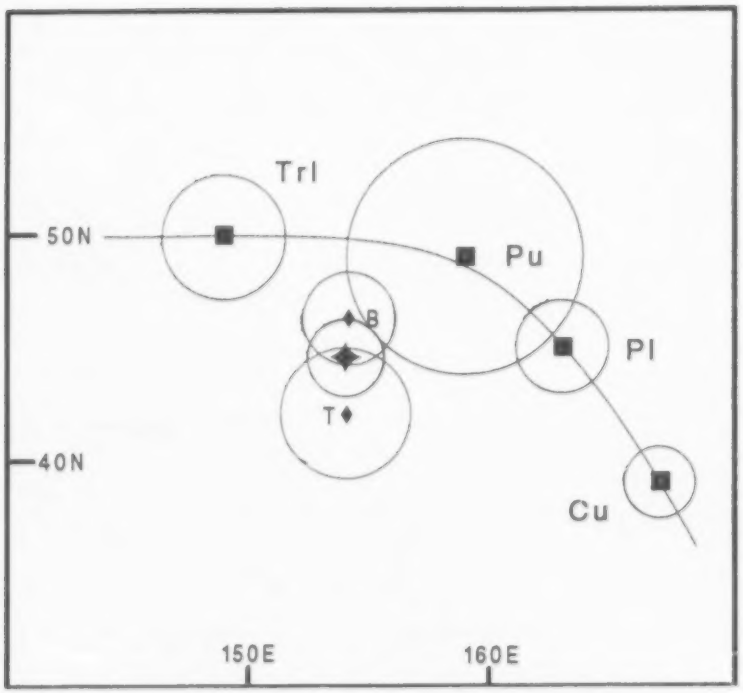

Figure 5.12. Paleomagnetic poles from the entire Basin Traverse (star) and from its lower (B) and upper (T) halves, compared to combined paleopoles for Europe and North America (from Van der Voo, 1990); circles indicate the 95% confidence level. Cu: upper Carboniferous, Pl: lower Permian, Pu: upper Permian, Trl: lower Triassic.

of approximately 450 km towards lower latitude. This appears very unlikely since it does not conform to the general APWP, and would therefore imply a regional motion. However, it must be noted that statistically the displacement does not have to be this large since the true B and T poles are not necessarily this far apart according to the size of their 95% confidence circles. The possibility of a regional tectonic displacement might thus be a viable hypothesis and merits further investigation.

Another interesting comparison is with other paleomagnetic poles obtained from the same region. Two previous studies of the Lodève Basin by Kruseman (1962) and Merabet and Guillaume (1988) have produced paleomagnetic poles, which are shown in Fig. 5.13 along with the Basin Traverse poles. A comparison reveals that the pole from the lower half of the Traverse (as well as the one from the complete Traverse) is not significantly different from the one previously obtained for the Upper Permian. This was expected since the horizons studied by Kruseman and by Merabet and Guillaume all correspond to the lower part of the Traverse. There is still a discrepancy with the pole from the upper half of the Traverse and again the trend is roughly orthogonal to the general Autunian to Thuringian trend. Therefore, the comparison does not shed any new light on the problem.

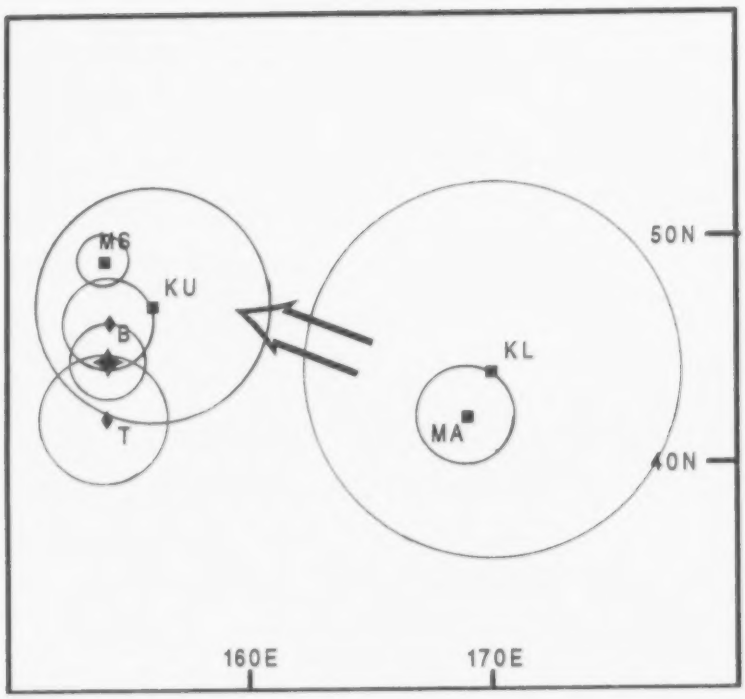

Figure 5.13. Paleomagnetic poles from the entire Basin Traverse (star) and from its lower (B) and upper (T) halves, compared to earlier results from the Lodève Basin.
KL and KU: lower and upper Lodève sandstones from Kruseman (1962). MA and MS: Lodève Autunian and "Saxonian" from Merabet and Guillaume (1988).

As a final remark, it should be noted that an alternative explanation for the apparent discrepancy of these poles could be the presence of an "inclination error" (King, 1955). This error, highly dependent on the shape of the particles, can be caused by an imperfect alignment due to a tendency for flat grains to lie horizontally rather than to align their magnetic moment parallel to the ambient field direction. Another possible cause of error is the rolling of rounded particles after their deposition (see Verosub (1977) for a review). The net effect is usually a shallowing of the inclination. To be invoked in our case, this inclination error would have to vary through the stratigraphic column and to be larger in the upper part of the Traverse. This is possible since the conditions of deposition vary towards lower energy environments as time progresses. On the other hand, we have seen in Chapter 3 that there are good reasons to believe that the magnetization is essentially post-depositional. Therefore, any initial inclination error acquired at the moment of deposition should have been erased. Finally, an examination of the inclination magnetogram for the Basin Traverse (see Fig.4.7 and 4.8) shows that , above 600 m, a majority of the samples possess positive inclinations, whereas below 600 m most inclinations are negative. If inclination errors were present, the necessary corrections would make both inclinations less shallow; therefore

negative inclinations would become more negative and positive inclinations more positive. The result would be an even greater discrepancy between both halves of the Traverse. We can therefore be certain that the inclination error cannot account for the slight discrepancy between the poles obtained in this study and the European mean paleomagnetic poles.

CHAPTER 6

SUMMARY AND CONCLUSIONS

In this final chapter I will review all the main aspects of the project, and show what general conclusions can be drawn from the results. I will also assess the success with which the main goals were achieved and make suggestions for any future work. According to the development of the work, it is appropriate to divide this chapter into contributions to the results from scalar (essentially magnetic intensity) and those from directional data.

6.1 Scalar magnetic properties of the Lodève strata

It was seen in Chapter 3 that perhaps the most interesting outcome of the present work was the discovery of well marked magnetic intensity variations with a characteristic "saw tooth" pattern. This was made possible by the use of small samples and sampling intervals (<1cm). In the context of the long-standing controversy about redbed magnetization, this discovery appears to be significant since it constitutes a new observation concerning these rocks so important for paleomagnetism.

Stacked, normalized intensity profiles suggest an exponential decrease with depth such that $M = Ae^{d}$ where M is the normalized magnetic intensity, d is depth, and A is a constant approximately equal to 2.5.

Of course, more important than the observations themselves are their interpretation and consequences regarding the process of magnetization. It was shown that despite all efforts made to detect differences in magnetic or petrographic properties able to explain the intensity patterns, none was found. This led me to propose that the intensity variations were due to varying efficiency of the magnetization acquisition process, and that this was most likely to occur where post-depositional remanent magnetization was involved.

The validity of the proposed model is certainly not proved, and the main weaknesses of the argument are due to the relative scarcity of samples corresponding to intensity peaks. Indeed, although very common, intensity peaks cover at best 2 or 3 samples, and eventually only a very few specimens were available for each of the various techniques used. The first goal of future work would therefore be to collect more specimens in the Lodève Basin with the specific purpose of sampling intensity peaks. Since these peaks are located at the top of sedimentary units this should be relatively easy. Another approach would be to try to simulate in the laboratory the

formation of these intensity peaks according to the proposed model. A column of about 20 cm of sediment saturated with water might be left in a container exposed to the ambient magnetic field. The top of the column would be mechanically disturbed and after drying, the magnetization would be measured at regular intervals to see if the intensity decrease towards the bottom is replicated. It would also be extremely interesting to know if similar intensity patterns are found in other redbed formations, and if their presence can be correlated with certain characteristics like the existence of a stable, primary magnetization. A systematic study of magnetic intensities in redbeds might shed new light on the old controversy and possibly provide a new approach to the understanding of the magnetization processes in rocks of this type.

6.2 Directional magnetic properties

The initial goal of the study was to obtain new insight into the Permian geomagnetic field and more particularly on the poorly known Kiaman interval (PCR), through the paleomagnetic study of a long sedimentary sequence. Despite many practical difficulties, 1220m of upper Permian strata were sampled, corresponding to approximately 10Ma, thus representing one of the longest continuous paleomagnetic record available to date.

The paleomagnetic pole obtained (154.1°E, 44.6°N, A_{95}=1.6) is concordant with other results from western Europe, and it is certainly an improvement over previous results from the Lodève Basin because of the much better coverage of the stratigraphic sequence. At this point the trend detected in the data series (see Fig.5.12) cannot be attributed to a unique cause but its potential tectonic implications merit further investigation, possibly by studying other Permian and Triassic formations in the same general region.

The first and most definite geomagnetic result is the total absence of normal polarities indicating that the end of the Kiaman was not reached. This places the termination of this superchron in western Europe at the very end of the Upper Permian.

One line of evidence suggests that the coherent directional variation patterns observed both in the Basin Traverse and the closely sampled sections constitute genuine recordings of the geomagnetic field. It was shown that the VGP dispersion is reduced ($\leq 10°$) compared to periods of high reversal rates ($\sim 13°$), although it is not as small as during the KN superchron ($\sim 7°$). This result is compatible with models linking PSV and reversal rates but is certainly not decisive. Clearly a major improvement would be a direct evaluation of the within site dispersion, as would be allowed by repetitive sampling at

exactly the same stratigraphic levels. This would permit a more accurate determination of the dispersion due to geomagnetic causes alone.

The maximum entropy spectra presented in Chapter 5 indicate that short period variations(10^2-10^3 yr) recorded in the closely sampled sections are similar to those of the recent past , but much longer periods in the range $2x10^5$ to $5x10^5$ yr are also present. The former seem, at least at one of the sites, to reflect linear pulsations of the field that are probably caused by a perturbing source which is stationary in the Earth's core. Other short period variations, and the long period ones, are represented by looping movements of the local field vector that are probably due to drifting sources. Both clockwise and counter-clockwise motions are present, with neither sense clearly predominating.

The long period variations are the more interesting since there are very few such observations available. Paleomagnetic records spanning several million years are indeed very rare, and the present work tends to demonstrate that the detailed study of long period features of the geomagnetic field, like the elusive dipole wobble, should prove feasible and fruitful, even for ancient geological epochs. A more detailed study of the Lodève Basin, using denser sampling and concentrating on the recognized zones where the variations are the most

marked, appears to be a promising project if one is willing to undertake the difficult sampling of the mudstones.

It is important for our understanding of the field mechanisms to know if the observed long period variations are particularly well developed during low reversal rate periods, or if they are a typical feature of the Earth's magnetic field at all times. The answer to this question in connection with the even more fundamental problem of the origin of polarity reversals lies in a better knowledge of the history of the geomagnetic field. This will be achieved only when more long paleomagnetic records from various locations and geologic times become available.

BIBLIOGRAPHY

Arthaud F., Megard F. and Séguret M., 1977. Cadre tectonique de quelques bassins sédimentaires, Bull. Centres Rech. Explo.-Prod. Elf-Aquitaine, Pau, 1(1), 147-188.

Baag C. and Helsley C.E., 1974. Geomagnetic secular variation Model E, J. Geophys. Res., 79, 4918.

Briden J.C., Smith A.G. and Sallomy J.T., 1971. The geomagnetic field in Permo-triassic time, Geophys. J. R. Astro. Soc., 23, 101-117.

Brunhes B., 1906. Recherches sur la direction d'aimantation des roches volcaniques, J. Phys., 5, 705.

Butler R.F., 1992. Paleomagnetism, Blackwell Scientific Publications.

Bullard E.C., Everett J.E. and Smith A.G., 1965. The fit of the continents around the Atlantic, Proc. Roy. Soc. London, A258, 41-51.

Clegg, J.A., Almond M. and Stubbs P.H.S., 1954. The remanent magnetism of some sedimentary rocks in Britain, Phil. Mag., 45, 583-598.

Collinson D. W., 1965a. The remanent magnetism and magnetic properties of red sediments, Geophys. J. R. Astro. Soc., 10, 105-126.

Collinson D. W., 1965b. Origin of remanent magnetization and initial susceptibility of certain red sandstones, Geophys. J. R. Astro. Soc., 9, 203-217.

Collinson D. W., 1966a. Magnetic properties of the Taiguati Formation, Bolivia, Geophys. J. R. Astro. Soc., 11, 337-347.

Collinson D. W., 1966b. Magnetic grain size effects and the remanent magnetesism of sediments, Earth Planet. Sci. Letts., 1,330-332.

Collinson D. W., 1967. The variation of magnetic properties among red sandstones, Geophys. J. R. Astro. Soc., 12, 197-207.

Collinson D. W.,1968a. An estimate of the haematite content of sediments by magnetic analysis, Earth Planet. Sci. Letts., 4, 417-421.

Collinson D.W., 1968b. Ferrous and ferric iron in red sediments and their magnetic properties, Geophys. J. R. Astro. Soc., 16, 531-542.

Collinson, D. W., 1969. Investigations into the stable remanent magnetization of sediments, Geophys. J. Roy. Astr. Soc., 18, 211- 222.

Collinson D. W., 1972. Micromagnetometer investigations of the remanent magnetization of the Bonito Canyon quartzite, Earth Planet. Sci. Lett., 15, 430-435.

Collinson D.W., 1983. Methods in palaeomagnetism and rock magnetism, Chapman and Hall, London, pp500.

Constable C.G., 1990. A simple statistical model for geomagnetic reversals, J. Geophys. Res., 95, 4587-4596.

Cox A., 1962. Analysis of present geomagnetic field for comparison with paleomagnetic results, J. Geomag. Geoelec., 13, 101-112.

Cox A., 1968. Lengths of geomagnetic polarity intervals, J. Geophys. Res., 73, 3247-3260.

Cox A., 1970. Latitude dependance of the angular dispersion of the geomagnetic field, Geophys. J. Roy. Astro. Soc., 20, 253-269.

Cox A., 1982. Magnetostratigraphic time scale, in A Geologic Time Scale (W.B. Harland et al., Eds.) pp. 63, Cambridge University Press, Cambridge.

Creer K.M., 1959. AC demagnetization of unstable Triassic Keuper marls from S.W. England, Geophys. J. R. Astro. Soc., 2, 261-275.

Creer K.M., 1962. On the origin of the magnetization of red beds, J. Geomag. Geoelec., 13, 86-100.

Creer K.M., Irving E. and Nairn A.E.M.,1959. Palaeomagnetism of the great Whin sill, Geophys. J. Roy. Astro. Soc., 2, 306-323.

David P., 1904. Sur la stabilité de la direction d'aimantation dans quelques roches volcaniques, C. R. Acad. Sci. Paris, 138, 41.

Dekkers M.J. and Linssen J.H., 1989. Rock magnetic properties of fine grained natural low temperature hematite with reference to remanence acquisition mechanisms in red beds, Geophys. J. Int., 99, 1-18.

Denham C.R., 1975. Spectral analysis of paleomagnetic time series, J. Geophys. Res. 80, 1897-1901.

Doell R.R. and Cox A., 1963. The accuracy of the paleomagnetic method as evaluated from historic Hawaiian lava flows, J. Geophys. Res., 68(7), 1997-2009.

Dunlop D.J., 1972. Magnetic mineralogy of unheated and heated red sediments by coercivity spectrum analysis, Geoph. J. Roy. Astr. Soc., 27, 37-55.

Elston D.P. and Purucker M.E., 1979. Detrital magnetization in red beds of the Moenkopi formation (Triassic), Gray Mountain, Arizona, J. Geoph. Res., 84, 1653-1665.

Ellwood B.B., 1984. Bioturbations: some effect on remanent magnetization acquisition, Geophys. Res. Lett., 11, 653-655.

Evans M.E. and Maillol J.M., 1986. A paleomagnetic investigation of a permian red bed sequence from a mining drill core, Geoph. J. Roy. Astr. Soc., 87, 411-419.

Fisher R.A., 1953. Dispersion on a sphere, Proc. Roy. Soc. London, 217, 295-305.

Hailwood E.A., 1989. Magnetostratigraphy, Special Report No. 19, The Geological Society, Blackwell Scientific Publications, Oxford, pp 84.

Harland W.B., Armstrong R.L., Cox A.V., Craig L.E., Smith A.G., and Smith D.G, 1990. A geologic time scale 1989, Cambridge University Press, Cambridge, pp 263.

Herrero-Bervera E. and Hesley C.E., 1983. Paleomagnetism of a polarity transition in the lower (?) Triassic Chugwater Formation, Wyoming, J. Geophys. Res., 88, 3506-3522.

Horrenberger J.C. and Rulhand M., 1981. Déformation progressive des sédiments permiens du bassin de Lodève (Hérault), Rev. Géol. Dyn. Géogr. Phys., 23(3), 225-234.

Hospers J., 1953-54. Reversals of the main geomagnetic field I, II and III, Proc. Kon. Nederl. Acad., Wet. B., 56, 467-491, 57, 112-121.

Irving E., 1977. Drift of the major continental blocks since the Devonian, Nature, 270, 304-309.

Irving E. and Parry L.G., 1963. The magnetism of some Permian rocks from New South Wales, Geophys. J. R. Astro. Soc., 7, 395-411.

Irving E. and Runcorn S.K., 1957. Analysis of the paleomagnetism of the Torridonian sandstone series of NW Scotland, Phil. Trans. Roy. Soc. Lon., 250, 83-99.

Irving E. and Ward M.A., 1964. A statistical model of the geomagnetic field, Pure Appl. Geophys., 57, 47-52.

Kanasewich E.R., 1981. Time sequence analysis in geophysics, University of Alberta Press, pp 480.

Khramov A.N., 1967. The Earth's magnetic field in the late Palaezoic, Izv. Earth Phys., 1967, 86-108.

King R.F., 1955. Remanent magnetism of artificially deposited sediments, Mon. Notic. Roy. Astr. Soc., Geophys. Suppl. 7, 115-134.

Kruseman G.P., 1962. Etude paleomagnetique et sedimentologique du bassin permien de Lodève, PhD thesis, Utrecht.

Lancelot J.R., de St André B. and de La Boisse H., 1984. Systématique U/Pb et évolution du gisement d'uranium de Lodève. Mineral. Deposita, 19, 44-53.

Larson E.E., Walker T.R., Patterson P.E., Hobblit R.P. and Rosenbaum J.G. 1982. Paleomagnetism of Moenkopi formation, Colorado plateau; basis for a long-term model acquisition of CRM in red beds, J. Geoph. Res., 87, 1081-1106.

Laversanne J.B., 1976. La sédimentation et les minéralisations uranifères du Permien du Lodèvois, Thèse Docteur-Ingénieur, Orsay.

Lee S. and Lilley F.E.M., 1986. On paleomagnetic data and dynamo theory, J. Geomag. Geoelec., 38, 797-806.

Lodève, 1982. Carte géologique de la France à 1/50 000, Lodève, BRGM.

Lowrie W., 1990. Identification of ferromagnetic minerals in a rock by coercivity and unblocking temperature properties, Geophys. Res. Lett., 17, 159-162.

Mazaud A., Laj C. and Bard E., 1989. A phenomenological model for reversals of the geomagnetic field, Proceedings of the NATO Advanced Study Institute on Geomagnetism and Palaeomagnetism, Kluwer Academic Publisher,pp 205-214.

McElhinny M.W., 1969. The palaeomagnetism of the Permian of Southeast Australia and its significance regarding the problem of intercontinental correlations, Spec. Pub. Geol. Soc. Austral., 2, 61-67.

McElhinny M.W. and Merrill R.T., 1975. Geomagnetic secular variation over the past 5 My, Rev. Geophys. Space Phys., 13(5), 687-708.

McFadden P.L. and McElhinny M.W., 1984. A physical model for palaeosecular variation, Geophys. J. Roy. Astro. Soc., 78, 809-830.

McFadden P.L., Merrill R.T. and McElhinny M.W., 1988. Dipole/quadrupole family modeling of paleosecular variation, J. Geophys. Res., 93, 11583-11588.

McFadden P.L., Merrill R.T., McElhinny M.W. and Lee S., 1991. Reversals of the Earth's magnetic field and temporal variations of the dynamo families, J. Geophys. Res., 96, 3923-3933.

Merabet N. and Guillaume A., 1988. Paleomagnetism of the permian rocks of Lodève (Herault, France), Tectonophysics, 145, 21-29.

Merrill R.T and McElhinny M.W., 1983. The Earth's magnetic field, Academic Press, London, pp 401.

Merrill R.T. and McFadden P.L., 1988. Secular variation and the origin of geomagnetic field reversals, J. Geophys. Res., 93, 11589-11597.

Merrill R.T. and McFadden P.L., 1990. Paleomagnetism and the nature of the geodynamo, Science, 248, 345-350.

Nmila A., Cabanis B., Dardel J., Saint Martin J. and Treuil M., 1989. Reliques volcaniques dans le remplissage permien du bassin de Lodève, C.R.A.S. Paris Serie II, 309, 1931-1938.

Odin B., 1986. Les formations permiennes, Autunien supérieur à Thuringien du "bassin" de Lodève (Hérault, France), Thèse Doctorat, Aix-Marseilles.

Odin B., Conrad G. and Stapf K., 1987. Les aspects de la sédimentation permienne, continentale et détritique à Lodève (Hérault, France): le role de la tectonique synsedimentaire et de la subsidence dans la dynamique du bassin, Géologie Alpine, Mém. h.s. No 13, 39-46.

Odin B., Doubinger J. and Conrad G., 1986. Attribution des formations détritiques rouges, du Permien du sud de la France, d'après l'étude du bassin de Lodève: implications géologiques, paléontologiques et paléoclimatiques, C.R. Acad. Sci. Paris (II), 302(16), 1015-1020.

Payne M.A. and Verosub K.L., 1982. The acquisition of post-depositional detrital remanent magnetization in a variety of natural sediments, Geophys. J. Roy. Astro. Soc., 68, 625-642.

Piper J.D.A., 1987. Palaeomagnetism and the continental crust, Open University Press, pp 433.

Robert P.H. and Stix M., 1972. a-effect dynamos, by the Bullard-Gellman formalism, Astron. Astrophys., 18, 453-466.

Ruhland M., Horrenberger J.D., Laversanne J., Lillie F., Gauthier-Lafaye F., and Heitz J.C., 1977. Analyse tectonique du bassin de Lodève, Hérault, géométrie et cinématique d'une zone en extension, C. R. Soc. Geol. Fr., Paris, 5, 263-265.

Runcorn S.K., 1955. Palaeomagnetism of sediments from the Colorado Plateau, Nature, 176, 505-506.

Santouil G., 1980. Tectonique et microtectonique comparée de la distension permienne et de l'évolution post-triasique dans les bassins de Lodéve, Saint Afrique et Rodez (France S.E.), Thèse 3e cycle, Montpellier.

Shive P.N., Steiner M.B. and Huyke D.T., 1984. Magnetostratigraphy, paleomagnetism, and remanence acquisition in the Triassic Chugwater Formation of Wyoming, J. Geophys. Res., 89, 1801-1815.

Smith A.G., Hurley A.M. and Briden J.C., 1980. Phanerozoic palaeocontinental world maps, Cambridge University Press, Cambridge, pp 102.

Smylie D.E., Clarke G.K.C. and Ulrych T.J., 1973. Analysis of irregularities in the Earth's rotation, in Methods in Computational Physics, V15 pp 391-430, Academic Press, New York.

Steiner M.B., 1983. Detrital remanent magnetization in hematite, J. Geoph. Res., 88, 6523-6539.

Tauxe L., Constable C., Stokking L. and Badgley C., 1990. Use of anisotropy to determine the origin of characteristic remanent magnetization in the Siwalik red beds of Northern Pakistan, Jour. Geoph. Res., 95, 4391-4404.

Tauxe L. and Kent D.V., 1984. Properties of detrital remanence carried by hematite from study of modern river deposits and laboratory redeposition experiments, Geoph. J. Roy. Astr. Soc., 77, 543-561.

Tauxe L., Kent D.V. and Opdyke N.D., 1980. Magnetic components contributing to the NRM of the Middle Siwalik red beds, Earth Planet. Sci. Lett., 47, 279-284.

Turner P., 1980. Continental red beds, Elsevier, Amsterdam, pp 562.

Verosub K.L., 1977. Depositional and postdepositional processes in the magnetization of sediments, Rev. Geophys. Space Phys., 15(2), 129-143.

van den Ende C., 1977. Paleomagnetism of permian red beds of the Dome de Barrot (S. France), PhD thesis, Utrecht.

van der Voo R., 1990. Phanerozoic paleomagnetic poles from Europe and North America and comparisons with continental reconstructions, Rev. Geophys., 28(2), 167-206.

van der Voo R. and French R.B., 1974. Apparent polar wandering for the Atlantic-bordering continents: Late Carboniferous to Eocene, Earth Sci. Rev., 10, 99-119.

Verosub K.L., Ensley R.A. and Ulrick J.S., 1979. The role of water content in the magnetization of sediments, Geoph. Res. Lett., 6, 226-228.

Watson G.S. and Beran R.J., 1967. Testing a sequence of unit vectors for serial correlation, J. Geophys. Res., 72(22), 5655-5659.

Wegener A., 1924. The origin of continents and oceans, (english translation by J.G.A. Skerl), Methuen, London, pp 212.

Zijderweld J.D.A., 1967. Demagnetization of rocks: Analysis of results, in Collinson D.W., Creer K.M. and Runcorn S.K.; Methods in paleomagnetism, Amsterdam, Elsevier, 254-286.

APPENDIX 1

DATA SETS

a) Samples used for rock magnetic experiments

SSt= sandstone; SiSt= siltstone.

Name	Litho.	Mass g	NRM Int. $10^{-6}Am^2/kg$
Thermal demagnetization (Fig.3.6)			
F2FI	SiSt	8.5	13.0
F2FM	SiSt	9.3	18.9
F2HH	SiSt	8.6	5.3
F2IB	SiSt	8.7	7.1
P3B	SiSt	7.4	26.5
P3ZD	SiSt	7.5	5.1
J1O	SSt	8.2	16.1
J1Z	SSt	7.4	2.8
J4R	SSt	7.6	14.9
J4ZD	SSt	7.7	1.1
AF demagnetization (Fig.3.7)			
F2FE	SiSt	7.8	13.5
F2FL	SiSt	9.6	14.5
P4B	SiSt	8.5	18.5
P4Z	SiSt	13.2	5.6
J5O	SSt	7.9	16.5
J5W	SSt	8.8	6.4
MAX IRM (Fig.3.9)			
F2KX	SiSt	6.2	22.9
F2KY	SiSt	4.9	15.3
F2KZ	SiSt	8.8	10.3
F2KZA	SiSt	8.5	9.7
F2KZB	SiSt	7.1	7.2
F2KZC	SiSt	8.3	6.8
IRM acquisition/destruction (Fig.3.10&3.11)			
P4B	SiSt	8.5	18.5
P5C	SiSt	7.4	15.1
P5ZC	SiSt	7.2	4.3
P5ZD	SiSt	11.2	2.4
P8B	SiSt	8.5	18.3
J2O	SSt	7.2	17.4
J2ZE	SSt	7.4	4.8
Thermal demagnetization of IRM (Fig.3.12)			
P8B	SiSt	8.5	18.3
P8C	SiSt	7.7	11.7
P8ZC	SiSt	10.6	4.4

b) Data from the Basin Traverse and closely sampled sections

Name: sample reference
Ty: sampling type; C=core, H=plastic top
L: lithology, 1=mudstone, 2=siltstone, 3=sandstone
Depth: in metres
Ma: mass in grams
Sus: initial susceptibility in S.I. units
M1: NRM moment in 10^{-9} Am^2
Fdec1: NRM declination before dip correction
Finc1: NRM inclination before dip correction
Bdec1: NRM declination after dip correction
Binc1: NRM inclination after dip correction
Th1: angular standard deviation of measurement
M2: clean (510°C) moment in 10^{-9} Am^2
Fdec2: clean declination before dip correction
Finc2: clean inclination before dip correction
Bdec2: clean declination after dip correction
Binc2: clean inclination after dip correction
Th2: angular standard deviation of 510°C measurement

Basin Traverse

Name	Ty	L	Depth	Ma	M1	Fdec1	Finc1	Bdec1	Binc1	Th1	M2	Fdec2	Finc2	Bdec2	Binc2	Th2
BLA06B	C	2	2	27	210	217	-5	218	-15	2	220	213	-16	214	-27	3
BLA07I	C	2	10	30	227	183	15	183	5	3	205	184	-12	183	-23	2
BLA07II	C	2	10	29	225	188	11	188	0	4	204	194	-12	193	-23	5
BLA08A	H	2	19	45	1141	216	8	216	-3	3	1024	208	-5	209	-16	1
BLA08B	H	2	19	48	815	209	7	209	-5	6	719	202	-5	202	-16	3
BLA09B	H	1	31	10	159	209	21	209	11	12	129	203	-5	203	-16	11
BLA12B	H	2	65	25	1257	226	3	224	-8	4	1436	209	-13	209	-23	3
BLA12C	H	2	65	20	3781	208	-11	206	-22	3	3062	204	-10	203	-22	3
BLA12D	H	2	65	20	3473	206	-11	206	-22	1	1277	200	-2	200	-13	3
BLA13A	H	2	76	52	1026	220	15	220	5	2	931	191	13	191	2	2
BLA13B	H	2	76	30	959	211	13	210	3	3	826	196	13	196	2	4
BLA14C	H	1	94	6	1168	219	14	219	4	2	872	216	10	216	0	3
BLA15A	H	1	99	8	356	210	7	210	-9	10	139	201	-11	201	-22	10
BLA15C	H	1	99	7	537	209	-7	210	-18	3	414	210	-12	211	-23	3
BLA17A	H	2	120	12	515	197	0	197	-15	5	424	196	-9	194	-24	4
BLA18A	H	1	145	45	348	204	50	207	35	5	275	192	8	192	-6	4
BLA19A	H	1	151	62	257	246	73	233	65	5	102	219	18	219	10	11
BLA20A	H	1	166	21	181	309	73	282	73	9	35	219	27	219	19	28
BLA20B	H	1	166	86	540	273	77	249	72	4	181	186	10	186	3	4
BLA20C	H	1	166	75	509	248	75	233	69	4	224	185	14	186	6	5
BLA21A	H	1	181	21	321	344	69	325	75	7	31	188	27	189	20	28
BLA22A	H	1	191	39	533	341	63	328	68	3	49	207	22	206	14	9
BLA23A	H	1	201	57	874	342	78	291	79	4	91	199	10	199	2	13
BLA24B	H	1	214	49	538	349	73	315	77	4	84	213	16	213	6	8
BLA25B	H	1	222	35	764	350	71	313	74	4	63	217	22	217	12	7
BLA26/3AH	1	231	41	410	326	75	288	75	3	61	204	18	204	9	10
BLA26/3BH	1	231	28	266	308	75	276	72	4	57	215	20	216	10	16
BLA26/2AH	1	241	47	636	348	68	323	72	5	59	203	10	204	0	14
BLA26A	H	1	259	54	1041	10	82	278	85	3	84	190	5	190	-4	13
BLA26B	H	1	259	35	397	344	65	322	69	7	49	213	19	213	9	18
BLA27A	H	1	269	17	201	341	70	311	73	4	27	206	21	207	11	29
BLA28B	H	1	279	34	380	314	79	270	76	3	79	204	11	205	2	11
BLA29A	H	1	288	35	201	341	75	299	76	5	40	164	44	171	20	28
BLA29C	H	1	288	52	783	359	78	304	82	3	94	206	21	206	11	10
BLA30B	H	1	299	68	839	333	74	296	75	4	133	196	18	197	9	8

BLA27A	H	1	269	17	201	341	70	311	73	4	27	206	21	207	11	29
BLA28B	H	1	279	34	380	314	79	270	76	3	79	204	11	205	2	11
BLA29A	H	1	288	35	201	341	75	299	76	5	40	164	44	171	20	28
BLA29C	H	1	288	52	783	359	78	304	82	3	94	206	21	206	11	10
BLA30B	H	1	299	68	839	333	74	296	75	4	133	196	18	197	9	8
BLA31B	H	1	307	27	293	358	73	324	78	4	35	197	49	200	19	26
BLA32A	H	1	337	34	765	355	72	323	77	2	50	197	22	198	12	20
BLA32B	H	1	337	43	954	351	70	330	74	4	47	168	35	178	20	25
BLA33A	H	1	347	51	705	345	72	311	76	4	95	207	13	207	3	11
BLA33B	H	1	347	37	825	324	68	300	68	7	111	207	1	207	-9	17
BLA34B	H	1	358	23	416	359	69	335	75	5	33	206	8	206	-1	20
BLA35B	H	1	367	29	339	326	78	281	76	3	44	201	7	201	-3	17
BLA35A	H	1	367	44	435	310	75	276	72	10	30	209	36	211	2	30
BLA37A	H	1	388	53	615	261	52	254	44	4	127	204	16	203	5	8
BLA37B	H	1	388	34	393	321	80	239	82	4	66	195	20	195	8	15
BLA40A	H	1	405	39	414	232	54	222	45	7	332	209	1	209	-10	5
BLA43A	H	1	434	23	322	331	80	238	86	5	35	239	43	219	2	21
BLA43C	H	1	434	6	42	315	80	237	81	3	4	169	9	169	-4	13
BLA44A	H	1	445	6	39	31	79	112	81	2	5	181	9	180	-4	17
BLA44B	H	1	445	6	34	280	80	216	77	1	6	185	15	185	2	15
BLA44C	H	1	445	44	379	339	79	242	86	4	52	206	11	205	0	20
BLA45AI	H	1	456	43	240	262	73	224	69	6	72	204	13	203	2	13
BLA45B	H	1	456	37	248	262	75	224	70	8	76	203	23	201	12	11
BLA46B	H	1	467	34	288	316	76	250	82	7	50	196	11	195	0	17
BLA48A	H	1	489	34	302	326	81	211	84	6	40	191	4	191	-9	24
BLA50A	H	1	511	34	247	235	77	204	68	8	67	214	13	212	3	12
BLA50B	H	1	511	4	25	301	81	213	80	2	5	204	21	202	10	6
BLA51A	H	1	522	47	441	322	82	202	83	5	91	181	13	180	0	29
BL145A	H	1	524	28	316	344	80	216	85	7	24	191	-6	191	-19	20
BL145B	H	1	524	61	5518	307	75	249	77	7	63	210	41	205	19	28
BL143B	H	1	545	49	227	279	60	255	60	8	59	200	19	199	6	13
BL140A	H	1	572	53	509	336	75	264	84	2	45	215	43	209	19	23
BL139A	H	1	581	20	176	253	76	217	68	10	54	203	14	202	1	9
BL139B	H	1	581	33	293	264	81	212	73	13	99	210	7	210	-5	14
BL137B	H	1	599	5	21	286	75	237	73	3	3	200	19	199	6	29
BL136A	H	1	609	30	130	263	86	194	75	14	41	248	17	210	11	28
BL136B	H	1	609	12	162	165	79	173	66	7	51	174	48	192	5	22
BL134A	H	1	627	6	40	349	83	190	82	3	4	203	19	201	6	19
BL133A	H	1	635	28	176	239	77	209	67	10	48	209	-7	211	-20	15
BL133B	H	1	635	37	149	216	56	206	47	4	78	209	-14	211	-26	6
BL132B	H	1	645	40	658	327	65	307	76	5	66	212	27	209	17	9
BL131B	H	1	653	61	474	356	77	260	87	6	74	206	27	203	17	6
BL129A	H	1	671	53	121	241	59	221	50	10	66	211	9	211	-1	9
BL127A	H	1	691	15	104	300	79	228	80	14	51	206	24	203	13	9
BL126B	H	1	699	57	318	273	80	212	76	5	54	209	6	209	-5	7
BL121B	H	1	740	53	381	290	81	201	79	3	72	200	-1	201	-12	20
BL116A	C	1	788	28	149	210	79	187	65	5	27	198	3	198	-11	3
BL116B	C	1	788	27	128	183	71	178	55	4	20	196	2	197	-13	5
BL115A	C	1	799	26	89	209	82	184	67	6	22	195	9	195	-6	4
BL115B	C	1	799	20	96	177	65	175	49	3	13	186	1	186	-15	6
BL114A	C	1	808	28	168	320	69	271	79	8	18	194	14	193	-5	4
BL113I	C	3	818	25	61	206	26	203	13	5	32	206	4	206	-10	2
BL113II	C	3	818	24	65	201	55	194	41	2	23	203	23	200	9	5
BL112A	C	1	830	28	87	252	54	233	48	3	28	208	1	209	-12	6
BL112B	C	1	830	27	98	224	50	213	39	5	18	194	9	194	-6	5
BL111A	C	1	840	28	110	238	77	203	66	4	24	199	-1	200	-15	5
BL110A	C	1	850	27	153	285	66	247	67	8	22	196	1	196	-14	3
BL110B	C	1	850	23	158	281	64	243	66	9	21	203	-2	204	-16	3
BL109A	C	1	860	29	76	208	54	201	39	3	20	195	2	195	-13	4
BL109B	C	1	860	29	77	204	49	198	34	4	17	192	-2	193	-17	5

BL108A	C	2	870	26	61	220	68	204	55	8	20	199	14	199	-2	7
BL108B	C	3	870	26	75	209	47	203	33	5	29	203	20	201	5	3
BL108CI	C	3	870	26	58	213	52	205	38	3	26	200	19	199	4	3
BL107A	C	1	880	26	136	168	80	175	64	6	34	200	3	201	-12	5
BL107B	C	1	880	26	128	271	67	238	63	10	31	210	0	211	-14	2
BL107C	C	1	880	28	120	223	67	207	53	4	29	206	-2	207	-17	5
BL106A	C	1	890	24	1	201	83	186	68	11	19	206	5	206	-10	5
BL106B	C	1	890	29	126	217	71	201	57	3	26	204	5	204	-10	4
BL106C	C	1	890	28	102	270	81	211	72	5	22	204	0	205	-15	3
BL105A	C	1	900	20	136	197	51	193	36	4	17	203	10	203	-5	5
BL105B	C	1	900	26	2	224	50	215	38	5	25	213	6	213	-7	7
BL104A	C	1	910	27	144	206	39	202	25	4	26	204	0	204	-14	2
BL104B	C	1	910	24	132	152	53	159	38	3	24	195	5	195	-11	3
BL103A	C	1	920	19	86	278	50	257	49	3	30	200	4	200	-12	3
BL103B	C	1	920	25	99	90	63	120	58	4	35	192	6	192	-10	5
BL103C	C	1	920	27	136	231	43	222	31	3	42	194	6	194	-10	3
BL102B	C	2	930	23	78	153	50	159	35	2	12	203	-7	204	-21	8
BL101A	C	1	940	27	122	68	59	98	61	3	21	212	-1	213	-14	6
BL101B	C	1	940	28	118	154	53	161	38	3	18	203	-11	205	-25	10
BL100A	C	2	950	27	128	197	74	189	58	4	25	221	-4	223	-16	6
BL100B	C	1	950	26	118	168	61	172	44	2	33	197	6	198	-9	5
BL99A	C	1	960	22	96	215	51	207	36	9	15	206	7	206	-9	5
BL99B	C	1	960	22	68	252	86	192	72	7	11	210	5	210	-9	7
BL99C	C	1	960	24	125	233	41	224	29	4	33	204	1	204	-15	8
BL98A	C	1	971	24	115	124	83	164	68	6	22	199	5	199	-11	4
BL98B	C	1	971	24	174	245	51	230	42	5	29	201	0	202	-16	3
BL97A	C	1	982	26	104	257	66	219	47	4	29	204	12	203	-4	4
BL97B	C	1	982	28	83	252	86	192	72	3	33	200	2	201	-14	4
BL97C	C	1	982	27	124	244	61	223	50	2	35	197	8	197	-8	4
BL96A	C	2	993	26	60	236	59	219	47	4	21	197	5	198	-11	4
BL96B	C	3	993	23	163	186	7	186	-11	3	78	189	4	189	-13	5
BL96C	C	3	993	31	124	184	16	184	-1	4	43	187	12	187	-5	8
BL95A	C	1	1003	29	105	183	51	182	34	3	22	180	3	180	-14	6
BL95B	C	1	1003	21	75	214	72	199	56	5	22	206	-2	208	-17	6
BL94B	C	2	1013	26	69	243	31	238	20	3	22	217	-5	218	-19	6
BL93A	C	3	1021	23	378	200	-4	200	-19	4	275	199	-5	199	-20	3
BL93B	C	3	1021	28	420	196	-7	196	-22	3	292	197	-10	197	-25	2
BL93C	C	3	1021	23	493	198	5	198	-10	2	330	199	4	199	-11	3
BL92AI	C	3	1024	8	325	190	15	189	0	5	81	195	7	195	-8	7
BL92BI	C	3	1024	29	387	195	10	195	-4	3	318	193	10	193	-5	4
BL92BII	C	3	1024	28	302	192	13	192	0	2	240	191	12	191	-2	3
BL90B	C	2	1053	27	77	187	15	187	2	5	26	192	5	192	-9	3
BL89A	C	2	1057	28	105	236	35	228	28	5	23	199	1	200	-12	6
BL89B	C	1	1057	26	90	268	50	252	49	5	32	218	-8	220	-18	4
BL88A	C	3	1064	22	191	194	-12	197	-29	6	124	186	-20	187	-34	5
BL88B	C	3	1064	28	351	180	-8	181	-25	13	243	181	-9	181	-23	7
BL88C	C	3	1064	29	284	177	-13	178	-31	2	223	177	-16	177	-30	4
BL85AI	C	3	1071	31	246	203	2	203	-10	3	205	203	-2	203	-14	4
BL85AII	C	3	1071	31	355	205	-1	206	-13	4	313	202	-6	203	-18	3
BL85BI	C	3	1071	31	143	200	3	200	-9	3	118	199	-5	199	-17	2
BL85BII	C	3	1071	32	149	206	9	206	-3	3	123	206	3	206	-8	2
BL83A	C	3	1087	22	106	216	20	214	10	10	67	206	6	206	-6	4
BL82C	H	1	1089	36	99	221	57	212	47	22	39	193	26	192	15	14
BL81A	H	1	1099	19	116	196	42	193	30	18	54	183	20	183	8	9
BL81C	H	1	1099	21	122	201	53	197	42	13	76	184	21	184	9	10
BL80B	C	1	1107	23	125	189	34	188	22	9	71	188	9	187	-3	1
BL80C	C	1	1107	25	251	190	30	189	18	4	155	190	23	189	11	2
BL79A	C	2	1110	29	268	199	24	198	14	3	150	200	10	199	-2	2
BL78B	C	3	1116	24	429	193	12	192	2	8	315	190	9	190	-1	2
BL76A	C	3	1132	30	298	200	16	199	6	3	196	199	5	199	-5	4

BL76B	C	3	1132	24	54	202	28	199	18	4	47	200	-4	201	-14	4
BL76C	C	3	1132	29	195	201	13	200	3	3	150	202	3	202	-6	2
BL75A	C	3	1142	31	415	198	4	198	-6	5	273	198	1	198	-9	3
BL75B	C	3	1142	30	378	201	6	201	-3	2	73	201	2	201	-8	0
BL75C	C	3	1142	28	439	204	5	204	-5	3	310	203	1	204	-9	1
BL75D	C	3	1142	29	401	194	8	194	-2	2	273	27	4	193	-6	1
BL74A	C	3	1157	23	84	200	28	198	19	8	40	192	1	192	-9	1
BL74B	C	3	1157	23	77	191	26	190	16	5	32	196	8	196	-2	2
BL74C	C	3	1157	29	99	197	1	197	-9	5	52	190	-15	192	-25	3
BL73A	C	3	1165	29	187	201	8	200	-2	8	113	195	-3	195	-13	4
BL73B	C	3	1165	25	112	204	12	204	3	3	74	199	-11	200	-21	5
BL73C	C	3	1165	21	65	225	50	219	43	7	59	198	19	198	8	2
BL73D	C	3	1165	23	50	198	23	196	14	11	46	190	-22	192	-32	5
BL72A	C	3	1170	25	211	203	5	203	-4	2	177	196	-6	197	-16	2
BL72B	C	3	1170	28	194	199	10	198	0	3	163	193	-5	193	-15	2
BL72C	C	3	1170	24	60	208	67	197	58	8	61	201	-3	201	-12	2
BL71A	C	3	1175	28	98	196	23	195	13	3	77	199	2	199	-8	2
BL71B	C	3	1175	24	68	222	46	214	38	3	37	206	10	205	2	3
BL71C	C	3	1175	24	59	218	46	211	38	5	32	202	15	201	6	3
BL70/2A	C	3	1179	24	124	190	6	190	-4	8	69	196	-1	196	-11	3
BL70A	C	3	1180	26	223	206	13	205	4	3	162	202	0	203	-9	1
BL70B	C	3	1180	22	25	225	35	220	29	9	12	205	-7	207	-16	3
BL70C	C	3	1180	21	26	237	43	228	38	8	12	208	7	208	-1	3
BL69/2A	C	3	1186	27	31	246	62	228	58	3	44	193	7	193	-4	6
BL69/2B	C	3	1186	29	54	202	24	200	15	9	42	200	7	200	-2	4
BL69	C	3	1189	28	224	205	10	204	1	1	173	202	1	203	-8	2
BL68/2A	C	3	1192	29	161	203	6	203	-3	2	104	199	-6	200	-16	1
BL68/2B	C	3	1192	29	162	206	6	206	-3	4	105	203	-3	204	-13	2
BL68I	C	3	1197	7	22	195	15	194	5	5	11	192	-3	193	-13	4
BL68II	C	3	1197	7	19	206	18	204	9	4	10	196	9	196	-1	9
BL68III	C	3	1197	6	19	199	21	197	11	7	9	194	4	194	-7	8
BL67/2A	C	3	1203	24	202	196	6	196	-4	3	149	195	-4	196	-14	1
BL67/2	C	3	1203	23	54	205	25	203	16	4	39	194	-3	195	-13	3
BL64	C	3	1207	29	184	199	15	198	5	2	124	198	2	198	-8	3
BL65A	C	3	1207	29	163	193	10	193	0	2	114	191	3	192	-7	2
BL65B	C	3	1207	23	58	212	35	208	27	3	24	200	16	199	6	2
BL65C	C	3	1207	23	75	208	39	203	30	4	24	208	23	206	14	4
BL65D	C	3	1207	23	73	203	30	200	20	2	30	196	9	195	-1	2
BL61	C	3	1209	19	466	207	45	202	45	4	18	203	16	202	7	7
BL58	C	3	1210	22	853	207	25	205	16	3	27	216	16	214	8	7
BL60	C	3	1210	22	1355	192	23	191	13	3	72	191	11	190	1	3
BL53	C	3	1212	19	890	205	37	201	28	4	40	199	23	197	14	2
BL50	C	3	1216	25	1006	210	28	210	19	2	75	202	4	201	-5	3
BL44	C	3	1217	18	1410	205	13	204	4	2	73	206	-2	207	-11	3
BL44I	C	3	1217	20	143	202	6	201	-3	3	76	203	-7	204	-16	1
BL45	C	3	1217	7	209	251	54	237	51	9	37	206	-2	207	-10	8
BL46	C	3	1217	13	83	205	32	202	23	5	46	206	-1	207	-10	3
BL47	C	3	1217	22	54	210	16	208	8	3	33	202	1	203	-9	5
BL38	C	3	1219	28	824	204	17	203	7	4	42	197	1	198	-9	3
BL41	C	3	1219	18	1943	193	18	192	8	2	116	192	7	192	-3	1
BL33	C	3	1220	13	1140	198	20	197	10	4	54	188	4	188	-7	4

Closely sampled sections

Site BLF

Name	Depth	Ma	Sus	M1	Bdec1	Binc1	Th1	M2	Bdec2	Binc2	Th2
BLF2LA	3	7.86	5.1	89	203	6	4	58	201	2	3
BLF2LB	9	8.02	4.4	110	203	4	2	71	202	1	2
BLF2LC	16	10.07	6.3	136	201	4	3	90	198	-1	3
BLF2LD	23	8.05	4.8	128	198	2	5	88	199	-3	3
BLF2LE	30	8.64	4.1	112	198	-1	3	74	198	-5	3
BLF2LF	37	7.34	4.5	114	197	2	3	78	201	-1	4
BLF2LG	43	7.7	3.3	119	195	-4	4	86	195	-8	4
BLF2LH	50	8.02	4.4	149	199	-2	4	101	201	-6	4
BLF2LI	57	8.2	4.2	138	198	-1	4	93	198	-4	3
BLF2LJ	64	8.56	4.	103	196	3	4	68	200	-2	4
BLF2LK	71	7.48	4.1	87	196	4	5	55	198	1	4
BLF2LL	78	7.16	3.9	76	195	5	6	54	198	1	5
BLF2LM	84	8.97	4.3	100	197	0	4	66	196	-5	4
BLF2LN	92	10.39	5.3	94	196	2	3	65	201	-4	3
BLF2LO	103	12.3	6.9	160	195	0	3	106	199	-3	3
BLF2LP	111	10.3	5.7	162	197	-1	4	110	197	-2	5
BLF2LQ	117	7.95	4.3	122	194	-1	4	86	199	-7	3
BLF2LR	124	7.63	4.4	124	195	2	3	86	197	-2	3
BLF2LS	130	7.94	4.2	150	195	-1	6	107	201	-2	5
BLF2LT	139	9.72	5.	184	198	-5	4	131	203	-5	4
BLF2LU	146	9.	5.	128	198	-5	3	92	202	-10	3
BLF2LV	153	7.59	4.2	88	197	-3	4	61	203	-6	3
BLF2LW	161	9.87	5.8	143	197	-2	4	102	205	-7	3
BLF2LX	168	8.64	5.2	136	203	-3	3	99	207	-10	3
BLF2LY	174	7.2	3.5	106	203	-5	3	73	207	-10	3
BLF2LZ	182	7.97	3.9	117	201	-2	3	83	207	-11	3
BLF2LZA	188	8.45	3.9	111	203	-1	5	81	208	-9	3
BLF2LZB	196	8.73	4.1	133	204	-7	5	93	207	-14	4
BLF2LZC	203	7.07	3.1	103	203	-8	4	74	208	-15	3
BLF2LZD	208	7.07	3.4	92	206	-6	3	64	206	-12	2
BLF2LZE	215	3.07	1.6	53	208	-3	8	38	212	-12	7
BLF2MA	221	6.76	4.2	118	195	8	3	85	200	-6	2
BLF2MB	228	6.14	3.5	79	195	1	3	56	200	-12	3
BLF2MC	236	9.73	5.	129	196	2	4	94	200	-10	3
BLF2MD	242	14.26	6.9	147	194	8	4	106	200	-3	3
BLF2ME	249	2.13	0.3	19	201	4	5	9	204	-6	13
BLF2MF	254	8.32	3.4	76	196	5	3	51	202	-7	2
BLF2MG	261	9.05	3.4	81	201	5	2	57	203	-7	2
BLF2MH	268	6.98	2.8	69	199	3	3	44	205	-6	3
BLF2MI	274	8.3	3.1	107	200	5	3	74	203	-1	3
BLF2MJ	281	7.41	2.4	97	199	5	4	65	199	-3	7
BLF2MK	288	8.56	3.5	81	206	2	7	53	206	-5	4
BLF2ML	294	6.4	2.4	48	206	10	3	28	207	-7	2
BLF2MM	300	7.19	2.5	58	207	6	3	35	208	-4	3
BLF2MN	306	7.16	3.	63	207	3	3	35	217	1	4
BLF2MO	311	6.4	3.2	62	207	6	2	38	205	-5	5
BLF2JA	323	7.71	3.6	76	205	-3	1	46	208	-10	4
BLF2JB	330	8.16	4.2	74	208	1	5	59	195	-4	5
BLF2JC	337	7.98	3.9	56	203	-3	3	39	206	-14	7
BLF2JD	343	7.03	3.2	54	202	-5	4	38	199	-11	3
BLF2JE	351	7.28	3.2	49	203	3	3	32	201	-7	4
BLF2JF	358	7.08	4.1	39	205	3	5	18	209	-14	15
BLF2JG	365	7.66	5.1	38	206	1	4	22	200	-10	4

BLF2JH	373	11.71	8.7	57	203	-2	4	34	198	-10	6
BLF2KA	380	5.58	4.2	35	203	10	5	20	211	-5	4
BLF2KB	386	7.82	5.2	63	196	12	3	30	194	5	5
BLF2KC	394	8.26	5.7	82	200	4	3	51	207	-9	4
BLF2KD	401	8.5	5.3	77	204	6	3	45	208	-4	3
BLF2KE	407	7.77	4.4	71	201	3	3	42	207	-10	2
BLF2KF	415	8.49	4.5	65	202	6	4	42	206	-7	4
BLF2KG	422	6.92	4.3	59	199	11	3	39	216	-3	3
BLF2KH	428	11.18	7.	82	196	10	3	52	201	-4	4
BLF2KI	435	5.46	3.2	41	204	10	4	26	202	-1	11
BLF2KJ	442	6.8	3.9	59	205	2	4	29	196	-7	8
BLF2KK	448	6.1	3.9	46	205	7	4	29	205	-6	3
BLF2KL	454	7.68	5.2	53	202	18	4	22	188	11	8
BLF2KM	461	8.81	5.9	67	201	16	4	30	194	6	8
BLF2KN	467	8.98	5.8	96	203	-3	5	67	206	-8	6
BLF2KO	474	10.67	5.9	115	201	-5	6	81	209	-13	7
BLF2KP	482	8.31	6.5	121	210	9	6	83	211	-1	5
BLF2KQ	490	13.75	8.	183	203	1	4	120	204	-7	3
BLF2KR	498	8.28	4.	242	199	-10	5	157	199	-8	9
BLF2KS	506	6.1	2.6	135	212	-12	5	89	213	-15	4
BLF2KT	515	8.34	3.2	63	205	-3	7	43	203	-10	7
BLF2KU	522	10.37	3.7	22	195	13	5	13	199	-15	11
BLF2KW	535	11.55	4.7	17	211	30	14	11	209	-9	12
BLF2KX	540	6.21	3.3	142	209	-6	4	100	208	-6	4
BLF2KY	550	4.9	3.3	75	219	5	3	42	217	6	7
BLF2KZ	557	8.77	5.4	91	214	-1	3	63	215	-5	4
BLF2KZA	563	8.49	5.7	82	213	0	4	52	217	-7	2
BLF2KZB	571	7.13	5.1	51	211	4	3	34	214	-11	7
BLF2KZC	578	8.31	6.	56	213	9	4	38	217	-8	5
BLF2KZ	586	10.49	7.4	76	214	13	4	52	218	-5	3
BLF2DA	598	14.21	9.	187	200	-2	3	142	199	-7	5
BLF2DB	605	8.04	5.7	65	201	5	5	45	201	-9	5
BLF2DC	612	9.2	6.9	76	204	2	4	52	203	-11	4
BLF2DD	619	7.3	5.5	47	205	7	3	30	204	-12	3
BLF2DE	626	7.59	5.5	58	203	-2	3	39	203	-14	4
BLF2DF	633	7.59	4.6	47	202	9	4	26	202	-5	5
BLF2DG	640	4.77	3.9	83	194	2	4	61	193	-5	3
BLF2DH	647	11.93	8.0	155	194	4	10	121	190	5	4
BLF2DI	655	8.39	5.6	85	197	-2	3	62	194	-11	3
BLF2DJ	662	9.38	8.3	114	198	-1	5	84	199	-11	7
BLF2DK	669	7.76	7.3	45	195	12	5	33	194	-8	5
BLF2DL	675	5.13	4.9	44	175	4	5	30	170	-7	5
BLF2DM	680	13.79	9.1	212	198	-1	3	167	198	-7	3
BLF2DN	687	8.78	5.2	93	202	-4	3	65	203	-12	3
BLF2DO	695	7.57	5.0	193	199	-2	5	148	202	-6	6
BLF2DP	702	9.56	5.5	152	202	1	3	111	200	-5	4
BLF2DQ	708	7.86	4.0	109	202	-5	4	75	199	-9	4
BLF2DR	714	4.40	2.2	90	203	-4	3	63	200	-9	4
BLF2DS	723	12.69	7.7	196	208	-1	4	138	207	-7	4
BLF2DT	730	8.84	6.1	160	210	-4	6	114	209	-12	7
BLF2DU	737	7.72	4.3	134	207	-4	4	98	208	-9	3
BLF2DV	745	8.01	4.5	114	208	-3	3	83	206	-6	5
BLF2DW	751	6.88	4.4	130	212	-2	4	97	212	-6	4
BLF2DX	758	8.57	5.1	168	194	0	4	133	189	-5	4
BLF2DY	765	8.34	4.4	124	210	-2	4	90	211	-7	4
BLF2ED	771	7.97	4.4	157	202	-5	4	104	202	-9	2
BLF2EE	779	9.23	4.5	175	201	-6	4	75	201	-10	13
BLF2EF	786	7.65	3.1	103	203	-3	4	67	206	-6	3
BLF2EG	792	8.49	3.7	104	206	-1	2	71	204	-8	3
BLF2EH	799	5.92	2.5	100	202	-4	2	68	205	-7	2

BLF2EI	806	10.88	2.9	150	203	1	8	99	201	-6	4
BLF2EJ	813	7.96	3.8	70	200	-4	5	49	199	-12	5
BLF2EK	820	8.54	4.5	237	198	-10	4	167	198	-15	4
BLF2EL	828	7.4	3.6	160	201	-5	3	110	200	-10	3
BLF2EM	834	10.68	5.0	291	198	-9	3	217	197	-12	2
BLF2EN	842	8.41	4.1	115	198	-10	5	81	193	-14	4
BLF2EO	849	7.14	3.1	100	198	-6	4	71	197	-12	3
BLF2EP	856	8.93	3.5	186	196	-10	3	123	194	-12	2
BLF2EQ	864	6.99	3.1	153	193	-2	4	106	194	-6	4
BLF2ER	870	8.9	3.4	89	198	2	3	55	197	-6	3
BLF2ES	877	9.22	3.9	126	198	1	3	86	197	-4	4
BLF2ET	885	10.07	6.4	276	197	4	3	203	195	-3	5
BLF2EU	891	8.68	5.3	203	195	-1	3	149	198	-7	3
BLF2EV	898	7.12	4.0	177	194	-1	3	121	194	-5	2
BLF2EW	905	6.76	3.9	127	195	-2	3	86	192	-6	2
BLF2EX	911	9.11	3.8	197	200	-7	4	140	197	-9	3
BLF2EY	918	7.5	3.3	154	200	-5	3	107	196	-12	3
BLF2EZ	926	8.8	5.	190	197	-3	2	138	194	-8	3
BLF2EZA	933	7.64	4.5	103	197	1	3	71	197	-10	4
BLF2EZB	939	7.74	3.2	126	198	-1	3	92	196	-9	5
BLF2EZC	947	6.33	2.8	85	196	-4	3	64	194	-9	2
BLF2EZD	954	7.95	4.3	102	197	1	3	68	196	-9	4
BLF2FA	1027	6.24	4.	113	199	-8	3	85	198	-9	4
BLF2FB	1034	5.43	2.	80	200	-8	3	61	196	-10	2
BLF2FC	1041	8.91	3.8	70	196	-8	9	68	194	-20	11
BLF2FD	1048	8.93	6.2	227	192	-11	4	170	191	-16	3
BLF2FE	1055	7.75	5.4	105	193	-8	3	52	189	-16	4
BLF2FF	1063	6.34	5.	118	197	-5	4	95	195	-11	3
BLF2FG	1069	10.66	8.6	238	199	1	3	188	195	-5	3
BLF2FH	1075	7.9	5.2	118	199	-4	4	88	195	-10	4
BLF2FI	1082	8.5	5.1	111	198	-4	5	79	195	-10	4
BLF2FJ	1089	7.95	6.3	226	194	-7	3	168	194	-10	3
BLF2FK	1096	8.58	4.5	187	197	-11	4	137	195	-11	4
BLF2FL	1105	9.55	4.8	139	201	-9	3	62	199	-15	3
BLF2FM	1114	9.33	4.	176	197	-8	2	138	192	-10	3
BLF2FN	1121	10.34	3.3	12	238	68	9	5	182	-26	11
BLF2GA	1138	9.52	3.5	71	196	-1	4	56	194	-11	4
BLF2GB	1144	6.05	1.7	25	209	-6	6	19	204	-19	6
BLF2GC	1150	7.8	2.8	39	201	-6	3	29	195	-15	3
BLF2GD	1156	5.56	1.9	73	189	-11	4	51	186	-16	5
BLF2HA	1164	10.31	3.4	83	195	-7	4	60	192	-16	4
BLF2HB	1170	8.28	2.6	55	199	-11	5	42	198	-16	6
BLF2HC	1177	7.42	3.4	48	197	-4	6	35	192	-14	5
BLF2HD	1185	7.52	3.1	62	201	-4	3	46	198	-14	4
BLF2HE	1192	10.65	5.1	71	211	-1	4	58	207	-9	5
BLF2HF	1198	7.46	4.5	48	200	4	6	35	196	-5	4
BLF2HG	1203	4.57	2.2	45	196	-2	5	48	192	-3	4
BLF2HH	1208	8.59	3.4	46	202	1	4	36	201	-5	5
BLF2HI	1214	7.72	4.4	78	194	-5	5	66	193	-13	3
BLF2HJ	1220	7.6	3.6	57	200	-7	4	45	197	-13	5
BLF2HK	1227	7.69	4.7	70	197	-3	6	56	195	-7	4
BLF2HL	1234	7.28	4.4	52	201	1	5	39	199	-6	5
BLF2HM	1242	8.47	4.9	53	200	1	5	42	196	-11	3
BLF2HN	1248	8.46	4.8	44	198	-2	5	35	197	-11	5
BLF2HO	1256	7.26	4.5	79	211	-5	3	66	210	-9	4
BLF2HP	1263	8.04	5.3	55	198	3	4	47	194	-6	5
BLF2HQ	1268	7.5	4.4	60	195	-2	5	52	193	-9	3
BLF2IA	1277	12.4	9.2	109	193	-1	4	89	193	-12	3
BLF2IB	1285	8.7	5.6	62	196	-3	4	48	195	-13	4
BLF2IC	1293	7.48	4.5	28	198	0	6	21	198	-11	8

BLF2ID	1299	8.9	6.1	144	196	-8	5	123	196	-10	6
BLF2IE	1307	6.16	4.8	80	199	-7	4	64	196	-12	3
BLF2IF	1313	11.36	8.7	59	194	-3	6	45	192	-13	7
BLF2IG	1320	5.5	4.3	24	197	6	3	19	194	-5	3
BLF2IH	1326	5.29	4.2	98	195	-2	3	80	193	-6	4
BLF2II1	1330	4.89	3.2	55	194	-8	3	45	190	-12	3
BLF2II2	1335	7.39	4.5	46	196	-2	4	36	193	-7	4
BLF2IJ	1340	6.87	3.4	32	199	0	3	27	195	-12	4
BLF2IK	1346	11.44	7.5	30	192	13	7	19	191	-10	5
BLF2IL	1353	9.16	5.9	65	198	-3	3	51	197	-13	2
BLF2IM	1360	6.71	3.8	38	194	-3	4	28	191	-12	3
BLF2IN	1367	8.39	4.6	53	193	0	4	43	192	-6	3
BLF2IO	1374	7.85	4.2	52	188	-8	5	43	190	-14	5
BLF2IP	1382	4.57	2.7	23	198	4	5	18	198	-5	8
BLF2IQ	1390	13.21	6.9	57	190	0	5	45	188	-12	9
BLF2AA	1397	10.4	6.5	152	198	-2	4	109	198	-6	5
BLF2AB	1405	7.78	2.	49	200	-4	5	37	196	-11	5
BLF2AC	1411	7.92	4.3	66	199	-3	4	23	197	-8	7
BLF2AD	1418	8.2	4.6	90	200	-2	3	68	197	-7	4
BLF2AE	1423	4.51	1.8	33	199	-1	5	25	198	-4	8
BLF2AF	1428	8.68	3.5	35	207	1	7	28	203	-11	5
BLF2AG	1435	7.45	4.3	104	201	-3	4	74	201	-8	3
BLF2AH	1441	5.34	2.	49	200	1	3	39	198	-5	3
BLF2AI	1446	7.59	4.4	100	202	-1	4	83	199	-3	5
BLF2AJ	1452	8.2	4.4	51	207	1	5	40	202	-10	5
BLF2AK	1459	7.57	3.6	26	206	10	6	23	197	-6	7
BLF2AL	1466	7.09	3.2	39	208	5	5	31	201	-5	3
BLF2BA	1471	8.56	5.2	63	204	3	4	51	201	-3	4
BLF2BB	1476	4.84	2.8	25	202	-4	5	20	194	-14	3
BLF2BC	1482	6.74	3.8	56	209	-8	6	48	204	-13	3
BLF2BD	1486	8.39	5.3	44	199	-3	4	40	195	-9	4
BLF2BE	1492	7.35	4.	34	196	1	5	25	193	-13	5
BLF2BF	1499	5.93	1.6	44	201	0	3	33	194	-9	4
BLF2BG	1506	11.37	6.8	76	188	6	8	57	185	-7	4
BLF2BH	1513	7.63	4.6	43	194	3	4	34	188	-9	3
BLF2BI	1520	7.48	4.3	38	194	-2	4	31	187	-11	4
BLF2BJ	1527	8.87	5.3	49	188	-1	4	42	186	-10	4
BLF2BK	1535	12.	6.2	73	184	2	4	61	180	-7	3
BLF2BL	1542	8.49	4.1	35	193	6	3	30	186	-8	7
BLF2BM	1549	7.79	3.9	32	197	7	4	24	188	-6	6
BLF2BN	1556	7.44	3.9	29	195	9	7	20	184	-8	5
BLF2BO	1563	8.12	3.8	26	194	6	3	23	188	-10	5
BLF2BP	1571	8.42	4.1	31	194	9	4	25	188	-7	6
BLF2BQ	1577	7.69	3.7	31	197	2	6	25	189	-12	4
BLF2BR	1585	8.6	5.1	34	196	7	5	25	187	-11	6
BLF2BS	1591	7.61	4.1	28	194	5	5	23	184	-8	4
BLF2BT	1598	8.99	5.1	38	190	-2	6	32	187	-12	6
BLF2BU	1606	8.89	5.2	57	184	-1	4	48	177	-11	4
BLF2BV	1613	8.07	4.2	43	183	-7	6	40	177	-16	5
BLF2BW	1621	4.68	2.1	82	184	-15	5	70	182	-14	6
BLF2BX	1625	5.06	3.4	68	187	-10	4	54	184	-10	7
BLF2BY	1633	13.92	9.6	167	182	-4	5	132	180	-9	5
BLF2BZ	1641	7.49	5.1	62	189	0	4	48	188	-9	2
BLF2BZA	1647	7.32	3.7	42	190	-8	5	37	187	-16	3
BLF2BZB	1654	7.27	4.	31	184	-5	3	29	179	-17	4
BLF2BZC	1661	6.75	3.4	28	187	0	7	22	181	-14	5
BLF2BZD	1668	5.28	3.3	40	181	-3	4	31	178	-7	8
BLF2BZE	1676	8.42	5.1	76	179	-3	5	61	175	-10	4
BLF2BZF	1683	6.87	3.6	15	190	1	6	28	184	-10	6
BLF2BZG	1688	5.38	2.9	16	206	19	7	11	184	-4	12

BLF2CA	1713	9.1	5.1	75	202	-5	5	58	202	-15	5
BLF2CB	1730	6.8	2.4	31	202	-2	5	25	197	-16	7
BLF2CC	1737	6.55	2.	35	201	-1	6	27	196	-10	6
BLF2CD	1744	13.75	5.2	113	208	-4	3	93	205	-9	6
BLF2CE	1751	5.71	2.8	47	205	-4	3	37	202	-11	5
BLF2CF	1756	6.41	3.2	44	201	2	4	33	197	-8	4
BLF2CG	1763	8.77	4.3	32	199	5	3	20	193	-5	7
BLF2CH	1770	8.14	4.4	27	202	7	4	21	196	-7	8
BLF2CI	1776	7.33	3.9	24	203	10	3	17	197	-8	7
BLF2CJ	1783	7.59	4.4	26	200	11	4	15	194	-6	6
BLF2CK	1790	8.47	2.5	30	196	1	6	17	191	-10	19
BLF2CL	1798	7.78	4.	29	200	7	4	16	196	-8	6
BLF2CM	1804	7.96	4.5	29	200	8	6	16	194	-8	6
BLF2CN	1811	8.05	5.6	29	199	7	5	19	198	-6	5
BLF2CO	1818	7.54	4.4	27	201	9	5	18	195	-7	6
BLF2CP	1825	8.42	4.5	32	202	14	4	23	198	-4	5
BLF2CQ	1832	7.3	3.5	27	202	14	4	18	198	-5	6
BLF2CR	1839	8.97	4.5	29	198	10	5	22	195	-8	4
BLF2CS	1847	7.73	3.1	28	200	7	4	20	199	-5	4
BLF2CT	1854	8.19	3.4	25	198	8	3	21	193	-10	7
BLF2CU	1861	7.61	3.6	25	199	11	5	17	194	-8	6
BLF2CV	1867	7.7	3.3	25	193	5	5	21	188	-8	4
BLF2CW	1874	7.63	3.1	27	193	1	5	20	192	-12	7
BLF2CX	1881	8.73	3.4	28	199	6	5	17	192	-8	11
BLF2CY	1888	7.28	3.8	86	199	-10	7	69	198	-14	9
BLF2CZ	1893	5.69	4.	94	197	-10	4	76	196	-12	3
BLF2CZA	1899	6.18	4.7	90	200	-4	3	72	196	-7	2
BLF2CZB	1904	3.32	2.2	40	199	-2	3	33	201	-6	4
BLF2CZC	1909	8.84	7.6	95	199	-1	2	76	199	-4	3
BLF2CZD	1917	4.55	2.8	67	195	-5	3	48	195	-8	4

APPENDIX 2

LABORATORY INSTRUMENTATION

a) Molspin Spinner Magnetometer

All measurements of intensity and direction of magnetization were performed on this instrument. A small head designed for regular 2.5cm cores or 2cm cubes was used for measuring cores and disks. The plastic top specimens were measured in a larger head designed for archeomagnetic purposes. To assess the uncertainty, repetitive measurements were carried out with 4 cores and 2 plastic tops, using both heads. The angular standard deviation (δ) calculated for 10 measurements is given below.

Cores measured with the small head

Sample Name	δ(degrees)
BL71	0.7
Bl108A	1.1
BL101B	1.5
BL44	2.3

Plastic tops measured with the large head (10 times)

Sample Name	δ(degrees)
BL133B	3.5
BLA44C	3.8

b) AF demagnetizer

The alternating field demagnetizer used in the present study was made in the Paleomagnetism Laboratory of the University of Alberta and is fully described by Murthy (Ph.D. Thesis, University of Alberta, 1969). It can reach peak field values of 0.18T.

c) Thermal demagnetization furnace

This furnace is located in a magnetically shielded room and can reach temperatures of 700°C. It is controlled by a micro-computer and the temperature can be set and stabilized with a precision <2°C. The control program, written in BASIC is given below.

```
-----------------------------------------------------------------
FURNACE CONTROL PROGRAM
J.M.MAILLOL 1989
VARIABLES:  SP(selected temp.),  TE(thermocouple reading),  ER
(temperature difference SP-TE)
-----------------------------------------------------------------

 1 CLS:CLEAR
 5 DIM SS(15)
 6 DIM ST(15)
***** THERMOCOUPLE CALIBRATION DATA ****************************
10 DATA -2676, -2405,-2064,-1709,-1350
15 DATA -962,-581,-186,207,618,1039,1431,1856,2263,2643,3030
16 DATA -19.7,50,105.2,158.3,210.2
17 DATA 259,308.3,356.2,404.1
18 DATA 450.1,494.7,543.9,587.6,633.8,682.6,731.6
20 FOR I=0 TO 15
25 READ SS(I)
30 NEXT I
40 FOR I=0 TO 15
50 READ ST(I)
60 NEXT
********* INITIALIZATION ***************************************
105 TF=0
110 AOR=&HFF70:BOR=&HFF72
```

```
120 ACR=&HFF71:BCR=&HFF73
130 AD=&HFF70:BD=&HFF72
140 C=0
150 TIMER=0
170CU=1
******** INPUT ROUTINES ****************************************
180 INPUT"DESIRED TEMP. ";TD
181 CLS
182 IF TD<50 THEN PRINT"TEMP. SHOULD BE AT LEAST 50":GOTO180
183 IF TD>731 THEN PRINT"TO HIGH ":GOTO180
184 INPUT"HOW LONG DO YOU WANT TO HOLD THIS TEMP.";RT:PRINT
185 IF TD>361 THEN PRINT"SWITCH VOLTAGE TO 208V":CM=13
186 IF TD<=361 THEN PRINT"SWITCHVOLTAGE TO 120V":CM=15
187PRINT:PRINT:INPUT"PRESS ENTER";ZZ
188 GOSUB 4000
189 CLS
200 *** SELECTION OF SETTINGS *********************************
210 IF SP>-800 THEN CC=1 ELSE CC=.4
220 GM=80:GA=60:OF=0:VM=3
230 IF SP>-1400 THEN OF=5:GA=30:VM=6
240 IF SP>-1000 THEN GM=60:GA=20:OF=6:VM=7
250 IF SP>-100 THEN VM=10:GM-90:GA=30:OF=3
260 IF SP>500 THEN GM=80:GA=20:OF=4:VM=15
270 GOSUB 3000
280 GOSUB 2000
282     IF     TE>SP     THEN     PRINT@229,"FURNACE     TOO     HOT
!":SOUND240,1:GOTO282
290 POKE BCR,&H38
295 PRINT@448,"SELECTED TEMPERATURE: ";TD
300 T1=TE
305 GOSUB 5000
310 SA=SP+OF
315 ********DISPLAY***********************************************
320 GOSUB 2000
330 N=N+1
350 T=TIMER:TIMER=0
360 TIME=TIME+(T+1)/3600
370 PRINT@69,USING"TIME: ###.##";TIME
380 PRINT@133,"TEMPERATURE: ";TX
390 PRINT@197,"HEATER: ";C
400 PRINT@261,"DEVIATION: ";ER
404 IF FT=1 THEN GOTO 410
405 IF TX=TD THEN FT=1:TF=TIME
410 GOSUB3000
420 ER=(SA-TEMP)
430 IF N>10 THEN GOSUB 1010
435 IF FT=1 AND (TI-TF)>RT THEN C=0:GOTO320
440 IF ER<0 THEN C=0:GOTO320
450 COR=(ER/GA)
460 IF CO>1 THEN CO=1
470 C=INT(COR*CM*CU*CC+.5):GOTO 320
1000 '********TURN ON/OFF PROP. CONTROL***********************
```

```
1020 N=0
1025 GOSUB5000
1030 DT=TE-T1
1040 T1=TE
1045 IF ER>9*GM THEN CU=1:RETURN
1050 IF DT>=VM AND ER>GM THEN CU=0:RETURN
1060 IF DT>=2 AND ER<=GM THEN CU=0:RETURN
1070 CU=1
1080 RETURN
2000 '*****************SET COUNTER*******************************
2020 POKE ACR,&H30:POKE AD,&HFF:     POKE ACR,&H34
2030 POKE AOR,C
2040 POKE ACR,&H3C:POKE ACR,&H34
2050 RETURN
3000 '***************READ TEMPERATURE***************************
3020 POKE BCR,&H38:POKE BD,&HC0
3030 POKE BCR,&H3C
3040 POKE ACR,&H30:POKE AD,0
3050 POKE ACR,&H34
3060 POKE BCR,&H34:POKE BCR,&H3C
3070 A=PEEK(BCR)
3080 IF A-127<1 THEN GOTO 3070
3090 POKE BOR,0
3100 FOR I=1 TO 100:NEXT I
3110 A=PEEK(AOR):B=PEEK(BOR)
3120 POL=B AND 32
3130 B=B AND 15
3140 TEMP=A+B*256
3150 IF POL=32 THEN TEMP=TEMP*-1
3160 POKE BOR,&HC0
3170 RETURN
4000 '*****************CONVERT TEMP>>S.P.************************
4020 F1=INT(TD/50)
4030 SP=SS(F1)+(TD-F1*50)/50*(SS(F1+1)-SS(F1))
4035 SP=INT(SP+.5)
4040 RETURN
5000 ***************** CONVERT SP>>TEMP ************************
5010 F2=INT((TE+2783)/378)
5020 TX=ST(F2)+(TE+2783-F2*378)/378*(ST(F2+1)-ST(F2))
5030 TX=INT(TX+.5)
5040 RETURN
```

d) Magnetically shielded room

This 2x2x2m room is covered with sheets of a special alloy (μ-metal) that provides a shielding effect from the ambient magnetic field. It houses a paleomagnetic furnace

and provides storage for samples before and during their analysis. In order to test the quality of shielding, measurements of the residual magnetic field inside the room were carried out. A contour map of the total field is given in Fig.A.1. It shows that away from the door, the field is always lower than 200 γ. Based on these measurements, the furnace was relocated to the N-E corner of the room (field < 60 γ), and the S-W corner was chosen to be the best storage place.

e) Other instruments

Bulk susceptibilities were measured on a commercial Bartington meter. IRM experiments were performed using a water-cooled electro-magnet providing a maximum field of 1.75T.

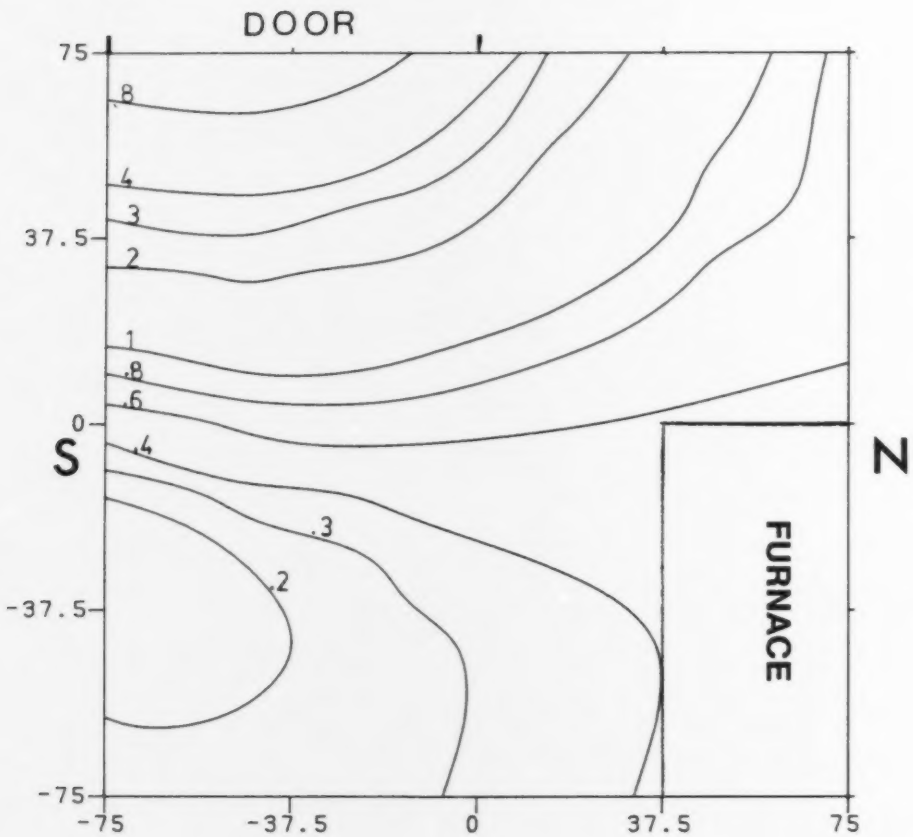

Figure A1. Contour plot of the field intensity in the magnetically shielded room. Field is in $10^2\gamma$ and distances in cm (origin in the center of the room).

APPENDIX 3

GEOMAGNETIC FORMULAS

a) Magnetic potential-Gauss coefficients

The Gauss coefficients mentioned in the discussion of the paleosecular variation models are found in the expression of the scalar magnetic potential (ψ) given below (Merrill and McElhinny, 1983).

$$\psi = \frac{a}{\mu_o} \sum_{l=0}^{\infty} \sum_{m=0}^{\infty} P_l^m \cos(\theta) \left\{ \left[C_l^m \left(\frac{r}{a}\right)^l + (1-C_l^m) \left(\frac{a}{r}\right)^{l+1} \right] g_l^m \cos m\phi \right.$$

$$\left. + \left[S_l^m \left(\frac{r}{a}\right)^l + (1-S_l^m) \left(\frac{a}{r}\right)^{l+1} \right] h_l^m \sin m\phi \right\}$$

where a is the Earth's radius and C_l^m and S_l^m are positive numbers between 0 and 1 which indicate the fraction of the potential associated with sources of external origin. The coefficients $(1-C_l^m)$ and $(1-S_l^m)$ indicate the fraction of the potential associated with sources of internal origin. The coefficients g^l_m and h^l_m are called the Gauss coefficients appropriate to the Schmidt polynomials P_l^m

b) Virtual geomagnetic poles (VGP)

At a given location on the Earth one can always calculate the position of the equivalent dipole that would cause the observed geomagnetic field direction. Of course, since the field is not purely dipolar this rarely corresponds to the true geomagnetic pole and the pole thus calculated is called Virtual Geomagnetic Pole.

If the latitude and longitude of the site are λ_s and ϕ_s and the declination and inclination at the site are D and I then the latitude λ_a and longitude ϕ_a of the VGP are given by

$$\sin\lambda_a = \sin\lambda_a\cos p + \cos\lambda_s\sin p\cos D$$

$$\phi_a = \phi_s + \beta \text{ (for } \cos p > \sin\lambda_s\sin\lambda_a)$$

or

$$\phi_a = \phi_s + (180°-\beta) \text{ (for } \cos p < \sin\lambda_s\sin\lambda_a)$$

where

$$\sin\beta = \sin p\sin D/\cos\lambda_a$$

Latitude is measured between 0° and ±90°, positive in the northern hemisphere and longitude is measured eastward from Greenwich, 0° to 360°.

p is the magnetic colatitude of the site, given by

$$\tan I = 2\cot p$$

and $-90° < \beta < +90°$.

APPENDIX 4

GLOSSARY

As suggested by the examination committee, this is a glossary of geological terms, which might help readers not familiar with geoscience vocabulary.

BIOCLASTIC: describes sediments made up of fragments of organisms.

BIOTURBATIONS: mechanical perturbations of unconsolidated sediments produced by the activities of living organisms.

CLASTIC: describes sediments made up of fragments produced by the breaking-up of earlier rocks.

DETRITAL: describes a process by which CLASTIC sediments are formed.

DIAGENESIS: the changes in mineral composition and texture that take place in a sediment after it has been deposited.

LACUSTRINE: of, or formed in or by, a lake.

LITHOLOGY: the general character of a rock, or a sedimentary formation, more particularly as seen in exposures and hand specimens.

PALYNOLOGY: the study of fossil spores and pollen.

PLAYA: intermittent desert lake.